The Effect of Manganese, Nitrogen and Molybdenum on the Corrosion Resistance of a Low Nickel (<2 wt%) Austenitic Stainless Steel

By

Asimenye Muwila

Submitted in fulfilment of the requirements for the degree

MSc: Materials and Metallurgy Engineering

In the Faculty of Engineering, The School of Process and Metallurgical Engineering, University of the Witwatersrand, Johannesburg

2006

Declaration

I declare that this dissertation is my own, unaided work. It is being submitted for the Degree of Masters of Science in Materials and Metallurgical Engineering in the University of the Witwatersrand, Johannesburg. It has not been submitted before for any degree or examination in any other university.

Asimenye Muwila
10th day of May 2006

Abstract

This dissertation is a study of the effect of manganese, nitrogen and molybdenum on the corrosion behaviour of a low nickel, austenitic stainless steel. The trademarked steel, Hercules^{TM}, has a composition of 10 wt% Mn, 0.05 wt% C, 2 wt% Ni, 0.25 wt% N and 16.5 wt% Cr. Eighteen alloys with a Hercules^{TM} base composition were made with varying manganese, molybdenum and nitrogen contents, to establish the effect of these elements on the corrosion behaviour of the steel, and to determine a composition that would ensure increased corrosion resistance in very corrosive applications. The manganese was varied in three levels (5, 10 and 15 wt%), the molybdenum in three levels (0.5, 1 and 2 wt%) while the nitrogen was varied only in two levels (0.15 and 0.3 wt%).

The dissertation details the manufacturing and electrochemical corrosion testing of these alloys. Preliminary tests were done on 50g buttons, and full-scale tests on 5 kg ingots. The buttons had a composition that was not on target, this was however rectified in the making of the ingots. Potentiodynamic tests were done in a 5 wt% sulphuric acid solution and the corrosion rate (mm/y) was determined directly from the scans.

From the corrosion test results, it was clear that an increase in manganese decreases the corrosion rate, since the 5 wt% Mn alloys had the highest corrosion rate, whereas the 15 wt% Mn alloys, the lowest.

The addition of molybdenum at 5 wt% Mn decreased the corrosion rate such that a trend of decreasing corrosion rate with increasing molybdenum was observed. At 10 and 15 wt% Mn molybdenum again decreased the corrosion rate significantly, but the corrosion rate value remained more or less constant irrespective of the increasing molybdenum content.

At nitrogen levels lower than those of Hercules^{TM} (less than 0.25 wt%) there was no change in corrosion rate as nitrogen was increased to levels closer to 0.25 wt%. For nitrogen levels higher than 0.25 wt%, corrosion rates decreased as nitrogen levels were increased further from 0.25 wt% but only at Mo contents lower than 1.5 wt%.

The Hercules^{TM} composition was developed for its mechanical properties. Microstructural analyses revealed that the 5 wt% Mn alloys were not fully austenitic and since the 15 wt% Mn alloys behave similarly to the 10 wt% Mn alloys, it was concluded that 10 wt% Mn was optimum for Hercules^{TM}. All the alloys tested had a much lower corrosion rate than Hercules^{TM}. Any addition of molybdenum thus improved the corrosion rate of this alloy. An alloy with a Hercules^{TM} base composition, 10 wt% Mn, 0.15 wt% N and a minimum addition of 0.5 wt% Mo would be a more corrosion resistant version of Hercules^{TM}.

Pitting tests were done on the 10 wt% Mn ingots in a 3.56 wt% sodium chloride solution. The results showed that an increase in molybdenum increased the pitting resistance of the ingots.

Immersion tests in a 5 wt% sulphuric acid solution at room temeperature on the 10 wt% Mn ingots confirmed that the ingots corroded by means of general corrosion.

Acknowledgements

The Lord

Thank you God for all the opportunities that You have afforded me. Without You none of this would be possible.

My Supervisors

I would like to thank Dr. M. Sephton for her patience, understanding, interest and invaluable advice. I would also like to thank Mr. R. Paton for his guidance.

Technical Assistance

Thanks to Jonathan Kerr, Joseph Moema, Patrick Mokaleng, Clement Dlamini and Edson Muhuma for sharing their technical knowledge on melting, preparing and examining samples. Thanks also to Bernard Joja for his SEM expert advice.

Institutions

I would like to thank Mintek for their sponsorship of my undergraduate, as well as postgraduate studies, and for the use of their facilities at what is now AMD (Advanced Materials Division). Thanks to the School of Process and Materials Engineering at the University of the Witwatersrand for allowing me to use their equipment and providing me with a computer and office space as well as the NRF for sponsoring my postgraduate studies.

Others VIP's

Thanks mum and dad for being so understanding and supportive even when you disagreed. Thanks Lusu and Ngata for making me laugh when I needed to. Ali and Chif thanks for your support. Mwaf - still missing you. Thanks Wes for your understanding and patience.

Table of Contents

Table of Contents

Table of Contents

List of Figures

List of Figures

List of Figures

List of Tables

1. Introduction

Nickel prices are notorious for being high and unstable and since austenitic stainless steels contain 8-10% nickel, price instability strongly affects the stainless steel industry. Nickel prices fluctuate because nickel is expensive to process and is not always readily available [Rama Rao and Kutumbarao, 1989]. The cost of nickel is currently averaging at $15000/tonne and is expected to increase [Moema e*t al.*, 2005]. This has once again sparked interest in the development of a low nickel austenitic stainless steel.

Reducing the nickel content in austenitic stainless steels significantly reduces their price. Nickel's ability to stabilise and form austenite is, however, an integral part in the processing of austenitic stainless steels, and if the nickel content is to be reduced appreciably, other austenite forming elements, such as carbon, nitrogen, manganese and copper, need to be used for the partial or complete replacement of nickel [Kerr, 2003; Lula, 1986]. These elements have the advantage of costing less than nickel.

There has been much research into replacing Ni with other austenizing elements [Lula, 1986; Turan, 1991]. Nickel shortages before World War II in Europe and in the United States during the Korean War initiated the replacement of nickel in austenitic stainless steels with manganese and nitrogen [Lula, 1986; Sedriks, 1979]. This led to the development of the now standard and commercial AISI 200 Series stainless steels. These steels are not, however, as popular as the 304 type steels because of their high tensile strength, hardness and work hardening rate, which make them difficult to form and they have poor corrosion resistance [Sedriks, 1979]. Other

low nickel austenitic stainless steels that have been developed in the past are listed in Table 1.1 [Cortie, 1995].

Table 1. 1: Prior art austenitic stainless steels with reduced contents of nickel [Cortie, 1995].

Alloys	Introduced by	Nominal Composition %						
		Cr	Ni	Mn	Cu	C	N	other
Type 201	USA, 1950	17	4.5	6.5	0	0.1	0.25	
203EZ		17	6	6	2	0.05		0.25S
YUS27A	Japan	18	6.5	1	2.2	0.05	0.07	
AL Type 211	Allegheny-Ludlum	17	5.5	6	1.5	0.05		
NHS-104	Nisshin Steel Co. Of Japan	15.5	0	10	3			
OKh17N3G4D2T	Former Soviet Union	17.5	2.9	3.7	2.5	0.1		0.2Ti
OKh18N2G9D2T	Former Soviet Union	18	1.6	9	2.4	0.05		0.2Ti
08Kh20N5G3D2	Former Soviet Union	20	5	3	2	0.08		

All the alloys listed in Table 1.1 have drawbacks, for instance YUS27A, which is susceptible to hot cracking and the Soviet grades which are duplex and have very high strength and thus low ductility which results in poor fabrication properties [Cortie, 1995]. There is therefore a need for a new low nickel austenitic stainless steel that will not replace any existing stainless steel, but merely provide an alternative for specific application and Mintek in conjunction with other engineering companies [Kerr, 2003] have recognised this need.

Mintek took on a three year project to develop and test a low nickel austenitic steel for construction applications [Kerr, 2003]. Such a stainless steel with a base

composition of 0.02-0.08% carbon, 1.8-2% nickel, 15-17% chromium, 9-10% manganese, 0.2-0.8% silicon and 0.2-0.3% nitrogen, which has a yield strength greater than 350MPa has already been produced [Kerr, 2003]. This alloy, called Hercules™, has good mechanical properties but was found, from preliminary tests, to have poor corrosion resistance. It is believed though that varying the manganese and nitrogen levels of the Hercules™ and adding molybdenum will improve its corrosion resistance.

This project dealt with the investigation of the corrosion resistance of Hercules™. Different alloys with a Hercules™ base composition but varying manganese, nitrogen and molybdenum levels were made so that the effect of these elements on the corrosion resistance of Hercules™ could be investigated. It is important for its acceptance in the stainless steel industry that Hercules™ have comparable corrosion resistance to popular and standard commercial stainless steels, such as AISI 304 and 201, and one of the aims of this project was to specify, if possible, the composition of a corrosion resistant variation of Hercules™.

The specific applications for which the new alloy is targeted and the type of corrosion which it is expected to experience, are listed in Table 1.2.

Table 1. 2: Possible applications for Hercules® and the corrosion attack common to these applications.

Target applications for the construction industry	Type of corrosion experienced
structural members	atmospheric, pitting, SCC, concrete
bars and profiles	general, pitting, SCC
fasteners	crevice, SCC
wall ties	general, crevice
rebars	pitting

From Table 1.2 it is evident that the alloy may suffer general, pitting and crevice corrosion as well as stress corrosion cracking. General and pitting corrosion were looked at in depth, in this project.

This dissertation consists of a literature survey (Chapter 2) and the procedure followed in making the different base alloys with variations in manganese, molybdenum and nitrogen (Chapter 3). It also describes the potentiodynamic, immersion and cyclic pitting tests (Chapters 4 and 5) that were used to determine the effect of the varying levels of these alloying elements on the corrosion resistance of Hercules™.

2. Literature Review

As mentioned in Chapter 1, this project deals with the corrosion behaviour of austenitic stainless steels, and this literature survey provides information on the general properties and corrosion behaviour of these steels. The effect of alloying elements such as nickel, molybdenum, chromium, nitrogen and manganese on microstructure and corrosion behaviour is also discussed.

2.1 Stainless steels

Stainless steels are ferrous alloys, which generally contain a minimum of 10% chromium for corrosion resistance, and are based on the binary Fe-Cr system, shown in Figure 2.1 [.Peckner and Bernstein, 1977; Honeycombe, 1981].

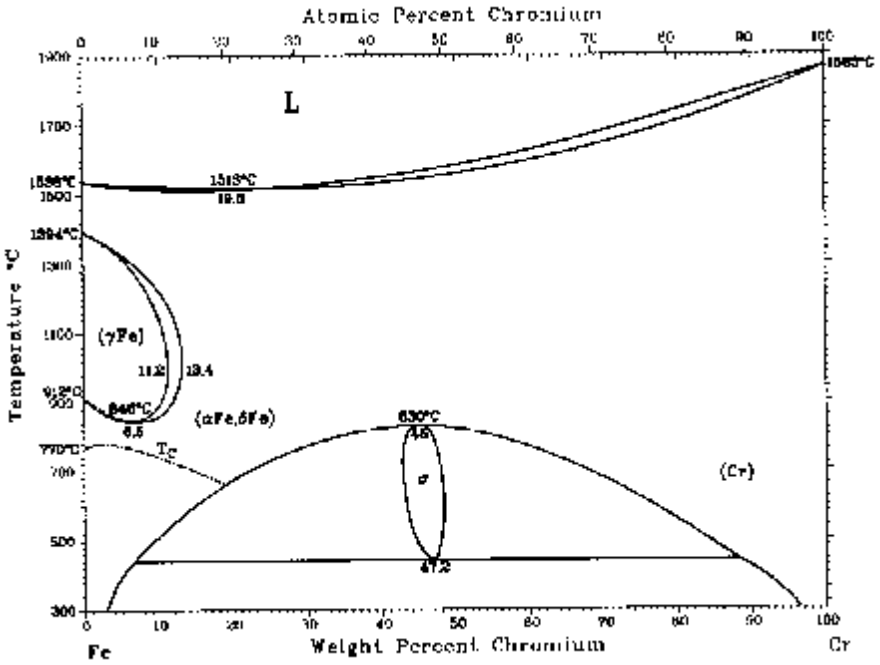

Figure 2. 1: The iron-chromium (Fe-Cr) phase diagram [Peckner and Bernstein, 1977;Honeycombe,1981].

This binary Fe-Cr diagram shows the phase transformations that occur in stainless steels at certain temperatures and compositions. Additions of specific alloying elements modify this binary system, producing different types of stainless steels such as martensitic (α'), austenitic (γ), ferritic (α) and duplex. Since chromium is a ferrite stabiliser, the ferrite (α) phase field on the Fe-Cr phase diagram is extensive while the austenite (γ) phase field is restricted to a small loop that does not extend beyond 12-13% chromium and temperatures lower than 800ºC. This austenite loop can, however, be expanded by the addition of a face centered (FCC) alloying element, such as nickel or manganese, to the binary Fe-Cr system. If the FCC element is added in sufficient amounts, the formation of the ferrite (α) phase is suppressed and a fully austenitic microstructure that is stable at room temperature can be obtained. When added to steel the atoms of the FCC elements substitute iron atoms in the crystal lattice [Vismer, 1997]. These FCC atoms diffuse slowly in iron, slowing down the kinetics needed for ferrite formation. Even though the amount of Ni required to form and stabilise austenite in steel is variable and is dependent on the ferrite forming elements, it is generally acceptable that a minimum of 8% nickel is needed to obtain an austenitic microstructure at room temperature. If, however, other austenite stabilising or forming elements (nitrogen for instance) are also added to the steel it may be possible to obtain a fully austenitic structure at room temperature with less than 8% nickel [Turan, 1991]

Alloying elements can thus be divided into two categories: austenite/ferrite formers and austenite/ferrite stabilisers. Austenite formers, such as nickel, actually increase the amount of austenite in the alloy, whereas austenite stabilisers, expand the austenitic field so that the austenite will be stable at lower temperatures than normal [Cortie, 1995]. An element can therefore be both an austenite former and stabiliser if it has the ability to expand the γ - field, so as to encourage the formation of austenite over wider compositional limits and also stabilise it at lower temperatures.

Ferrite formers, on the other hand, increase the tendency for delta-ferrite formation by decreasing the austenite loop so that the austenite is unstable and transforms to ferrite upon cooling [Vismer, 1997]. Delta-ferrite is a BCC (body centered cubic) phase that is stable between 1394ºC and 1538ºC (melting temperature of steel) [Pickering, 1992]. Delta-ferrite is rich in chromium and other ferrite stabilisers and is undesirable because it depletes the surrounding matrix of chromium and molybdenum, forming areas that are susceptible to pitting attack [Sedriks, 1986]. Delta-ferrite can also transform to hard and brittle sigma phase after long-term exposure at elevated temperatures, thus decreasing the toughness and ductility of the steel.

The effects of alloying elements on the formation of austenite and ferrite have been investigated and Schaeffler diagrams, as illustrated in Figure2.2, have been developed to predict the maximum amount of ferrite (F), austenite (A) and martensite (M) that can be expected in the microstructure at room temperature in terms of the nickel and chromium equivalents [Peckner and Bernstein, 1977; Lula, 1986].

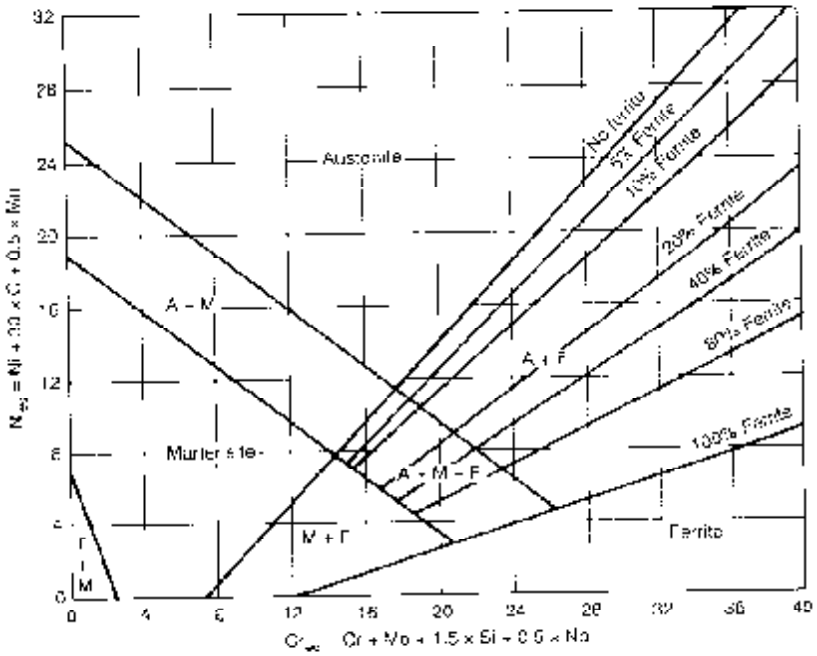

Figure 2. 2: Schaeffler diagram [Peckner and Bernstein, 1997; Lula,1986]

Schaeffler diagrams were constructed for predicting weld metal microstructures, but can be used as a guide when trying to predict if a certain as cast stainless steel will be fully austenitic at room temperature. The nickel and chromium equivalents have been determined using the most common austenite and ferrite forming elements respectively, as in equation 2.1 and equation 2.2 [Peckner and Bernstein, 1977].

Chromium equivalent = (%Cr) + 2(%Si) + 1.5(%Mo) + 5(%V) + 5.5(%Al) + 1.75(%Nb) + 1.5(%Ti) + 0.75(%W) **Equation 2.1**

Nickel equivalent = (%Ni) + (%Co) + 0.5(%Mn) + 0.3(%Cu) + 30(%C) + 25(%N) **Equation 2.2**

Values in the above equations are in weight percentages. The austenite forming elements contribute towards the nickel equivalent and the ferrite forming elements to the chromium equivalent.

Depending on composition, the austenite formed in steel may be stable or metastable. Metastable austenite transforms to martensite either by quenching to temperatures below M_s (martensite start temperature) or by deformation at temperatures below M_d (temperature below which martensite forms due to plastic deformation) [Vismer, 1997]. The austenite stabilising effect of an element depends on its ability to depress the M_s and M_d temperatures. The M_s temperature is calculated as shown in equation 2.3 [Peckner and Bernstein, 1977; Vismer, 1997].

$M_s = 502 - 810(\%C) - 1230(\%N) - 13(\%Mn) - 30(\%Ni) - 12(\%Cr) - 54(\%Cu) - 46(\%Mo)$ **Equation 2.3**

From the coefficients of N and C in the M_s equation it is evident that these elements significantly reduce the M_s temperature.

It is desirable to have a stable austenitic microstructure because it is easily weldable, tough and has better corrosion resistance than ferritic or martensitic microstructures. This is why the austenitic stainless steels are the largest group of stainless steels used today [Rama Rao and Kutumbarao, 1989; Sedriks, 1979]. These steels, classified as the AISI 200 and 300 series [Cortie, 1995; Peckner and Bernstein, 1977], are of interest to this project, since the AISI 304 and 201 along with the Hercules™ were used as control alloys during corrosion testing (refer to chapter 4 and 5).

2.1.1 Type 304 stainless steels

Type 304 steels are general-purpose chromium-nickel stainless steels that have good corrosion resistance and good formability [Harvey, 1982; Sedriks, 1979]. Type 304L is a low carbon version of 304 and has similar corrosion behaviour, but superior intergranular corrosion resistance. Table 2.1 lists the typical compositions of type 304 steels.

Table 2. 1: General composition of AISI type 304 stainless steels in wt% [Harvey, 1982]

	Element						
Alloy	**Cr**	**Ni**	**Fe**	**C(Max)**	**Mn(Max)**	**S(Max)**	**P(Max)**
AISI 304	18-20	8-10.5	bal.	0.08	2	0.5	0.045
AISI 304L	18-21	8-12.5	bal.	0.03	2	0.03	0.045

These steels can easily be drawn and formed because of their high ductility and good strength [Harvey, 1982].

2.1.2 Type 201 stainless steels

Type 201 steels, as mentioned before, are part of the AISI type 200 stainless steel series (austenitic chromium-nickel-manganese stainless steels) that were developed in

the 1950's because of nickel shortages at that time [Lula, 1986; Sedriks, 1979]. These steels have a general chemical composition as listed in Table 2.2 [Harvey, 1982]

Table 2.2: General chemical composition of AISI type 201 stainless steel in wt%[Harvey, 1982]

Alloy	Cr	Ni	Fe	C(max)	Mn	Si(Max)	S(Max)	P(Max)
AISI 201	16-18	3.5-5.5	bal.	0.15	5.5-7.5	1	0.03	0.06

These steels use nitrogen, in conjunction with manganese, to form and stabilise austenite [Levey, 1995]. They have high work hardening rates and higher yield strengths than the 300 series [Harvey, 1982; Levey, 1995]. Typical uses of these steels include shallow drawn cooking ware, automotive trim, window frames and doors. These steels can be drawn, bent, roll formed and end formed.

2.1.3 Hercules® Alloy

Hercules™ is a low nickel (<2 wt%) austenitic stainless steel developed by Mintek. It is fully austenitic at room temperature and has a yield strength >400 MPa in the hot rolled and annealed condition. Hercules™ has a base composition as listed in Table 2.3:

Table 2.3: Chemical composition of Hercules® alloy in wt%.

Alloy	Cr	Ni	Fe	C	Mn	N	Si
Hercules	16.5	2	bal.	0.05	9	0.25	0.5

2.2 Corrosion resistance of stainless steels

2.2.1 General corrosion

Stainless steels have excellent corrosion resistance because they are able to form a very thin, passive layer of chromium oxide (Cr_2O_3) that protects them against corrosive environments [Kincer and McEwan, 1993; Peckner and Bernstein, 1977; Pickering, 1979; Sedriks, 1986]. This film forms in the presence of oxidising agents, and is protective in that it has the ability to self-heal in a variety of environments [Colombier and Hochman, 1965; Newman, 2001; Sedriks, 1979]. Opinions differ on how the passive film protects stainless steels [Raja *et al.*, 1999]; some authors state that chromium-oxy-hydroxide (Cr-O-OH) is formed instead of chromium oxide and that the Cr-O-OH has better protective properties than the Cr_2O_3 [Hashmito and Asami, 1979]. Nevertheless the film is essential in maintaining the corrosion resistance of stainless steels.

When stainless steel is protected by the oxide film it is said to be in a passive state as it is not experiencing accelerated corrosion. [Sedriks, 1986]. The corrosion behaviour of stainless steels is known as active-passive behaviour and can be measured using electrochemical methods. Measurements of the corrosion of stainless steels produce characteristic anodic polarization curves that reveal the general and localised corrosion behaviour of these steels. A typical anodic polarisation curve of stainless steel in sulphuric acid has been redrawn from Sedriks [1986] and is illustrated in Figure 2.3:

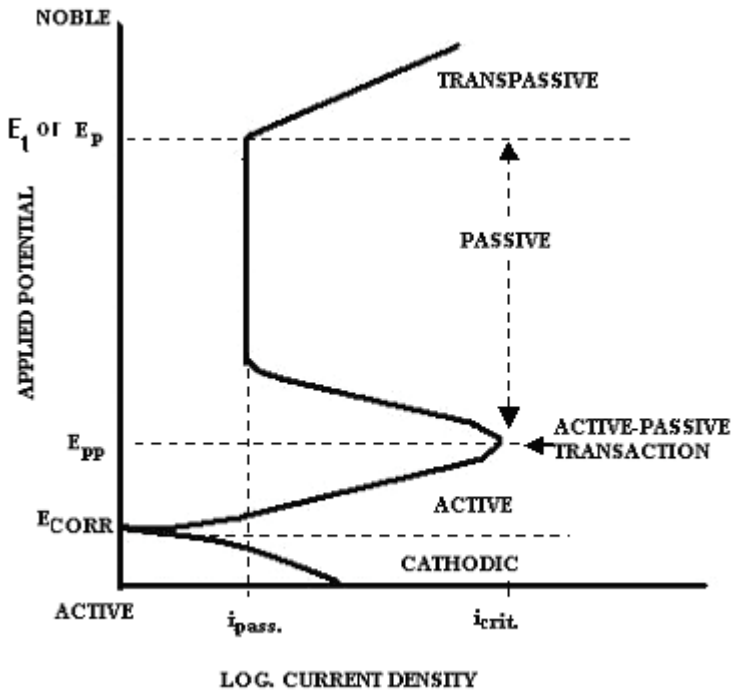

Figure 2. 3: Anodic polarization curve of stainless steel in sulphuric acid solution [Sedriks, 1986]

Stainless steels corrode in the active region, which exists at potentials below the passivation potential (E_{pp}). When the maximum current, called the critical current density (i_{crit}) is reached, the current density drops to a very low value, called the passive current density (i_{pass}), and passivation (formation of the protective Cr_2O_3 layer) is initiated. i_{crit} represents the point of maximum anodic dissolution. During passivation the metal still corrodes, but at a significantly lower rate. When the transpassive region (E_p) is reached the metal starts to corrode at high rates again. The potential value of E_p is dependent on the corrodent. In chloride-free aqueous sulphuric acid solution E_p represents the point of oxygen evolution by the electrolysis of water and is called E_t (representing the beginning of transpassive behaviour). In chloride solutions, however, this point represents the breakdown of the passive film due to pit formation and is called E_p. E_{corr} is the corrosion potential and is the point at which the total rate of all the anodic reactions equals the total rate of all cathodic reactions. The current density at E_{corr} is called the corrosion current density, i_{corr},

which is a measure of corrosion rate since it is directly proportional to metal dissolution [Jones, 1996; Peckner and Bernstein, 1977; Trethewey and Chamberlain, 2002, Vismer 1997]. i_{corr} cannot be measured directly but with the use of a counter electrode, reference electrode and a potentiostat it can be determined indirectly [Jones, 1996]. From the polarisation curve i_{corr} can be determined using either Tafel extrapolation or polarization resistance[1].

i_{corr} values can be converted into mm/y by using Faraday's Law, which relates current flow (I) to mass reacted (m) in an electrochemical reaction as in equation 2.4 [Jones 1996].

$$m = \frac{Ita}{nF}$$ **Equation 2. 4 [Jones, 1996]**

Where F is Faraday's constant (96500 coulombs/equivalent), n is the number of electrons transferred during the reaction, a is the atomic weight and t, the time.

Dividing equation 2.4 through by t, the surface area (A) and density (D), yields a formula, as in equation 2.5, that can find corrosion rate (r) in mm/y if the current density is known.

$$r = 0.00327\frac{ai}{nD}(mm/yr)$$ **Equation 2. 5 [Jones, 1996]**

Equations 2.4 and 2.5 are valid for pure metals only. For an alloy the determination of the equivalent weight (a/n in equation 2.5) is required. The equivalent weight (EW) of an alloy is the weighted average of a/n of the major alloying elements in the alloy as calculated with equation 2.6 [Jones, 1996].

[1] Full explanation of the Tafel extrapolation and polarization resistance methods can be found in Jones, 1996. Pp 143-165.

$$EW = N_{EQ}^{-1}$$

and **Equation 2. 6 [Jones, 1996]**

$$N_{EQ} = \Sigma\left(\frac{f_i n_i}{a_i}\right)$$

Where f_i, n_i and a_i are the mass fraction, electron exchange and atomic weight respectively. Major elements are assumed to be those that are added in amounts of more than 1 wt% to the alloy.

Stainless steels have good corrosion resistance in oxidizing acids such as nitric acid, but they show poor resistance to sulphuric acids at low concentrations and temperatures. Due to passivation, general corrosion of stainless steels occurs mainly in strong acids and alkaline environments and the severity of the corrosion depends on the severity of the solution and the type of steel [Kincer and McEwan, 1993]. Passivity however increases the possibility of pitting corrosion as discussed in the next section.

2.2.2 Pitting corrosion

Metals such as stainless steels and aluminium that depend on a passive film for corrosion resistance are especially susceptible to pitting corrosion when local breakdown of the film occurs. This happens primarily in environments containing very aggressive ions such as chlorides [Jones, 1996, Kincer and McEwan, 1993]. These aggressive ions penetrate the passive film when a certain potential is reached and destroy it at weak points such as grain boundaries and inclusions. The pitting resistance equivalent (PRE) is used to indicate the pitting resistance of stainless steel and is given in equation 2.7 [Frankel, 1998; Levey, 1995; Peckner and Bernstein, 1977]:

PRE = (%Cr) + 3.3(%Mo) + 16(%N) **Equation 2. 7**

This equation has been developed to explain the influence of alloying elements on the pitting resistance of stainless steels. The higher the pitting resistance of an alloy, the more resistant it is to pitting corrosion. [McEwan, 1994]. The PRE equation has limitations because it only considers the effect of molybdenum, nitrogen and chromium on the pitting resistance of stainless steel and the effects of microstructure on pitting are ignored [McEwan, 1994].

As mentioned, for pitting to occur on stainless steels the presence of aggressive ions is needed [Schollenberger, 1995]. These ions in most cases are chloride ions from salt solutions or from chloride bearing compounds such as hypochlorites. The presence of an oxidising agent, such as oxygen, cupric or ferric ions, that can maintain passivity on the surface surrounding the pit is also necessary. Low pH values and static conditions further promote pit formation. Figure 2.4 is an illustration of the pitting process where metal M is being pitted by an aerated sodium chloride solution:

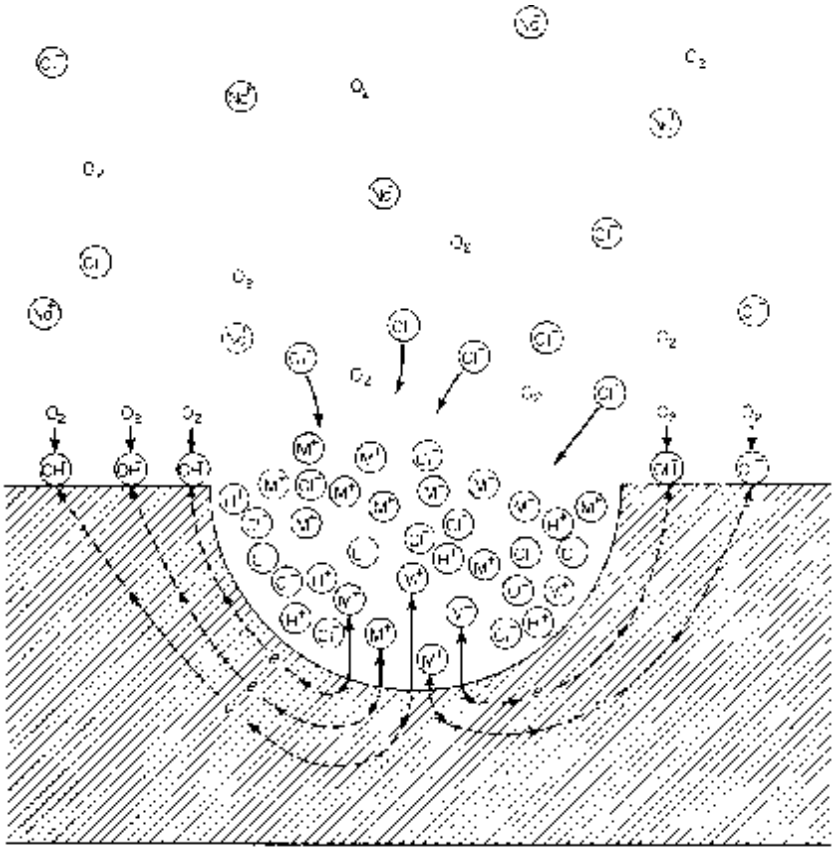

Figure 2. 4: Autocatalytic process occurring in a corrosion pit [Fontana and Greene, 1982].

M dissolves rapidly producing a high concentration of positively charged metal ions in the pit. These ions attract negatively charged chloride ions into the pit to maintain neutrality and this causes a high concentration of MCl ions to build up in the pit. A high concentration of hydrogen ions also builds up in the pit. Both chloride and hydrogen ions promote the dissolution of most metals and their presence accelerates the entire pitting process. The solubility of oxygen in the pit is very limited, so the cathodic oxygen reduction reaction occurs on the metal surface around the pit, protecting these surfaces cathodically and ensuring that the pit remains anodic. This introduces a situation where corrosion is occurring at a small anode near a large cathode, worsening the corrosion in the pit. Pitting is an autocatalytic process in that

as long as there are enough chlorides in the pit preventing repassivation, and provided the oxidizing agent keeps the surrounding cathodic surface passivated, the pit will grow. [Fontana and Greene, 1982; Jones, 1996; Schollenberger, 1995].

Manganese sulphides are a major cause of pitting corrosion in manganese bearing stainless steels. Sulphides form from sulphur that is present as an impurity or an intentional addition to the steel to improve machinability [Sedriks, 1983]. Manganese sulphides dissolve to form H_2S in acid solutions, such as those found in active pits or crevices. It has been suggested that the formation of H_2S makes the formation of passive films more difficult and that it also promotes the breakdown of the passive film in stainless steel [Sedriks, 1983]. Manganese sulphides in stainless steels are anodic with respect to the rest of the steel; they will thus corrode when exposed to a harsh environment, exposing bare metal to pitting attack[2]. In fact, any defect in the metal, inclusions or grain boundaries for example, will act as sites for pit initiation. It is therefore important to try and avoid these when making steel alloys. The pitting resistance of an alloy can be determined by examining its pitting potential (E_p) on the anodic polarisation curve. Generally the more noble the E_p value, the more resistant the alloy is to pitting corrosion [Sedriks, 1979].

2.2.3 Corrosion of control alloys

The three control alloys of concern to this project, as mentioned before, are the AISI 304, AISI 201 and Hercules^{TM} alloys. AISI 304 is the bread and butter of the stainless steel industry in that it has excellent corrosion resistance in numerous types of environments. When fully austenitic, the AISI 304 steels are very resistant to corrosive attack in nitric acids, but moderately resistant to sulphuric acids [Peckner and Bernstein, 1977]. AISI 304 in 5 wt% sulphuric acid at 25°C has been found to

[2] For pitting mechanisms suggesting how manganese sulphide inclusions can initiate pit propagation in stainless steels refer to Sedriks, 1983 and Blom and Degerbeck, 1983.

have a corrosion rate of 0.1-1 mm/y [Avesta Sheffield, 1994]. In an environment containing halogens, AISI 304 steels have poor corrosion resistance.

The AISI 201 steels resist corrosive attack for relatively long periods in industrial and marine atmospheres, but have poorer corrosion resistance than the AISI 304 stainless steels [Harvey, 1982]. Researchers have found AISI 201 to have a corrosion rate >1 mm/y in 5 wt% sulphuric acid at room temperature [Avesta Sheffield, 1994].

Preliminary electrochemical tests done on Hercules™ indicated that it has a higher corrosion rate than AISI 304, but comparable to 201 in the hot rolled and annealed condition. Its corrosion rate was found to be 2.8-35 mm/y [Kerr, 2003; Moema and Papo, 2005]. The higher corrosion rate is probably due to it having a lower chromium content than AISI 304. Chromium plays an important role in the formation of the passive layer of stainless steels, as is discussed in the following section.

2.3 Effect of alloying elements on the corrosion behaviour of stainless steels

Alloying elements play a significant role in determining the corrosion behaviour of stainless steels. The most important effects are the increase of corrosion resistance by the addition of elements such as chromium, nickel and molybdenum, but also a decrease in corrosion rate by the addition of elements such as sulphur and manganese. The stability of the passive film formed on austenitic stainless steels is also dependent on alloy composition in addition to temperature, passivation time and the working environment [Bastidas *et al.*, 2002].

Copper is another alloying element that has been found to be beneficial to the corrosion resistance of stainless steels in sulphuric acid environments [Cortie, 1995,

Sibanda *et al.*, 1994], but it will not be considered in this project since it will not be added to the alloy.

Alloying elements usually work best in conjunction with one another when improving corrosion behaviour of a metal [Sedriks, 1979]. For example, chromium alloyed in conjunction with molybdenum gives the best results in terms of corrosion resistance for austenitic stainless steels. In the next section the effect of chromium and nickel on corrosion behaviour and microstructure of stainless steels is discussed along with those of the elements of interest to this project: nitrogen, manganese and molybdenum.

2.3.1 Effect of chromium

Chromium is the most important alloying element for corrosion resistance because it forms a large part of the oxide layer (Cr_2O_3) that protects the stainless steel from corrosive environments [Frankel, 1998; Lula, 1986; Peckner and Bernstein, 1977; Raja *et al.*, 1999]. At least 12% chromium is needed for an alloy to be resistant to corrosion over an extended range of potential, pH and oxidising power [Audouard, 1993; Cortie, 1995]. Increasing the chromium content beyond 12-13wt% can allow steels to passivate in more aggressive environments [Peckner and Bernstein, 1997; Vismer, 1997].

Experiments done on Fe-Ni-Cr alloys in a sulphuric acid solution revealed that increasing the chromium content of the alloy to levels above 12% decreases the i_{pass} and shifts the E_{pp} (active-passive transition point) towards the active region, thus expanding the passive region and improving the corrosion resistance of the metal as illustrated in Figure 2.5 [Sedriks, 1986].

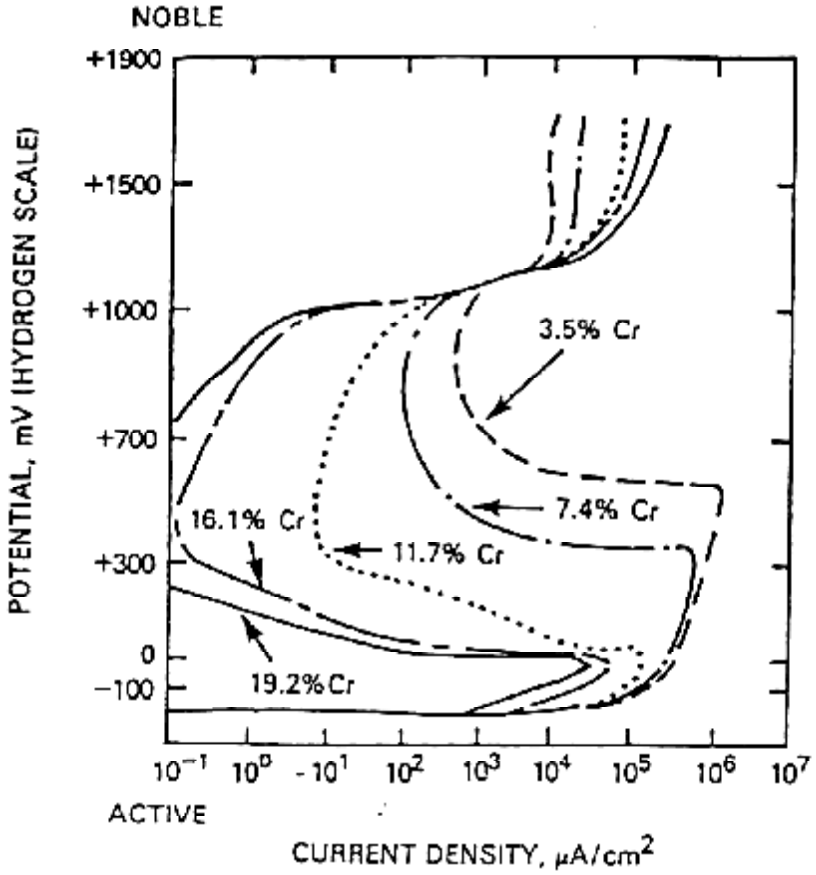

Figure 2. 5: Effect of chromium content of FeNiCr alloys on their anodic polarisation behaviour in 2N H_2SO_4 at 90˚C. The nickel content was in the range of 8.3% to 9.8% [Sedriks, 1986]

The presence of chromium also improves the pitting resistance of stainless steel in sulphuric acid by hindering the effects of sulphide ions [Hajjaji *et al.*, 1995]: sulphide ions exist in steel mailnly as manganese sulphides but they can also contain iron and chromium. Sulphides (manganese sulphides especially), as mentioned in section 2.2.2, are detrimental to the pitting corrosion resistance of stainless steels. Increasing the chromium content in the steel, however, increases the amount of chromium present in the sulphides, thus decreasing the amount of manganese in the sulphides.

Chromium-rich sulphides are more resistant to pit nucleation than manganese-rich sulphides [Hajjaji *et al.*, 1995].

Chromium also improves pitting resistance by increasing the pitting potential of stainless steels to noble directions as illustrated in Figure 2.6.

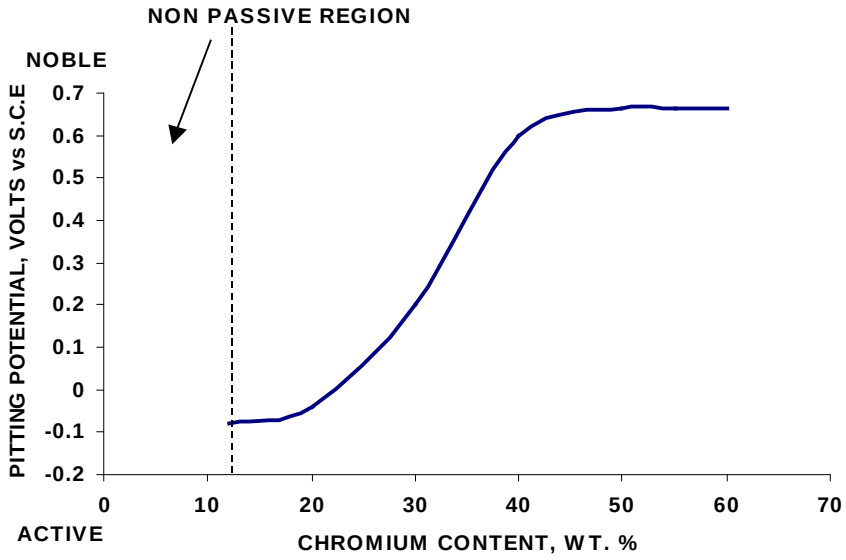

Figure 2. 6: Effect of chromium content on pitting potential of Fe-Cr alloys in a deaerated 0.1 N NaCl solution at 25°C [after Sedriks, 1979].

Chromium is essential in controlling the corrosion of stainless steels, but it can be detrimental when it forms chromium carbides at critical sensitisation temperatures. Chromium carbides are target sites for the initiation of pits [Sedriks, 1986; McEwan, 1994]. Chromium increases the solubility of carbon in austenite hence increasing the chances of sensitisation and decreasing the corrosion resistance of the steel [Sedriks, 1979]. Chromium can also have a negative effect on the properties of austenitic stainless steels since it is a ferrite former, but this effect can be counteracted by the addition of nickel which slows down the kinetics of the austenite-to-ferrite

transformation and makes it possible for an austenitic microstructure to exist at room temperature [Levey, 1995; Turan, 1991].

2.3.2 Effect of nickel

It has been found that increasing the nickel content at specific chromium contents of Cr-Mn-Ni alloys in boiling 65% nitric acid decreases the corrosion rate of the steel as illustrated in Figure 2.7 [Gross, 1980].

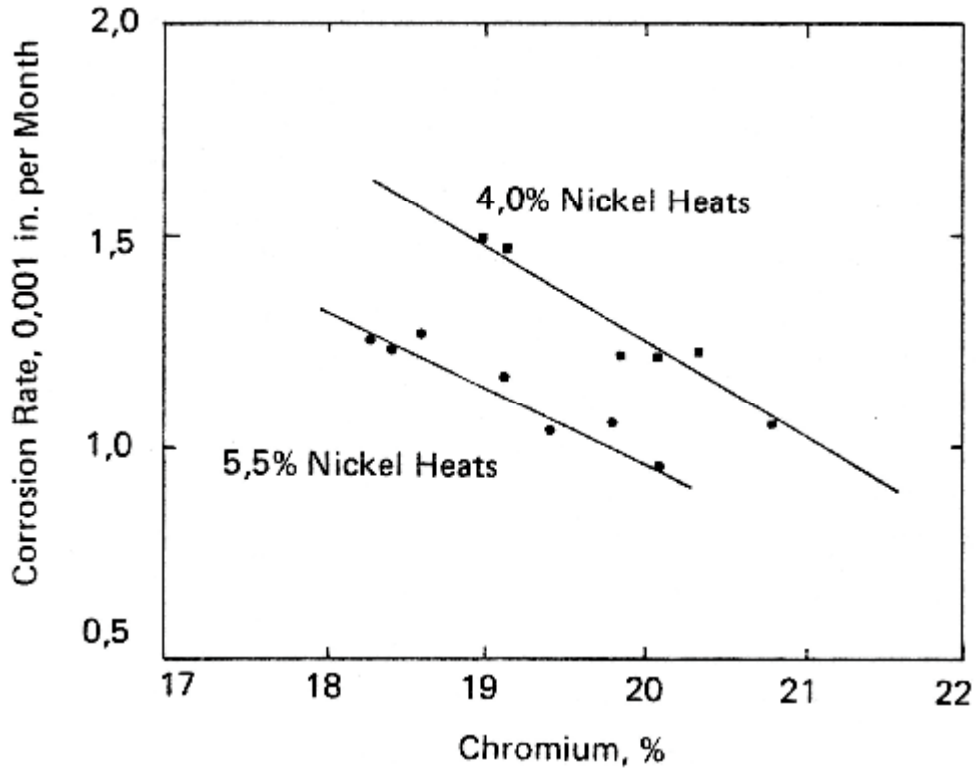

Figure 2. 7: Effect of increasing nickel on two heats of Cr-Ni-Mn steel in 65% nitric acid [Gross, 1980]

Researchers have also found that an increase in the nickel content to levels higher than 8%, increases the corrosion resistance of the stainless steel to weak oxidizing acids and chloride solutions by shifting the pitting potential of the metal to more

noble directions, thus expanding the passive region of the stainless steel and improving the corrosion resistance of the metal [Peckner and Bernstein, 1977; Pickering, 1979; Sedriks, 1986]. This effect is illustrated in Figure 2.8 [Sedriks, 1979].

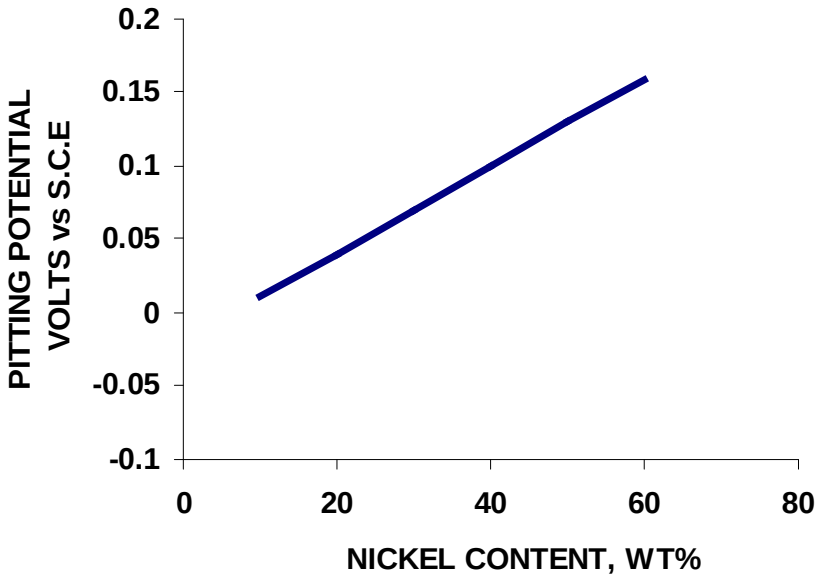

Figure 2. 8: Effect of nickel on pitting potential of Fe-15%Cr alloys in a deaerated 0.1 N NaCl solution at 25°C [after Sedriks, 1979].

An indirect way in which nickel improves corrosion resistance (if added in sufficient amounts) is by preventing the formation of delta-ferrite which, as discussed earlier, can lead to a reduction in the corrosion resistance of the austenitic stainless steels [Lula, 1986; Sedriks, 1979]. The Fe-Cr-Mn system without Ni does not produce fully austenitic stainless steels at low carbon contents and this could reduce their corrosion resistance [Banerjee *et al.*, 1990]. Nickel also improves the corrosion resistance by reducing the solubility of carbon in austenite, hence reducing the chances of sensitisation and intergranular corrosion [Sedriks, 1979].

Nickel can be detrimental to stainless steels in that it decreases the solubility of nitrogen, thereby limiting the nitrogen that could improve corrosion resistance and strength of the metal [Turan, 1991].

2.3.3 Effect of manganese

Manganese is an austenite former that can be used to replace nickel since it has the ability to extend the austenite loop and stabilize it at room temperature [Cortie, 1995; Lula, 1986; Peckner and Bernstein, 1977; Wellbeloved 1990]. Manganese also has the advantage of being less expensive than nickel. As a rule of thumb, when replacing nickel with manganese in austenitic stainless steels, the ratio of Mn:Ni is 2:1 [Lula, 1986]; because manganese is a weaker austenite former than nickel and has to be added in larger amounts to produce a fully austenitic microstructure [Gross and Robinson, 1981].

Manganese aids nitrogen solubility and is almost always used in conjunction with this element. Manganese in general is deemed to have a negative effect on the corrosion resistance of stainless steel and has also been found to weaken the passive film, increase i_{pass} and thus decrease the protectiveness of the film [Gross and Robinson, 1981]. Figure 2.9 shows the negative effect of manganese on the corrosion resistance of 17.5% Cr, 4% Ni steels in 65% nitric acid [Gross, 1980].

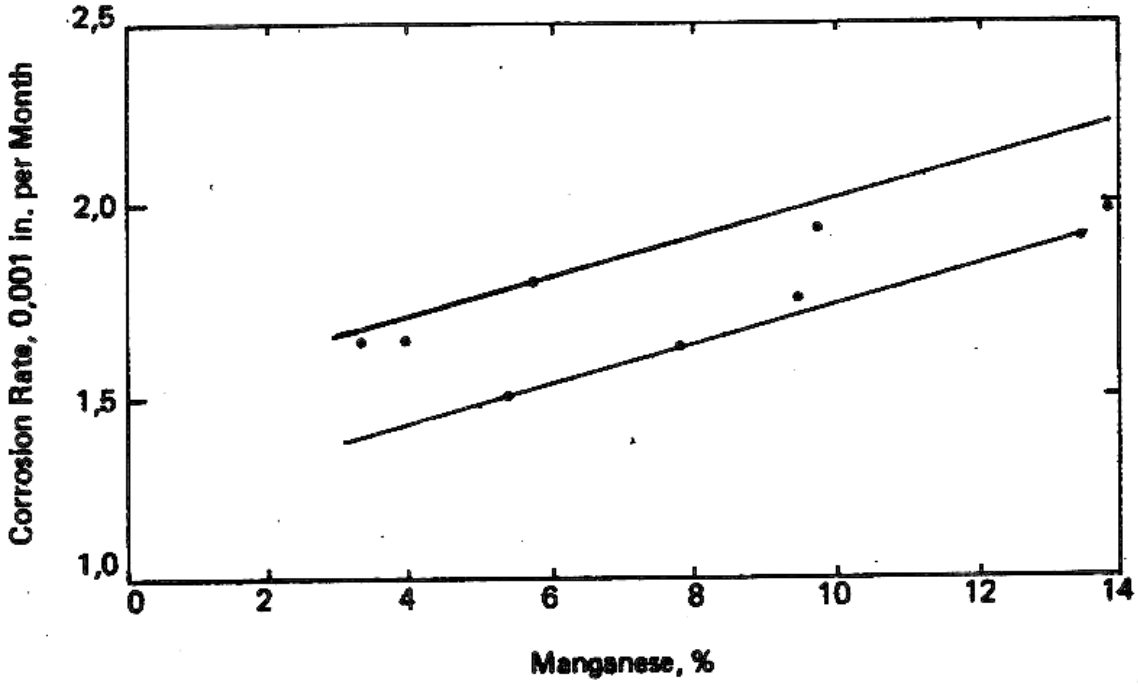

Figure 2. 9: Effect of manganese content on corrosion of 17.5% Cr, 4% Ni steels in 65% nitric acid [Gross, 1980].

Manganese is also detrimental to the pitting resistance of austenitic stainless steels because of the formation of manganese sulphide inclusions which are found in most commercial steels [Frankel, 1998]. These inclusions (as discussed earlier) are favourable sites for pit initiation in stainless steels. Maintaining low manganese levels (of about 0.2% for example) causes the formation of chromium sulphides as opposed to manganese sulphides, thus making it more difficult for pits to form [Sedriks, 1986].

2.3.4 Effect of molybdenum

Molybdenum has an overall beneficial effect on the general corrosion resistance of stainless steels as illustrated in Figure 2.10, where the polarisation curves show that molybdenum decreases both the critical and passivation current densities, making it easier for the metal to passivate.

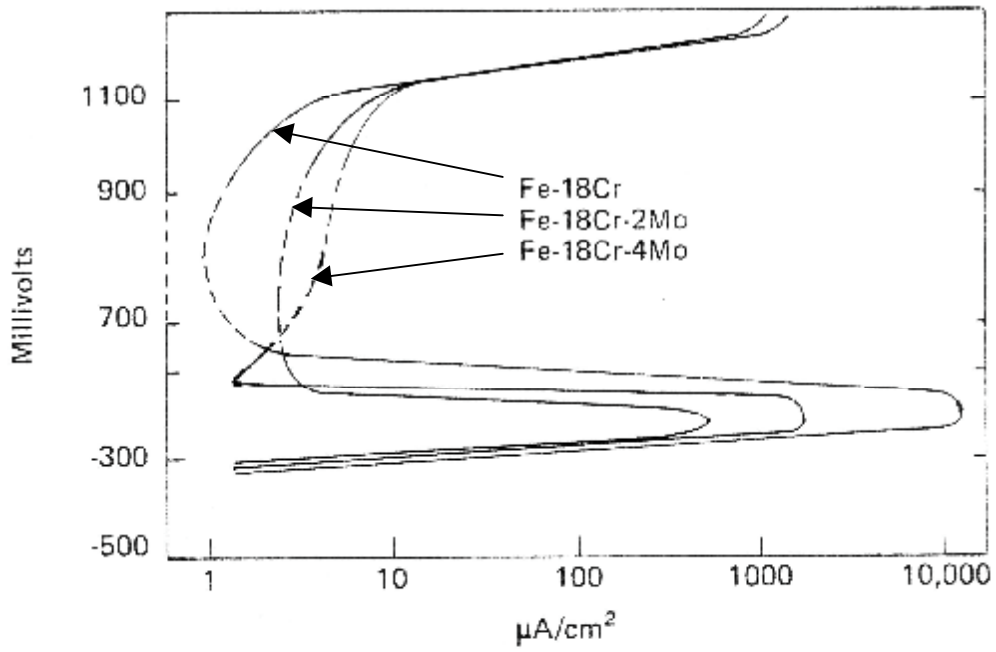

Figure 2. 10: Effect of molybdenum content on the anodic polarisation curves of an Fe-18% Cr alloy in 1N H_2SO_4 [Gross 1980].

Although not clear in this figure, molybdenum has also been found to affect the passivity of stainless steels by moving the pitting potential (E_p) in the noble direction, hence expanding the passive region and improving corrosion resistance. This is illustrated in Figure 2.11 [Sedriks, 1979 and 1986].

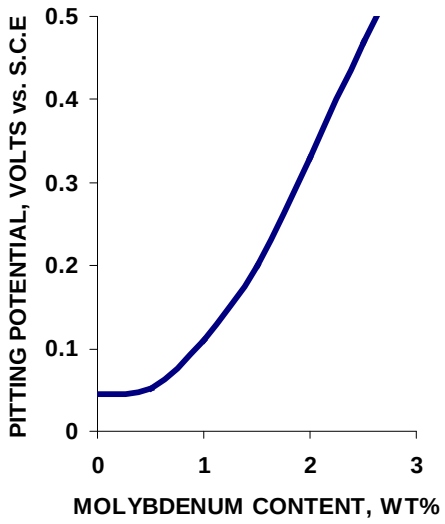

Figure 2. 11: Effect of molybdenum on pitting potential of Fe-15% Cr-13% Ni alloys in deaerated 0.1N NaCl solution at 25°C [after Sedriks; 1986].

According to Sedriks [1986], the exact mechanism by which molybdenum influences passivity is not really understood, but it seems to hinder the breakdown of passivity by pitting, as well as the growth kinetics of pitting. Some researchers suggest that molybdenum improves the pitting resistance of stainless steels in chloride environments by forming Mo^{6+} oxide in the passive film, which blocks the penetration of Cl^- [Lu *et al.*, 1993] or that it combines with cations in the pits to form molybdenum oxyhydroxide or molybdate (MoO_4^{2-}) at the active surface sites, thus blocking the active sites during dissolution [Frankel, 1998; Ilevbare and Burstein, 2001]. Molybdate is insoluble and reduces the amount of free metal ions in the pit solution, thus decreasing the diffusion of chloride ions into the pit and also decreasing the diffusion of metal cations out of the pit. This reduction in diffusion reduces the rate of dissolution significantly, resulting in the decrease of the size of the pits [Ilevbare and Burstein, 2001; Sumita *et al.*, 2004]. The reduction in free metal ions in the pit by molybdate also reduces the chances of forming stable pits because the critical concentration of metal ions needed for the transition of metastable pits into stable pits cannot be built up [Ilevbare and Burstein, 2001].

It has also been suggested that molybdenum improves passivity by promoting the formation of Cr-O-OH (which has better protective properties that chromium oxide) and hence improve the corrosion resistance of the steel [Lu *et al.,* 1993].

In context of this project molybdenum has the disadvantage that it is a strong ferrite former that needs to be balanced out with nickel and nitrogen and it is relatively expensive [Schollenberger, 1995].

2.3.5 Effect of nitrogen

Since the nitrogen content of the atmosphere is 79%, N is present in all steel alloys, as a result of atmospheric pick-up during manufacturing [Levey, 1995]. Stainless steels, however, have a deliberately higher nitrogen content. Nitrogen is useful to stainless steels not only because it is a strong austenite former and stabilizer, as is evident from its high coefficient in equation 2.2, but also because it strengthens the steel by means of solid solution strengthening. This occurs through nitrogen decreasing the stacking fault energy and hence increasing the work hardening rate, without unfavourably affecting the ductility and fracture toughness of the metal [Iorio *et al.*, 1994; Levey, 1995; Turan, 1991; Vismer 1997].

The beneficial effect of nitrogen on the corrosion resistance of austenitic stainless steels has been attributed to it homogenising the microstructure by eliminating delta-ferrite and stabilising the austeniteic microstructure [Jargelius-Pattersson, 1999].

It is important to consider nitrogen solubility when using it as an alloying element so that unwanted ingot effects, such as porosity, and difficulties during hot working of the metal can be avoided. Alloys made with nitrogen additions tend to form porosity due to nitrogen coming out of solution during solidification [Iorio *et al.*, 1994]. If the solubility limit of nitrogen in the microstructure is exceeded then chromium nitride

precipitates will form in the matrix and these are detrimental to the corrosion properties of the material because they form chromium-depleted zones in the matrix which are susceptible to pitting attack [Levey, 1995]. To ensure the solid solubility of nitrogen in chromium-containing austenite, nitrogen levels of 0.3% or above require relatively high levels of manganese (e.g. 4%) [Sedriks, 1986]. This is because manganese aids the solubility of nitrogen and a lower amount of manganese would not be sufficient in providing good nitrogen solubility. In conventional austenitic stainless steels, the solubility of nitrogen is about 0.2 wt% [Jargelius– Pattersson, 1994].

Factors that influence nitrogen solubility in iron alloys are composition, crystal structure, temperature and the pressure of gaseous nitrogen in the atmosphere above the alloy [Iorio *et al.*, 1994]. Elements such as nickel, carbon, silicon and copper decrease nitrogen solubility while chromium, manganese and molybdenum increase it [Iorio *et al.*, 1994; Levey, 1995; Vismer, 1997].

There is much debate as to the effect of nitrogen on the general corrosion resistance of stainless steels in acids [Levey, 1995]. Nitrogen has been found to have an adverse effect on the corrosion resistance of stainless steels in different acid mediums [Levey, 1995] but it has also been found to improve the corrosion resistance of molybdenum-free austenitic stainless steel. The addition of nitrogen to the molybdenum free-steels, has been found to be beneficial to the development of passivity in sulphuric acid as is illustrated in Figure 2.12 [Gross 1980], since an increase of nitrogen in austenitic stainless steels decreased i_{pass} and i_{crit}, making passivation easier.

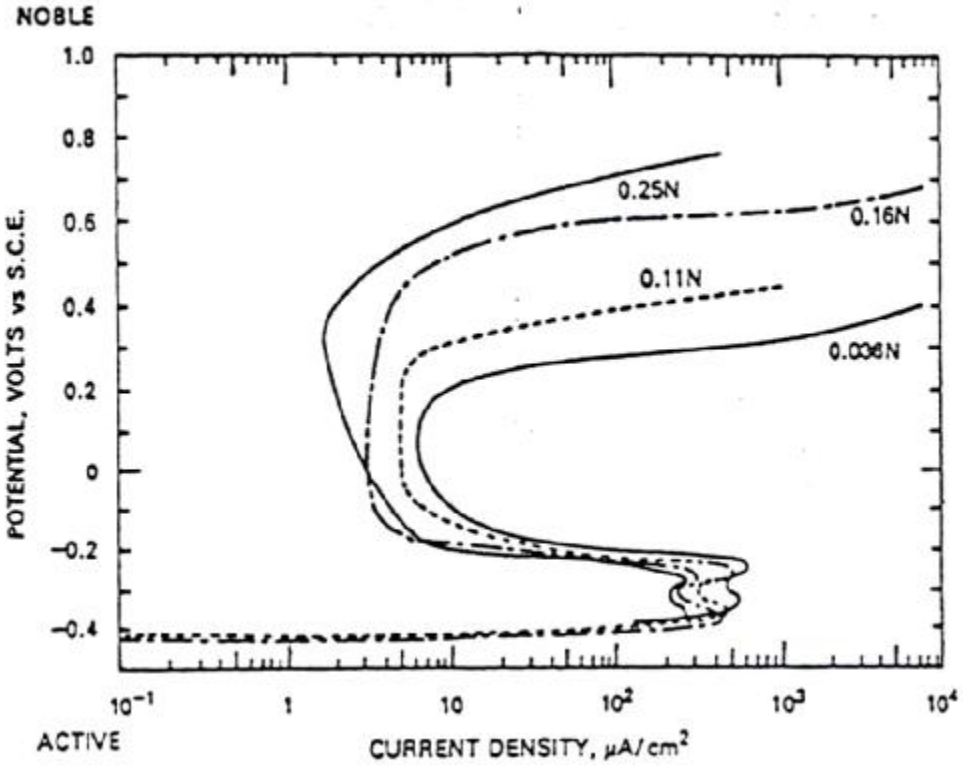

Figure 2. 12: Anodic polarisation curves for 18% Cr-8% Ni SSs containing various amounts of nitrogen, tested in a hydrogen-purged 1N H2SO4 + 0.5 M NaCl solution at ambient temperature [Gross 1980].

There seems, however, to be an agreement that nitrogen improves the general corrosion resistance of duplex and martensitic stainless steels more significantly than of the austenitic stainless steels. Nitrogen additions to austenitic stainless steels have a small to moderate effect on improving their general corrosion resistance. Ferritic stainless steels have a low solubility for nitrogen, so the addition of nitrogen is detrimental to the corrosion resistance of these steels.

When considering pitting corrosion however, small additions of nitrogen improve the pitting resistance of austenitic stainless steels, provided the solubility limit is not exceeded [Brigham and Tozer, 1974; Frankel, 1998; Levey, 1995,; Rondelli *et al.*, 1995; Sedriks 1983] as shown in Figure 2.13:

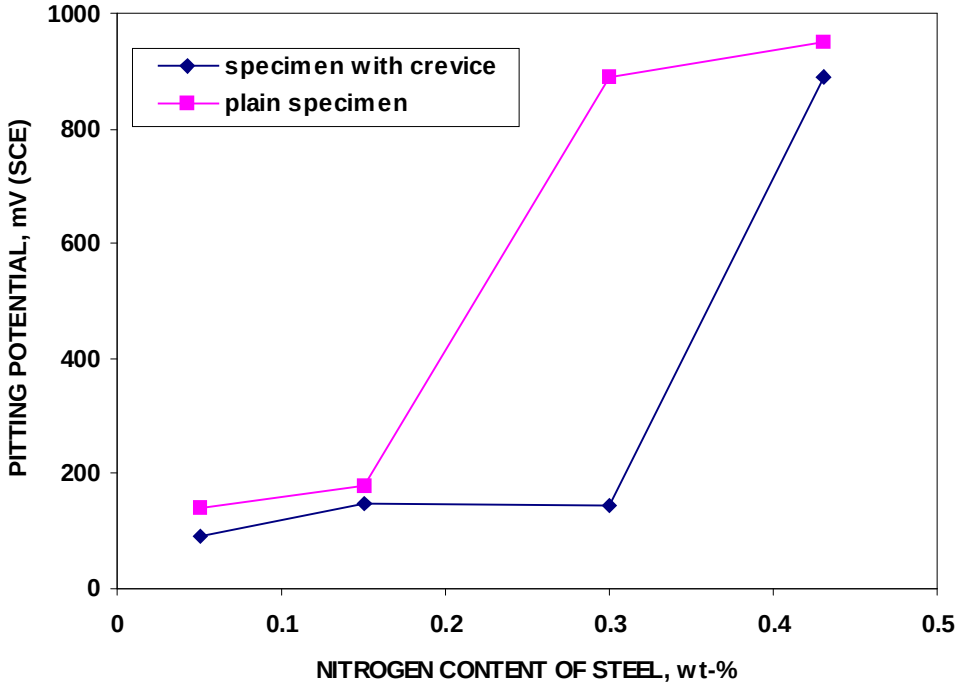

Figure 2. 13: Effect of Nitrogen content on pitting potential of 22Cr-20Ni-4Mn-2.8Mo-0.03C-0.01S stainless steel in aerated aqueous solution containing 0.6 M NaCl and 0.1 M NaHCO3 [after Sedriks 1983].

The beneficial effect of nitrogen in improving pitting resistance can also be seen by its high coefficient in the PRE equation (equation 2.7).

There are many opinions offered to explain how nitrogen improves the localised corrosion of stainless steels. One suggestion is that nitrogen in solid solution dissolves to form ammonium ions (NH_4^+) according to equation 2.8 [Baba *et al.*, 2002; Jargelius-Patterson, 1999]:

$$N + 4H^+ + 3e^- \rightarrow NH_4^+ \qquad \textbf{Equation 2. 8}$$

These ammonium ions consume protons during pit initiation, thus increasing the pH and helping to passivate the pit before it can become a stable growing pit [Jargelius-Patterson, 1999; Levey 1995]. These ammonium ions could further hydrolyse to form species such as NO_2^- or NO_3^- which are inhibitors of corrosion. Inhibitors can stifle the action of the chloride ion as a pitting agent [Shams *et al.*, 1999]. Ammonium ions could also combine with active oxidants such as free chlorine and bromine to form chloramines or bromo-amines which are less active products and therefore are less aggressive to the metal [Jargelius-Patterson, 1999].

Investigators have also suggested that nitrogen concentrates at the passive film/metal interface to stabilise the film and prevent attack of anions such as chlorides. This nitrogen is suggested to aid the repassivation of the film and increase the pitting corrosion resistance of the film [Baba *et al.*, 2002].

Nitrogen further improves pitting resistance of stainless steels by expanding the passive region of the metal through the shifting of the pitting potential (E_p) in a nobler direction [Sedriks, 1986]. This effect is more beneficial in stainless steels containing molybdenum because the E_p is shifted even further in the noble direction when molybdenum is present, thus providing maximum expansion of the passive region of the metal [Sedriks, 1986].

The synergistic effect of nitrogen and molybdenum in improving pitting and general corrosion resistance of stainless steel is a significant factor to consider. For example, once the molybdenum has shifted the pitting potential to higher values than normal and if sufficiently high potentials are reached, nitrogen can then accumulate at active dissolution sites, blocking them from the harsh environment [Jargelius-Patterson, 1999]. It has also been suggested that molybdenum and nitrogen interact to form a protective layer on the surface of the steel. Nitrogen is thought to promote the formation of molybdenum nitrides which inhibit the dissolution of molybdenum in the transpassive region, retaining the molybdenum in the passive film [Jargelius-

Patterson, 1999]. Nitrogen may also form ammonia ligands which raise the local pH, thus promoting the formation of molybdate, which assists in the formation of ammonium, further improving the passivity of the stainless steel [Jargelius-Patterson, 1999].

Improvement in grain boundary corrosion resistance has also been attributed to nitrogen additions, because when sensitisation temperatures are reached, the nitrogen can diffuse faster than the carbon to the grain boundaries so that chromium nitride (Cr_2N), rather than chromium carbide ($Cr_{23}C_6$), precipitates are formed [Turan, 1991]. Although the area around the grain boundaries is depleted of chromium, the depletion is not as severe as when chromium carbide precipitates are formed.

In conclusion, alloying elements have important effects on the corrosion behaviour of stainless steels: Figure 2.14 is an overall summary of their effects [Sedriks, 1986]

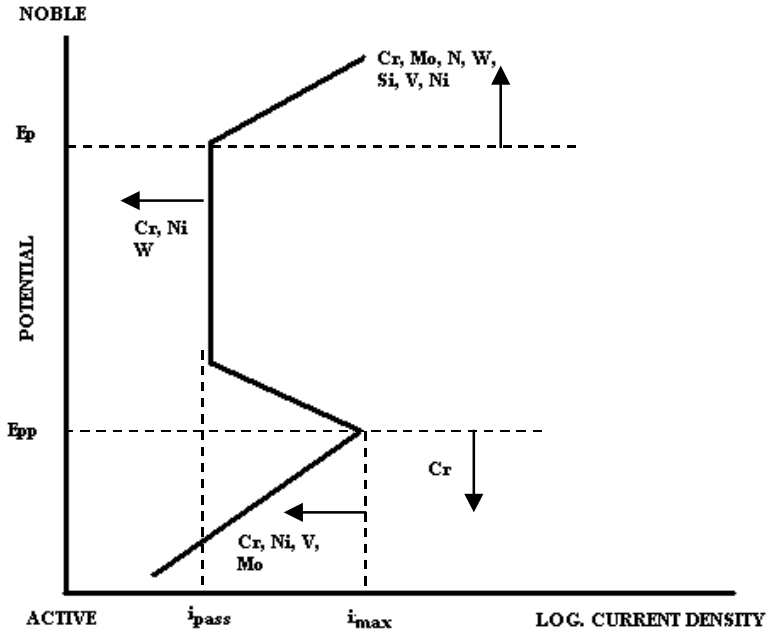

Figure 2. 14: Schematic summary of the effect of alloying elements in stainless steels on the anodic polarization curve [after Sedriks, 1986]

Chromium, molybdenum, nitrogen and nickel are beneficial to the corrosion resistance of stainless steels since they improve passivity by decreasing the critical current density and the passivation current. Manganese has been found to be detrimental to the corrosion resistance of stainless steels.

2.4 Effect of microstructure and processing on the corrosion behaviour of stainless steels

Microstructure is affected by alloying elements, which in turn affects the corrosion resistance of the stainless steels. Other factors that play a part in determining the microstructure are the processes and methods used to produce and treat the material. Castings have inhomogenous structures, rolling and extrusion methods can cause the material to have texture, while elongated grains, hot working and annealing can

produce anisotropy in the microstructure. All these factors will affect the corrosion behaviour of the material [Simpson, 1990]. Cold worked or plastically deformed parts of a metal are more susceptible to corrosion than if the metal was annealed [Callister, 1994]. This is because the worked part of a material stores a great deal of energy, making it more active or anodic compared to the rest of the material. Delta-ferrite and manganese sulphide inclusions, as already mentioned, decrease corrosion resistance. In fact, any irregularity or inclusion in the microstructure can provide a site for pit nucleation.

The pitting potential of stainless steels in chloride solutions has been found to depend highly on the degree of cold work and the orientation of the sample [Simpson, 1990]. It has been found that the pitting potential decreases with cold work and that it is higher in the longitudinal than transverse direction. It has also been concluded from experiments done on austenitic stainless steels in acid solutions that passivation in the longitudinal direction is ten times easier than that in the transverse direction at 30% cold work [Simpson, 1990].

From the literature survey it is evident that there are a number of factors that can simultaneously affect the corrosion resistance of stainless steel. Stainless steels can suffer both general and pitting corrosion depending on the nature of the steel and the environment. Researchers have found molybdenum and nitrogen to improve the general corrosion resistance of austenitic stainless steels, but not as effectively as they improve the pitting corrosion resistance. Manganese increases nitrogen solubilty of stainless steels but it forms manganese sulphides which are detrimental to the corrosion resistance of stainless steels. The correct balance of the alloys however can produce a steel that has good mechanical and corrosion resistance. Alloying elements can thus act individually or synergistically in determining the corrosion behaviour of stainless steels.

The alloys that were investigated in this project were all based on the Hercules™ alloy with variations in manganese, molybdenum and nitrogen. The aim was to find a combination of these alloys so that a more corrosion resistant version of the currently existing Hercules™ can be found. The original Hercules™ has no molybdenum additions and it is assumed that the addition of molybdenum could improve the corrosion resistance of this alloy. This is all discussed in the next chapters.

3. Production of the alloys

A matrix of eighteen alloys were designed to systematically analyse the effect of varying levels of Mn, N and Mo on the corrosion behaviour of the Hercules™ steel. Firstly, trial melts of 50g buttons were made to establish the alloying practice and allow for initial corrosion testing. This gave valuable information that enabled the successful production of 5kg ingots. The melting and production practice, targeted and actual chemical composition, as well as microstructures of these alloys are discussed in this chapter.

3.1 General

The alloys that were made for this investigation were targeted at a Hercules™ base composition of 0.04 wt% C, 16 wt% Cr, 2 wt% Ni, 0.5 wt% Si, and 0.01 wt% P. Mn, N and Mo were varied in two or three levels, as listed in table 3.1 to produce eighteen test alloys.

Table 3. 1: Target composition (wt%) matrix of alloys made

Alloy	Mn (±0.5)	N (±0.02)	Mo (±0.05)
Alloy 1	5.0	0.15	0.5
Alloy 2	5.0	0.15	1.0
Alloy 3	5.0	0.15	2.0
Alloy 4	5.0	0.30	0.5
Alloy 5	5.0	0.30	1.0
Alloy 6	5.0	0.30	2.0
Alloy 7	10.0	0.15	0.5
Alloy 8	10.0	0.15	1.0
Alloy 9	10.0	0.15	2.0
Alloy 10	10.0	0.30	0.5
Alloy 11	10.0	0.30	1.0
Alloy 12	10.0	0.30	2.0
Alloy 13	15.0	0.15	0.5
Alloy 14	15.0	0.15	1.0
Alloy 15	15.0	0.15	2.0
Alloy 16	15.0	0.30	0.5
Alloy 17	15.0	0.30	1.0
Alloy 18	15.0	0.30	2.0

Feed material used in the production of the eighteen alloys consisted of recarburiser, Cr(aluminothermic), remelt Fe, Mn (electrolytic), FeMo (0-50mm), nitrided Mn, Ni (cathodes) and Si (pure). The amount of feed material needed to make the required alloys was calculated using a programme called "Meltfeed" that has been developed by Mintek. This programme can calculate, in grams, the amount of feed material needed to produce an alloy of desired composition. The required weight percent of each element desired in the alloy and the type of feed material to be used are entered into the programme, which then calculates how much of each feed material needs to be weighed out to produce the desired product.

Inevitably, there are some losses during the making of alloys, especially with regard to C, Mn and N, and extra feed material is added to compensate for these losses. Knowledge of the amount of extra feed material to add is based on experience. According to K.P Mokaleng of Mintek, an extra 10% C and Mn and an extra 15% N is usually added to compensate for losses. The eighteen alloys were thus manufactured with the above mentioned extra feed material.

3.2 Melting procedure

When making alloys, inclusions and impurities are a major concern, since they can affect corrosion results. Great care was thus placed in melting the alloys. The 50g buttons and 5kg ingots were both melted in an argon atmosphere and the procedures followed to melt these alloys are discussed in this section.

3.2.1 The 50g buttons

The 50g buttons were made in a button arc furnace in an argon atmosphere. The furnace was first flushed with argon three times to remove oxygen before filling it with Ar. Pure Ti was melted in the button arc furnace prior to melting the feed material to ensure the removal of any residual oxygen. The heavier feed materials were melted first, while the lighter recarburiser and nitrided manganese were melted last. This was done to ensure that the light material did not blow away during melting. Once the feed material was melted into a button, the button was remelted two more times to ensure homogeneity. The button was then left to cool in the furnace.

The eighteen buttons were approximately 30 mm in diameter and were homogenised at 1200ºC for four hours and quenched. The buttons were then sand blasted to remove some of the oxide layer and, using a Feritscope ® MP30 ferritescope, the magnetic content of the buttons was measured. The buttons were manufactured with

the intent of them having an austenitic microstructure. Austenite is not magnetic, thus a ferritescope reading of 0 would be ideal. It was noted, however, in previous experiments [Kerr, 2003] that a ferritescope reading of less than 10 usually meant that the alloy was austenitic. The magnetic readings of all eighteen buttons were taken on a 40-grit ground surface. Figure 3.1 illustrates the results of the average of ten ferritescope readings taken per sample. All ferritescope readings can be found in Appendix A, table A1.

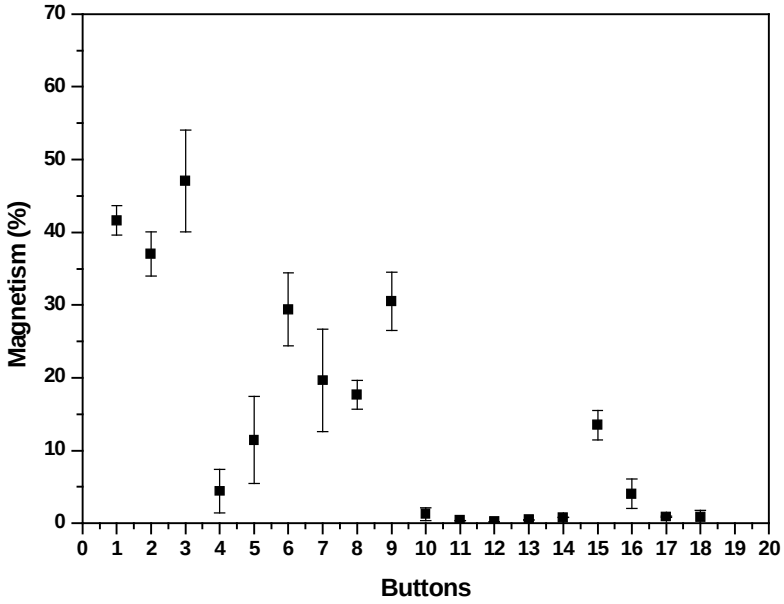

Figure 3. 1: Average ferritescope readings for the eighteen manufactured buttons.

In Figure 3.1 the error bars indicate standard deviation which was calculated from the mean, according to ASTM standard G65, pp 370-373. The results of the ferritescope readings, in Figure 3.1, show that buttons 1 to 3 and 5 to 9 had a high magnetic content (> 10%) (button 4 was an exception). The magnetic content of buttons 10 to 14 and 16 to 18 was much less than 10% (button 15 was an exception). The magnetic content of these buttons could be due to either ferrite or martensite as both these phases are magnetic. The buttons were quenched from the austenitic region, and this could have caused martensite to form in the microsturucture. This martensite could

be causing the high magnetism in buttons 1 to 9. It was thus decided to reheat buttons 1 to 9 at 1050°C and air cool these alloys, to try and eliminate any martensite that could have formed during quenching. After normalising the magnetic content of buttons 1 to 9 was again measured and Figure 3.2 illustrates the results obtained.

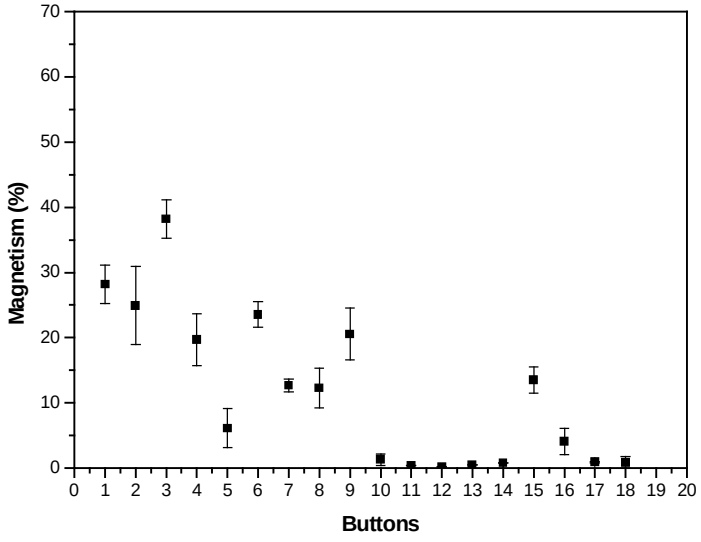

Figure 3. 2: Average ferritescope readings taken for the nine buttons after reheating at 1050°C and air cooling.

Figure 3.2 has been drawn using the same scale as Figure 3.1 for ease of comparison. The magnetic contents of buttons 1 to 9 decreased somewhat, with the annealing treatment. Button 4, however, had an increased magnetic content. This could possibly be due ferrite formed during air cooling. With quenching, no austenite to ferrite transformation occurs because of the rapid cooling rate, but the reheating to temperatures in the austenitic region and air cooling would cause ferrite formation if the austenite was not sufficiently stabilised to room temperature. Therefore, air cooling might have eliminated martensite from buttons 1 to 9, but probably assisted in forming ferrite.

3.2.2 The 5kg ingots

The 5kg ingots were manufactured in a vacuum furnace in an argon atmosphere using the same feed material as the 50g buttons. The vacuum furnace was flushed five times before filling with argon. The recarburiser, nitrided manganese and silicon were melted last for the same reason given in section 3.2.1. The molten material was then cast into a mould and cooled for about 45 minutes. After casting the ingots were sectioned to remove the shrinkage pipe and this was used for spectrometry and ferritescope readings. Results of ferritescope readings for the ingots are given in Figure 3.3 and those of the chemical analysis are discussed in section 3.2.3, in conjunction with those obtained for the 50g buttons.

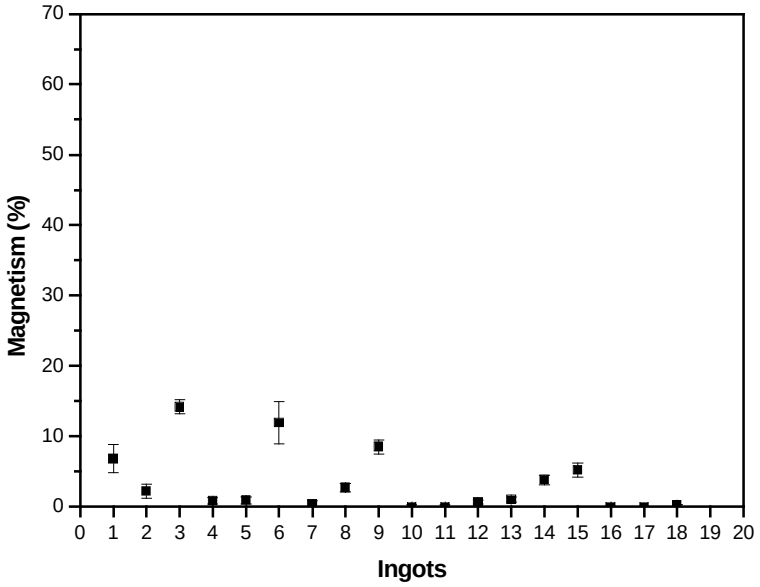

Figure 3. 3: Average ferritescope readings taken for the eighteen manufactured ingots.

Most of the 5kg ingots had a magnetic content of less than 10% with the exception of ingot 3 and 6. This was a much better result than that obtained for the 50g buttons since a lower magnetic reading indicates a lower ferrite/martensite content. The aim

was to produce austenitic stainless steel material (with no or very minimum ferrite/martensite for testing).

3.2.3 Results of chemical analysis for the buttons and ingots

Chemical analysis of all alloys was done on a 1200-grit surface finish. The bulk chemical composition of the alloys was determined using spark emission spectrometry. In order to obtain the nitrogen content of the alloys, drillings were taken from each sample and burned via a plasma combustion method. The chemical analysis for the key alloying elements, Mn, N and Mo, are shown in figures 3.4 to 3.6, and the rest of the composition analysis results along with tables (Tables A2 and A3) of the composition can be found in Appendix A. In the following figures alloys 1 to 6 are the 5 wt% Mn, alloys 7 to 12 have 10 wt% Mn and alloys 13 to 18 have 15 wt% Mn. Results for reference alloys AISI 304, 201 and Hecules™ are typical composition values from literature as referenced in Appendix A.

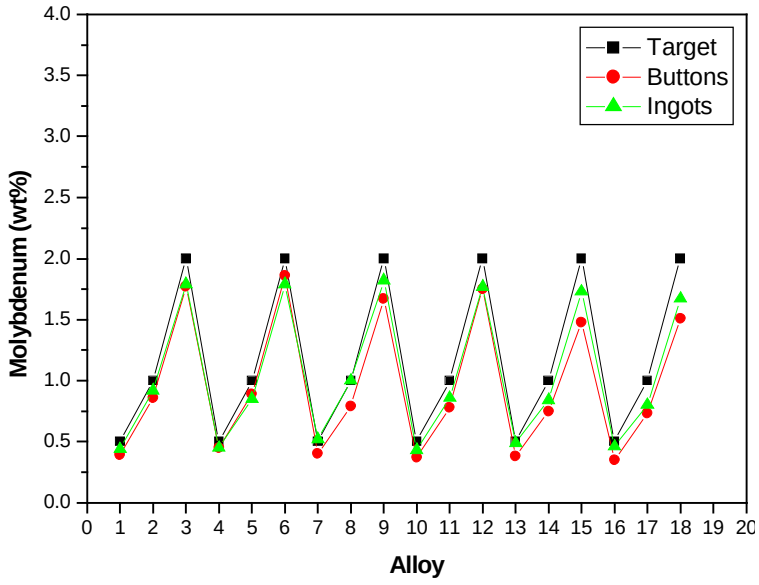

Figure 3. 4: Molybdenum content of buttons and ingots made.

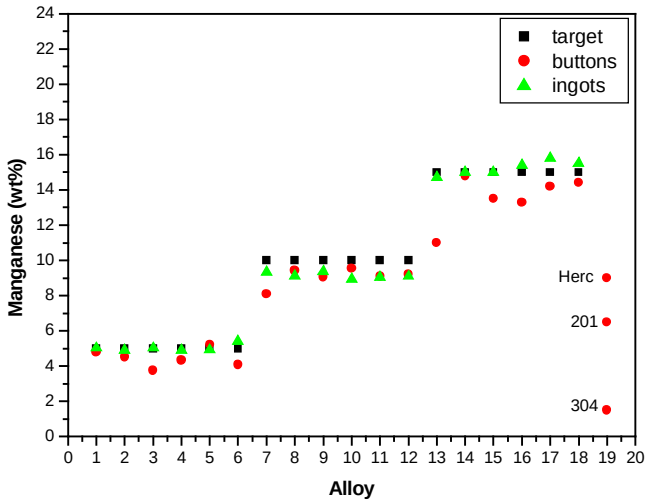

Figure 3. 5: Manganese content of buttons and ingots made.

The actual Mo and Mn contents of the alloys (figures 3.4 and 3.5) were generally close to target and in the instances where they deviated from target the difference was small. No reference values are shown in Figure 3.5 since reference alloys typically have no molybdenum content. One significant deviation to note though was the Mn content of alloy 13 for the 50g buttons, which was much lower than expected. The C, Ni and Cr contents in Appendix A (Figures A1 to A3) were also within the target range. The N content of the alloys, however, deviated significantly from target, as illustrated in Figure 3.6.

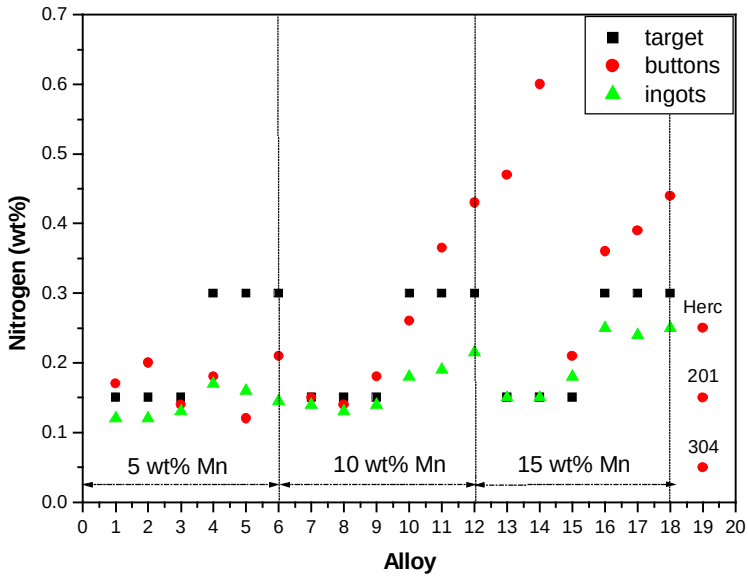

Figure 3. 6: Nitrogen content of buttons and ingots made.

Referring to the actual nitrogen content of the 50g buttons in Figure 3.6, the N content seems to increase above target from button 11 to 18. These buttons all have Mn contents of 10 wt% and more. An increase in Mn content increases the N solubility in stainless steel and this could be the reason for the high N contents of buttons 11 to 18. It was not possible though to get high N contents of 0.3 wt% for the 5 wt% Mn buttons 1 to 6. It was also not possible to attain high N contents for the 5kg ingots. The N content for the ingots was either on or below target, never above.

Figure 3.7 is a diagram showing the solubility of N as a function of both Mn and Cr content at 1600°C and 0.80 atm N_2 partial pressure [Kerr, 2003]. This diagram shows the maximum solubility of N for a given Mn/Cr combination, and can be used to explain why in some instances the N level was above or below target.

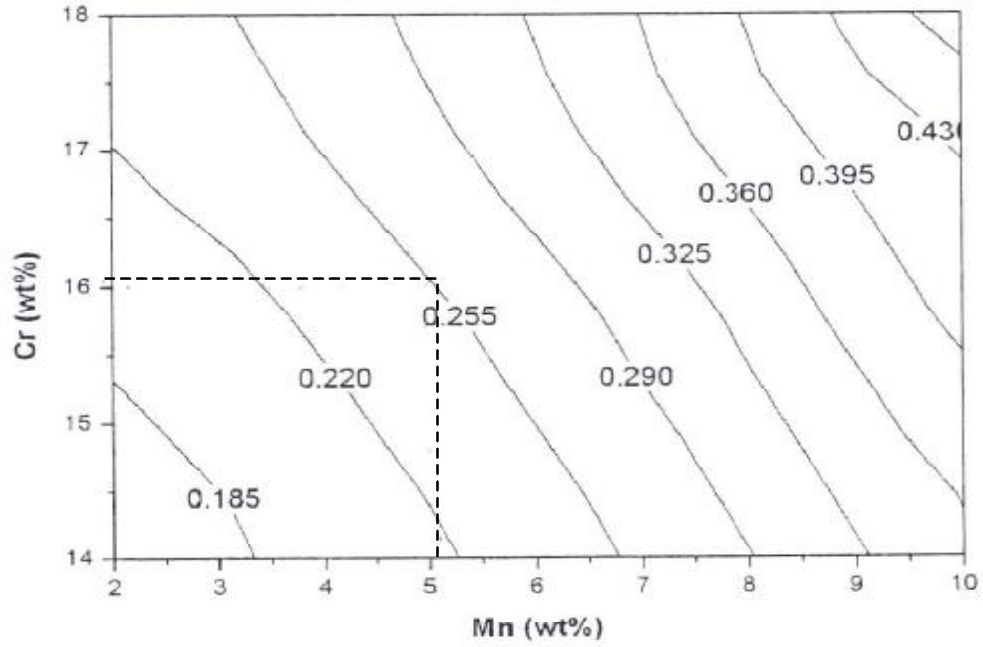

Figure 3. 7: Solubility of nitrogen (wt%) in the liquid phase at 1600ºC and 0.80 atm N_2 partial pressure [Kerr, 2003]

Figure 3.7 shows that, at 1600ºC and 0.80 atm N partial pressure (atmosphere saturated with nitrogen) a 5 wt% Mn alloy will dissolve a maximum of only 0.255 wt% N in the liquid phase. Since the buttons and ingots were made in an Ar atmosphere where there was minimal (if any) N, then it could be expected that the N solubility at 5 wt% Mn would be lower. This observation is supported in Figure 3.6, where none of the 5 wt% Mn buttons or ingots could attain a N content of 0.3 wt%.

At 10 and 15 wt% Mn, it should be possible to attain 0.3 wt% N, according to Figure 3.7, but this was not the case for the buttons and ingots. Some of the 50g buttons (alloys 11 and 12) at 10 wt% Mn and all the buttons at 15 wt% Mn (alloys 13 to 18) had a much higher N content than desired. It was not possible to get this high level of N for the ingots. The deviation from target for the ingots was however not as erratic as that for the buttons, and both the buttons and ingots were rolled, as discussed in the following section.

3.2.4 Rolling and heat treatment

3.2.4.1 The 50g buttons

The 50g buttons were rolled to a thickness of approximately 4.5 mm (± 55% reduction). Buttons 1 to 9 (which had the highest magnetic content) were difficult to roll because they work hardened easily and cracked after a few passes while buttons 10 to 18 rolled easier and showed only slight cracking. The rolling history of all the alloys is shown in Table B1 of Appendix B. The ferritescope readings (magnetism (%) also shown in the table) of the buttons increased during rolling, suggesting that the alloys have metastable austenite which transforms to martensite upon cold rolling at temperatures below the $M_{(d30)}$[3] temperature. This is to be expected since it was found in literature that manganese steels have a high work hardening rate [Harvey, 1982; Levey 1985]. After rolling the alloys were annealed at 1100°C and air cooled to eliminate the effects of cold rolling.

3.2.4.2 The 5kg ingots

After chemical analysis, the 5kg ingots were soaked at 1200°C for four hours for homogenisation. Following that, the ingots were hot rolled according to the following rolling sequence:

37-35-33 mm **à** reheat for 5 min at 1050°C **à** 30-28-26 mm **à** reheat for 5 min at 1050°C **à** 23-21-19 mm **à** water quench.

After quenching the alloys were annealed at 1100°C for 2 hours and air cooled so that any segregation or tension that was built up during quenching could be eliminated.

[3] $M_{d(30)}$ =413 - 462(C+N) - 9.2Si -8.1Mn - 13.7Cr - 9.5Ni - 18.5Mo - 18.5Cu - 3Co [Angel, 1954; Paton *et al*, 2004]

3.3. Microstructures of the alloys

Microstructural analyses were done only on the 5kg ingots, as discussed below. The 50g buttons had been destroyed after drillings were taken for nitrogen analysis.

3.3.1 Predicting the microstructure

As discussed in Chapter 2, Schaeffler diagrams are commonly used to predict the microstructure of welds but they can be used to give a good indication of the expected microstructure of as cast stainless steels depending on composition. Using these diagrams, Mintek has developed a spreadsheet-based programme called "AlphaGamma" that is able to predict the microstructure of an alloy depending on its Ni and Cr equivalents. "AlphaGamma" uses emperical formulae to predict various properties of stainless steels such as microstructural phases, yield strength and tensile strength. Schaeffler diagrams, as shown in Figure 3.8, are divided into different regions (martensitic (M), austenitic (A), ferritic (F) or a combination of these) into which an alloy's microstructure would fall depending on its Ni and Cr equivalents. "AlphaGamma" is also able to predict the %ferrite, M_s and $M_{d(30)}$ temperatures of an alloy and a table of these parameters has been inserted on the Schaeffler diagram.

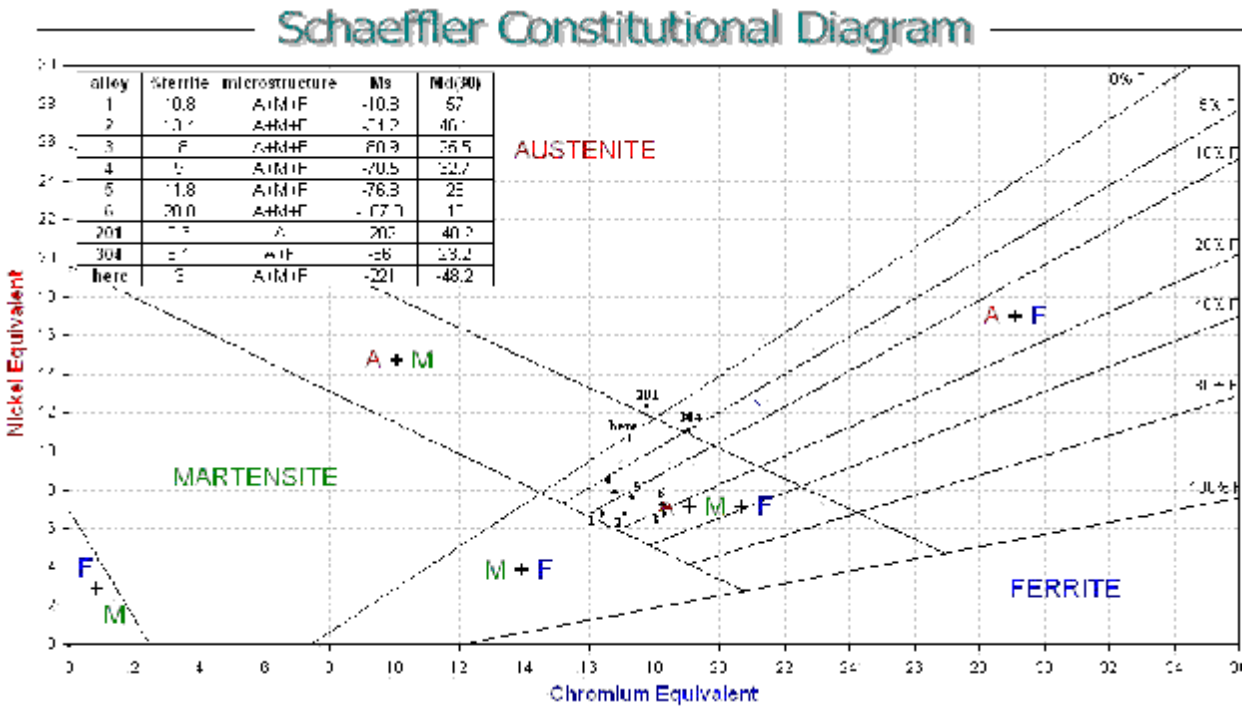

Figure 3. 8: Schaeffler diagram for the 5wt% Mn ingots, AISI 201, 304 and Hercules™ are also indicated here for reference.

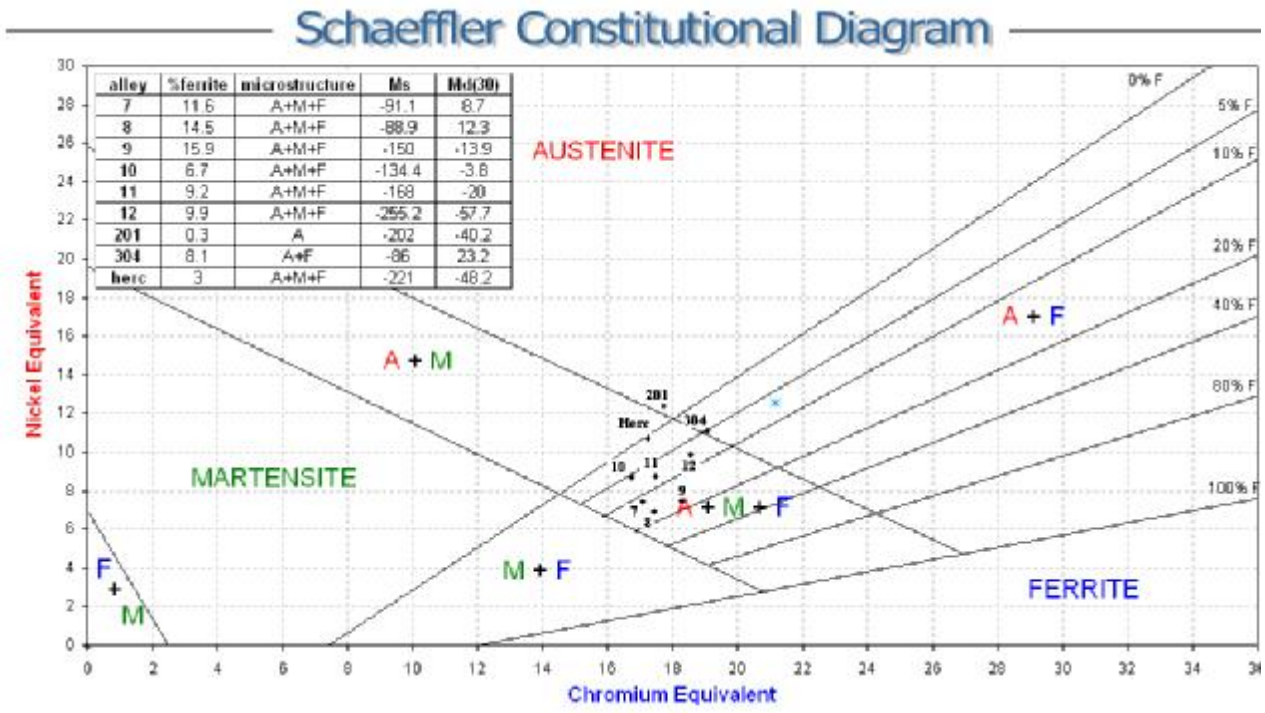

Figure 3. 9: Schaeffler diagram for the 10wt% Mn ingots, AISI 201, 304 and Hercules™ are also indicated here for reference.

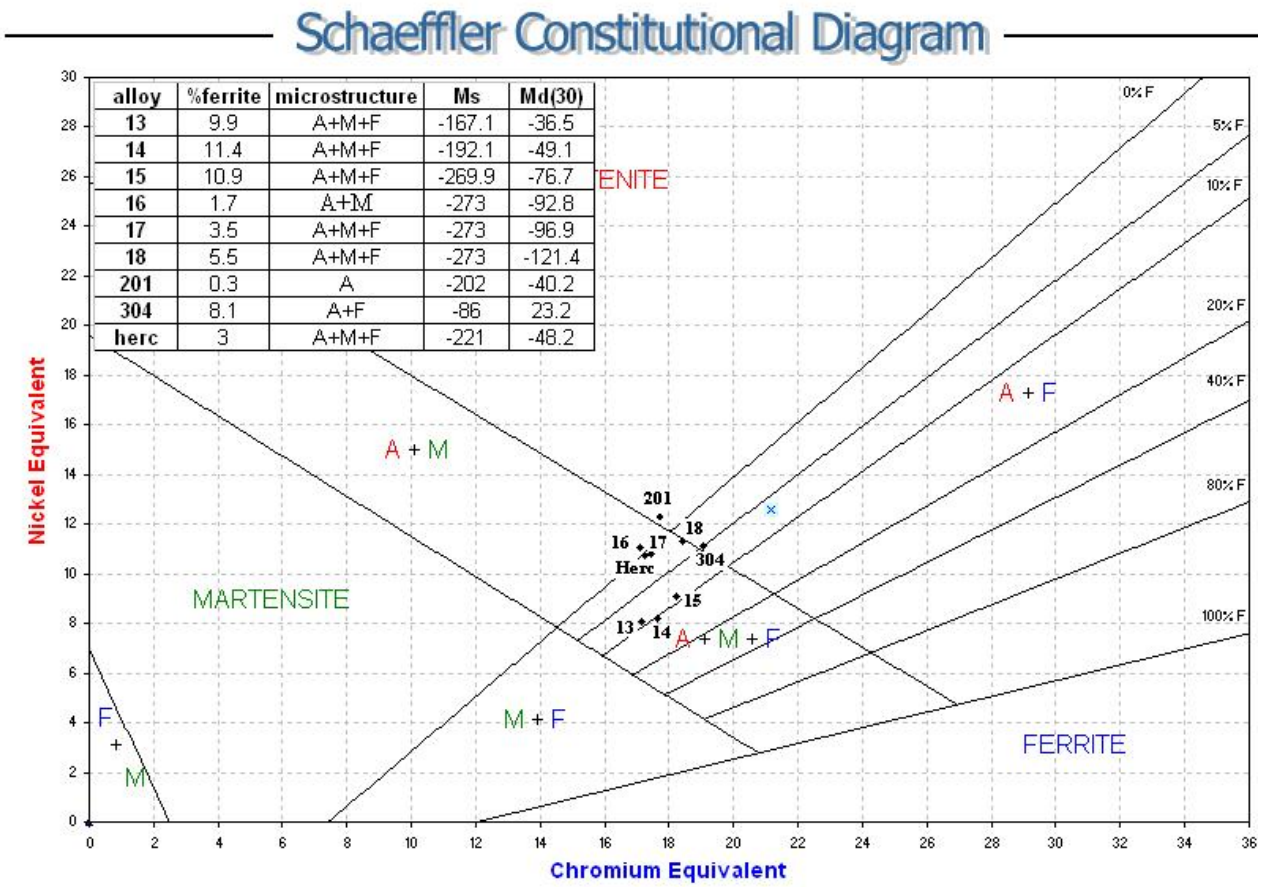

Figure 3. 10: Schaeffler diagram for the 15wt% Mn ingots, AISI 201, 304 and Hercules™ are also indicated here for reference.

Referring to Figures 3.8 to 3.10, all the ingots were predicted to have austenite, martensite and ferrite in their as cast microstructures, except for ingot 16 (Figure3.10), which was predicted to have only martensite and austenite. All the M_s temperatures for the as cast ingots were predicted to be below room temperature and the $M_{d(30)}$ temperatures varied depending on composition. The ingots' microstructures were however examined in the hot rolled annealed condition since this is the state in which they will be used and since schaeffler diagrams predict only as cast microstructures, Figures 3.8 to 3.10 will be used merely as a guide to detect any major anomalies in the final ingot microstructures.

3.4 Actual microstructure

3.4.1 Optical microscopy

From the 5kg ingots, material was cut transverse to the hot rolling direction, mounted and etched to reveal the microstructure. Two etchants were used: 10% oxalic acid and 75% potassium hydroxide (KOH). Both etchants were used to electro-etch the alloys according to the parameters listed in Table 3.2.

Table 3. 2: Etchants used for electro-etching

Etchant	**10% Oxalic acid**	**75% KOH**
Contents	10g oxalic acid, 100 ml water	45g KOH, 60 ml water
Structure it reveals	General structure. Attacks austenite particularly well but not delta-ferrite or martensite	Reveals delta-ferrite as dark brown and reveals austenite as a light phase. Can also reveal martensite
Example of structure revealed	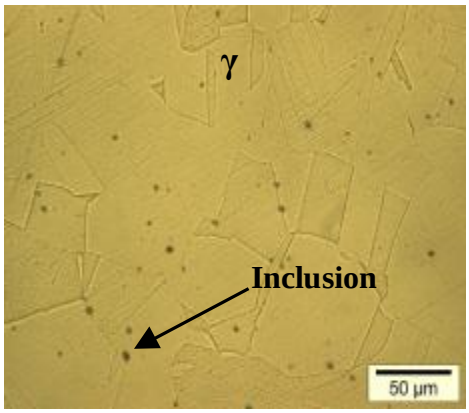	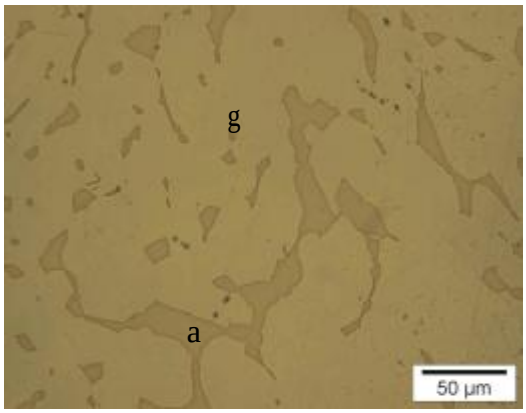
Voltage	2.5 V	6 V
Time	2-6 sec	90 sec

The full set of microstructures of the alloys are given in Appendix C. From the microstructural analysis it was found that all the ingots were mostly austenitic with some ferrite, except for alloy 1 which had some lathe martensite. Hot rolling and annealing would have altered the phase distributions as predicted by the schaeffler diagrams, but since no microstructural analysis was done on the as cast sample this could not be verified.

The ingots had varying ferrite contents (as measured on the hot rolled annealed ingots) which would have an effect on the corrosion properties of each ingot. Ferrite is detrimental to the corrosion resistance of stainless steels in that it decreases the corrosion resistance. The effect of chemical composition on ferrite content was thus investigated. Figures 3.11 to 3.13 illustrate the effect of nitrogen, molybdenum and manganese on the ferrite content of the alloys.

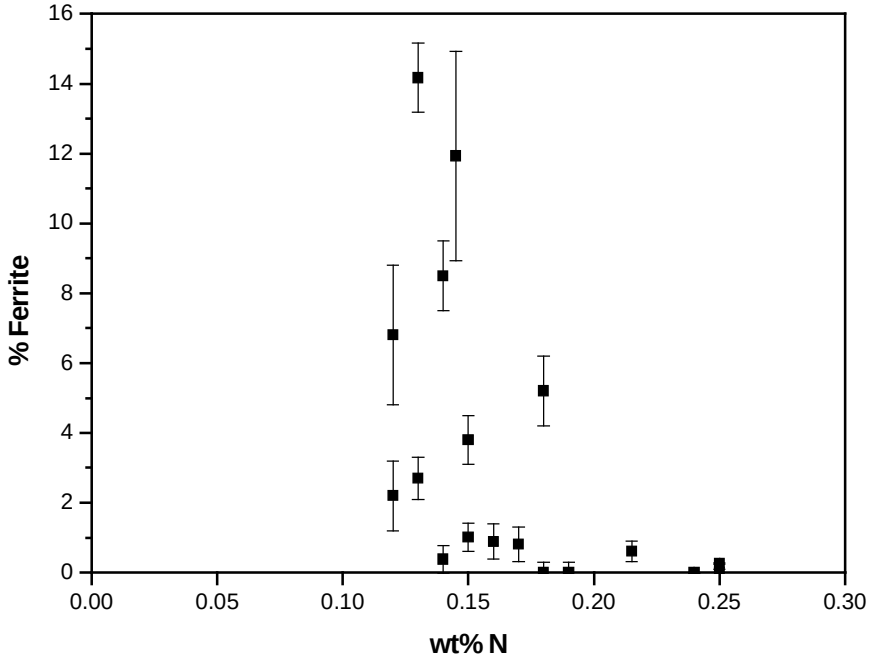

Figure 3. 11: Effect of nitrogen on ferrite content of 5kg ingots.

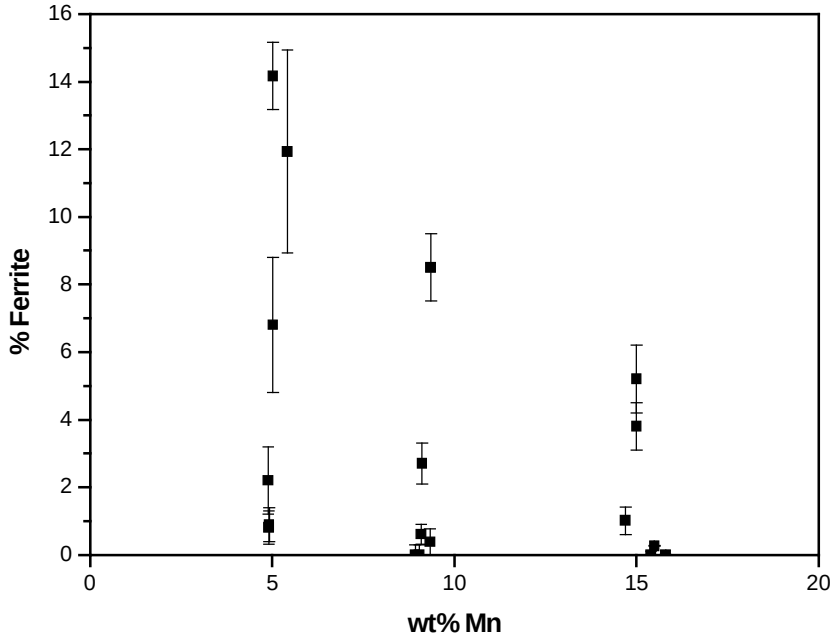

Figure 3. 12: Effect of manganese on ferrite content of 5kg ingots.

In Figures 3.11 and 3.12, there is roughly a general decrease in ferrite content as both N and Mn increase for the ingots. An increase in N should decrease the ferrite content of the ingots since N is an austenite former that hinders ferrite formation. Mn aids N solubility, thus an increase in Mn could increase the N content in the ingots, which in turn could be decreasing the ferrite content of the alloys. Mn is also an austenite former that could decrease the ferrite content of the ingots when added.

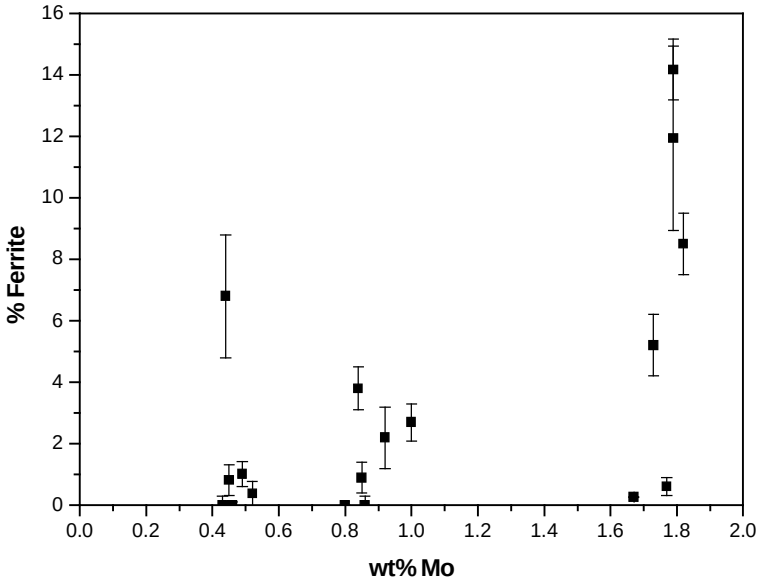

Figure 3. 13: Effect of molybdenum on ferrite content of 5kg ingots

An increase in Mo (Figure 3.13) seems to increase the ferrite content of the ingots, especially at contents greater than 1.6 wt% Mo. This is to be expected since Mo is a strong ferrite former and an increase in Mo would increase the amount of ferrite in the ingots.

3.4.2 Hardness tests

Hardness tests were done on the hot rolled annealed 5kg alloys using a Vickers hardness tester. Ten diamond indentations were made per alloy with a 30kg load. The average values are shown in Figure 3.14 and the actual figures can be found in Appendix B (Table B2). At this point reference alloys (Hercules^{TM}, AISI 201 and 304) were not physically tested, values in the following figures are from literature as referenced in the Appendix B. The reference alloys were only tested at a later stage, once all alloys were available and the number of alloys to be tested had been reduced. Reference alloy results can thus be assumed to be from literature unless otherwise stated.

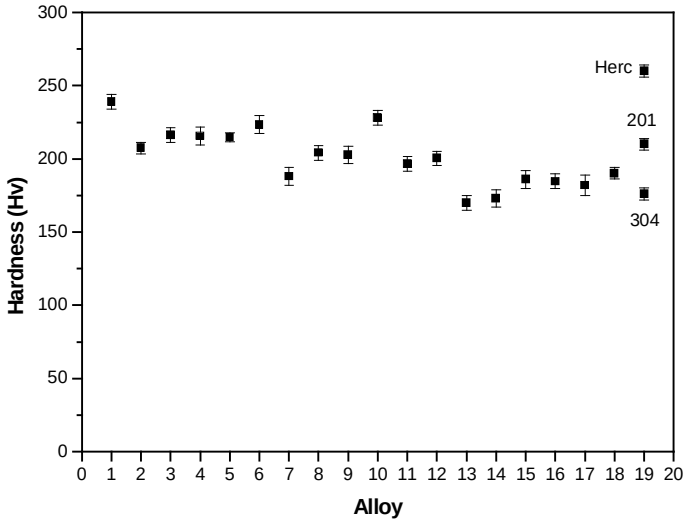

Figure 3. 14: Hardness of the 5kg ingots.

There are no significant changes in hardness between the different ingots. According to literature (section 2.4.5), N is supposed to increase the strength of stainless steels (which in turn increases the hardness) without affecting the toughness. This is, however, not evident in the hardness test results. It must be noted though, that the change in N is not large, ranging from 0.12-0.25 wt%. The hardness values in Figure 3.14 range from 181.9-239 Hv. Hercules™ has a general hardness of 260 Hv.

In summary, Mn, N and Mo have an effect on the microstructure and ferrite content of the alloys made. Mn and N decrease the ferrite content while Mo increases it. 5 wt% Mn is not enough to produce an austenitic microstructure at 0.5 wt% Mo and 0.1 wt% N. The effect of Mn, N and Mo on corrosion is discussed in Chapter 4.

4. Effect of alloying elements on corrosion behaviour of Hercules ä-based alloys

After chemical and microstructural analyses of the eighteen alloys, general corrosion testing was conducted on them to determine the effect of the varying amounts, and combinations, of Mn, N and Mo on the corrosion rate and behaviour of the alloys. The procedure and results are discussed in this chapter.

4.1 Testing procedure for general corrosion

The buttons and ingots were in the same condition prior to testing since they had all been heated into the austenic region and then air cooled as discussed in section 3.2. To determine the general corrosion behaviour of the alloys, corrosion tests were carried out using potentiodynamic testing methods on a 600-grit ground surface and in a 5 wt% sulphuric acid solution. A three-electrode corrosion cell consisting of a working electrode, reference electrode and counter electrode was used to carry out the corrosion tests. A saturated calomel electrode was used in all cases as the reference electrode. There were slight differences in the corrosion cell set-up used to test the buttons and ingots, these are discussed below. The experimental procedure followed for testing the buttons and ingots for corrosion is listed in Table 4.1.

Table 4. 1: Testing procedure for general corrosion of the alloys.

	50g buttons	5 kg ingots
Solution	5 wt% H_2SO_4	5 wt% H_2SO_4
Environment	Naturally aerated, static solution at room temperature	Naturally aerated, static solution at 25°C.
Scan range	The scan was started at -600mV vs. SCE and stopped at 1200 mV vs. SCE	The scan was started at –600 mV and stopped at 1200mV vs. SCE .
Scan rate	60 mV/min	10 mV/min
Reference electrode	Saturated calomel electrode (SCE)	Saturated calomel electrode (SCE)
Counter electrode (CE)	Platinum wire	Graphite electrode
Working electrode (WE)	Test piece was clamped directly to the corrosion cell using a carbon steel nail for electrical contact.	The 5kg ingots were machined into 5 mm diameter cylindrical buttons, which were mounted into a sample holder and immersed in the solution
Corrosion cell	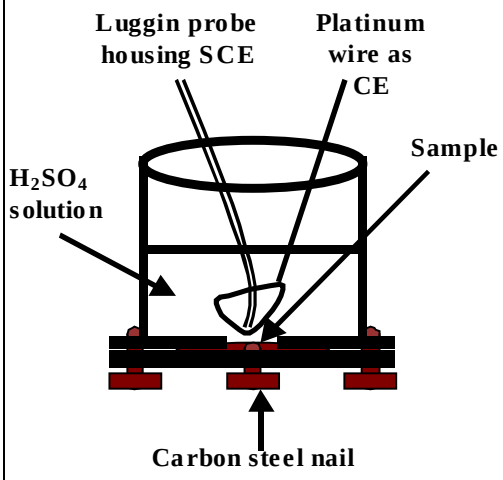	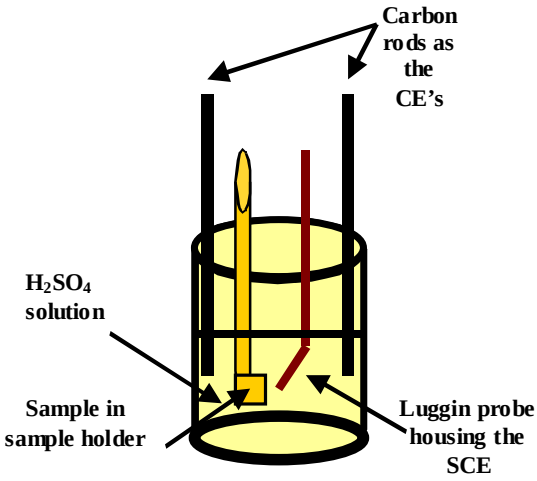
Description of test conditions	The reference electrode was housed in a Luggin-Haber Capillary. To minimise error due to IR-losses the capillary was place about 1cm from the working electrode. The alloy surface was cleaned by conditioning at -700 mV for 600 seconds prior to scanning to ensure that a reproducible surface was achieved for all alloys to be tested	The corrosion cell was placed in a water bath to keep the solution at 25ºC. The alloys were not stabilized prior to testing so as to avoid stabilization in the passive range since this would yield much lower corrosion rates than desired. The alloys were also not conditioned.
Potentiostat	Schlumberger FI1286	ACM Instruments AutoTafel potentiostat

All scans were done in duplicate and the results obtained are discussed in section 4.2.

4.2 Results of corrosion tests

The results of the buttons and the ingots are discussed together for comparison purposes. Scans obtained for both buttons and ingots were similar in that they all had more that one E_{corr} as illustrated in Figure 4.1.

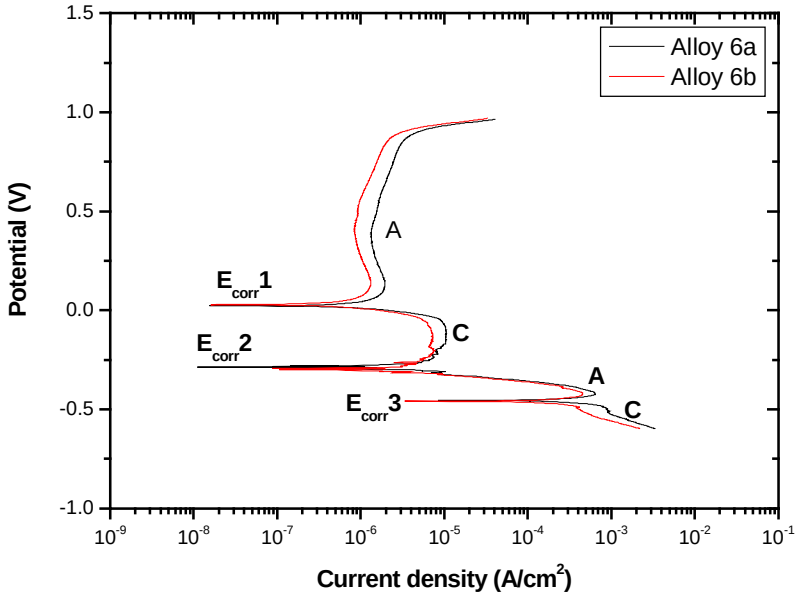

Figure 4. 1: Example of scans obtained for both ingots and buttons.

As shown in the figure, the scans had more than one cathodic "nose" at E_{corr}'s 1, 2 and 3. These noses are due to the actual cathodic curve intersecting the actual anodic curve more than once, as illustrated in Figure 4.2. (Figure 4.2 is merely an illustration and is not drawn from values in Figure 4.1)

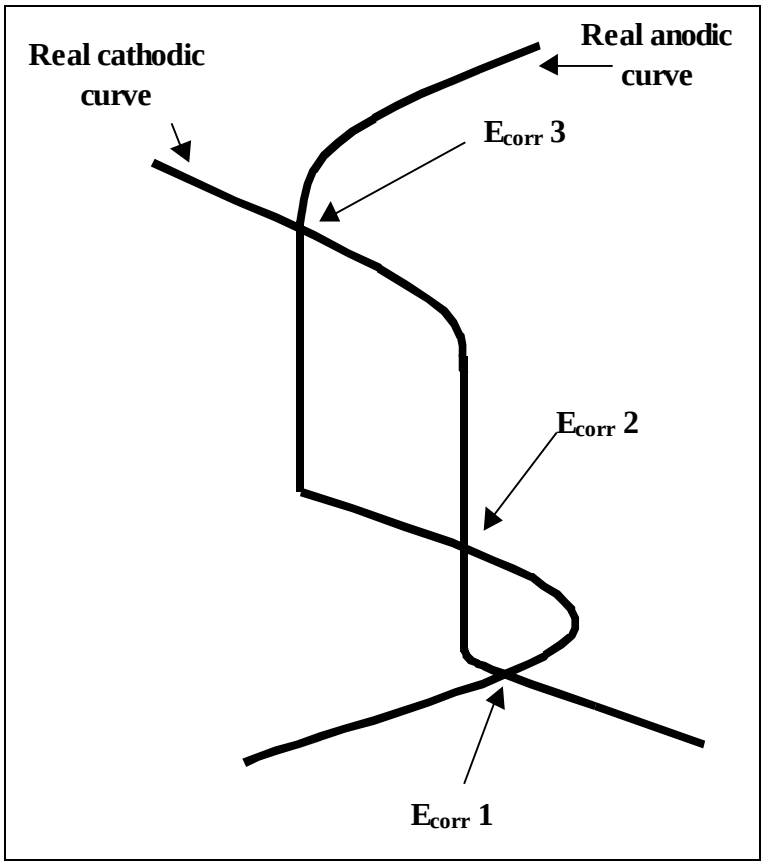

Figure 4. 2: Evans diagram showing the origin of a cathodic nose [Kerr *et al.*, 2003]

When an alloy is placed into the solution, there are times when the anodic and cathodic reactions are equal and it is at these points that the corrosion potential values are registered by the potentiostat. The full set of potentiodynamic scans obtained for corrosion testing of the buttons and ingots and tables of values obtained are given in Appendix D and E.

4.2.1 Calculating corrosion rate

The corrosion current density was calculated by determining the polarisation resistance (R_p) of each alloy from the scans. Polarization resistance is defined as the slope of the voltage-current density curve in the range ±30mV vs. E_{corr} [Jones, 1996].

This range is not restricted to being 30 mV, it can be as small as 15mV or even 10 mV from E_{corr}. In this project, R_p was calculated directly from the potentiodynamic scan, by drawing the above mentioned range on a linear scale and then calculating the slope at the origin, as shown in Figure 4.3.

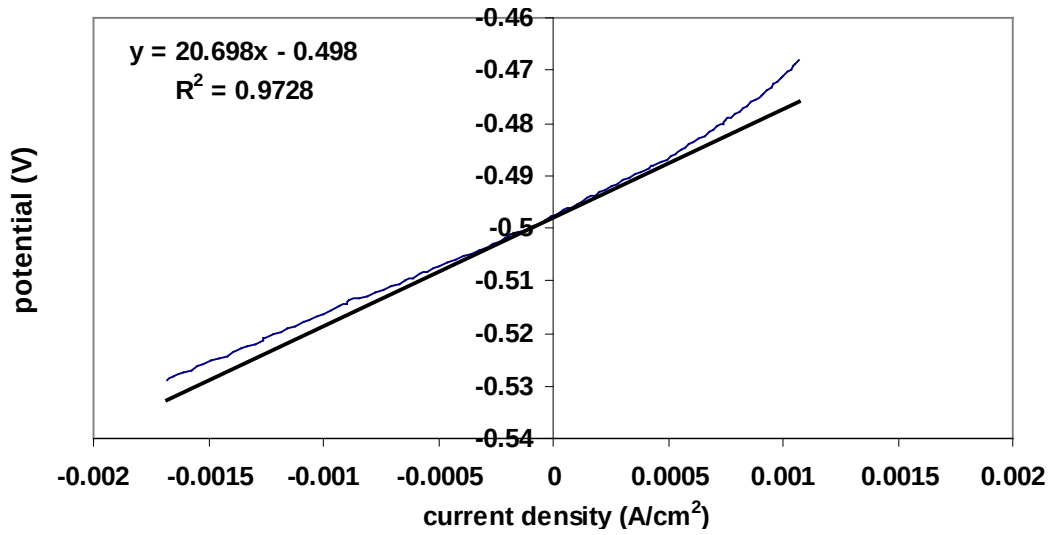

Figure 4. 3: calculation of R_p from the potentiodynamic curve.

From Figure 4.3 the slope and hence R_p is 20.698 Ω. cm^2 and i_{corr} can be found using equation 4.1 [Jones 1996].

$$R_p = \frac{B}{i_{corr}} \qquad \textbf{where} \qquad B = \frac{b_a \times b_c}{2.3(b_a + b_c)} \qquad \textbf{Equation 4. 1}$$

Subscripts a and c stand for anodic and cathodic, respectively, while ßa and ßc are Tafel slopes. ßa = ßc = 0.1 was used as is explained in Jones (1996, pp 146-149).

4.2.2 Corrosion rate as a function of Mn, N and Mo content

i_{corr} values obtained from the corrosion test results of the alloys were converted to mm/y as described in section 2.2.1 and the results were as in figures 4.4 to 4.6. Tables of actual corrosion values are tabulated in Appendix D (Table D1) and Appendix E (Table E1). At this point it was important to observe the trends that Mo, N and Mn had on the corrosion rate, i_{pass} and i_{crit}. Although AISI 304 and Hercules were tested for corrosion for the ingots, AISI 201 was not yet available for testing. It was thus decided to use reference values from literature for ease of comparison of the ingots and button results. The values as indicated in the following graph are as cited in Moema and Jones, 2005. Reference alloys were however tested in Chapter 5.

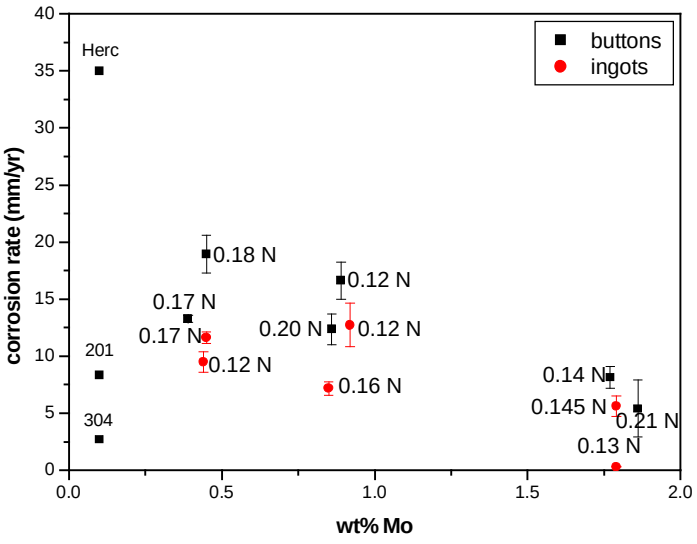

Figure 4. 4: Corrosion rate of 5 wt% Mn buttons and alloys.

For both buttons and ingots, an increase in molybdenum, at 5 wt% Mn, seems to lead to a decrease in the corrosion rate of the alloys (Figure 4.4). The corrosion values at 5 wt% Mn were higher for the 0.5 and 1 wt% Mo buttons and ingots than for those having molybdenum content greater than 1.5 wt%. An increase in nitrogen also seems to decrease corrosion rate except at the 0.5 wt% Mo level. Nitrogen does not,

however, seem to have a significant effect in decreasing corrosion rate, since the drop in corrosion rate at the respective molybdenum contents is not great. This is to be expected since, as noted in chapter 2, nitrogen has a small to moderate effect on improving the corrosion behaviour of austenitic stainless steels.

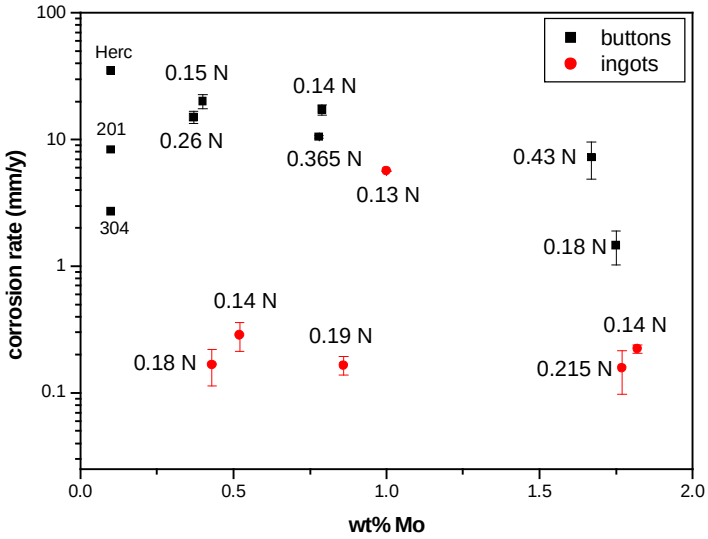

Figure 4. 5: Corrosion rate of 10 wt% Mn buttons and ingots.

The corrosion behaviour of the 50g buttons and 5kg ingot alloys differed markedly for the 10 wt% Mn alloys (Figure 4.5). The corrosion rate of the buttons again seems to decrease as molybdenum and nitrogen content increases, but there is no significant changes in the corrosion rate of the ingots as the Mo and n increase. For the buttons, the corrosion rates of the 0.5 and 1 wt% Mo were again higher than for those containing more than 1.5 wt% Mo. It seems that for the button samples a molybdenum content of greater than 1.5 wt% is needed to lower the corrosion rate at 5 and 10 wt% Mn. The buttons again had generally a higher corrosion rate than the ingots at the respective molybdenum contents except for ingot 8 (0.13 N) which had a much higher corrosion rate than the rest of the ingots.

Referring to figures 3.1-3.3, the buttons, at 5 and 10 wt% Mn, had a higher magnetic content than the ingots and this could be affecting their corrosion rates since a high magnetic content refers to a higher ferrite or martensite content (which both increase the corrosion rate). Microstructural analysis was not done on the buttons, thus making it impossible to determine the effect of microstucture on the corrosion rate.

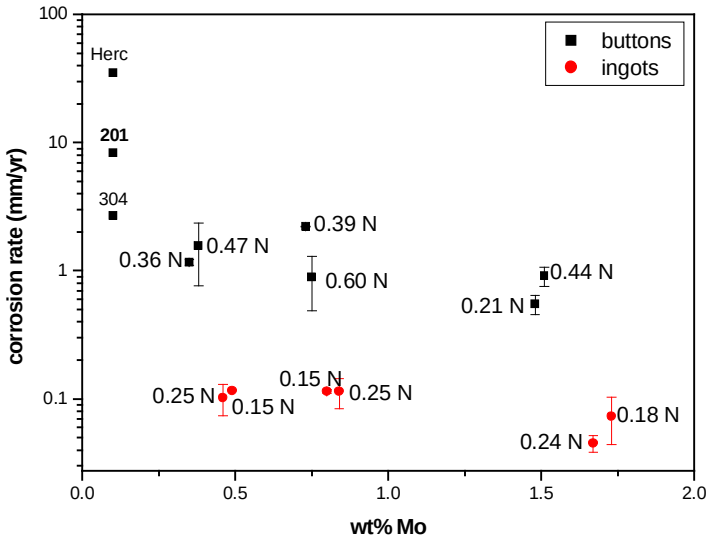

Figure 4. 6: Corrosion rate of 15 wt% Mn alloys

At 15 wt% Mn (Figure 4.6) there seems to be no significant change in corrosion rate as molybdenum or nitrogen increases for either buttons or ingots. The corrosion rate at 15wt% Mn is lower than that at 5 or 10wt% Mn for the buttons. It seems therefore that as the manganese content increases, much less molybdenum is needed to lower the corrosion rate of the buttons and ingots, since low corrosion rates for the alloys could be obtained with 0.5 wt% Mo at 15 wt% Mn but not at 5 wt% Mn. The ingots again had a lower corrosion rate than the buttons.

4.2.3 Passivation current density (i_{pass}) of the alloys

The passivation current density of the alloys were also calculated from the potentiodynamic scans obtained during corrosion testing and the results are shown in Figure 4.7. The lower the passivation current density of an alloy the better its corrosion resistance.

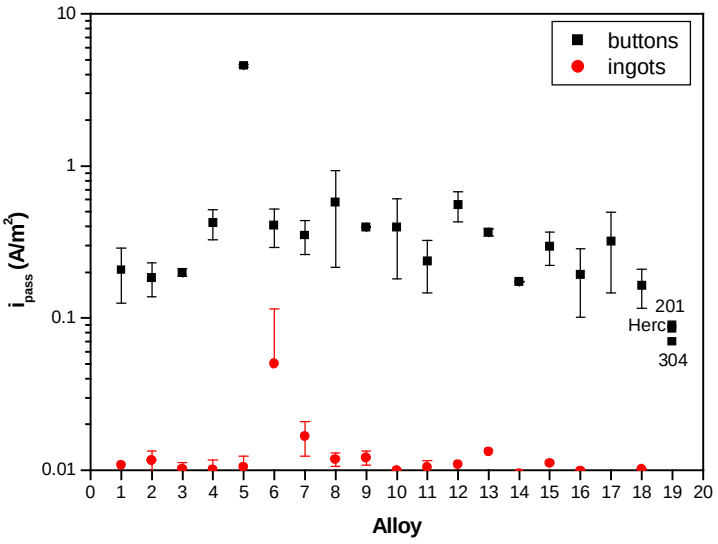

Figure 4. 7: i_{pass} for the buttons and ingots.

The i_{pass} values did not vary significantly from alloy to alloy. i_{pass} for the 50g buttons was in the region of 0.4 A/m^2, except for button 5, which had a much higher passivation current density. It should be noted that button 5 had severe porosity, which most probably affected the corrosion test results. The ingots had an average passivation current density lower than the buttons.

4.2.4 Critical current density (i_{crit}) of the alloys

The critical current density is an indication of how easily an alloy can passivate. The lower the critical current density the easier the alloy passivates. The critical current density for both the buttons and ingots were also calculated from the potentiodynamic scans, and is shown in Figure 4.8.

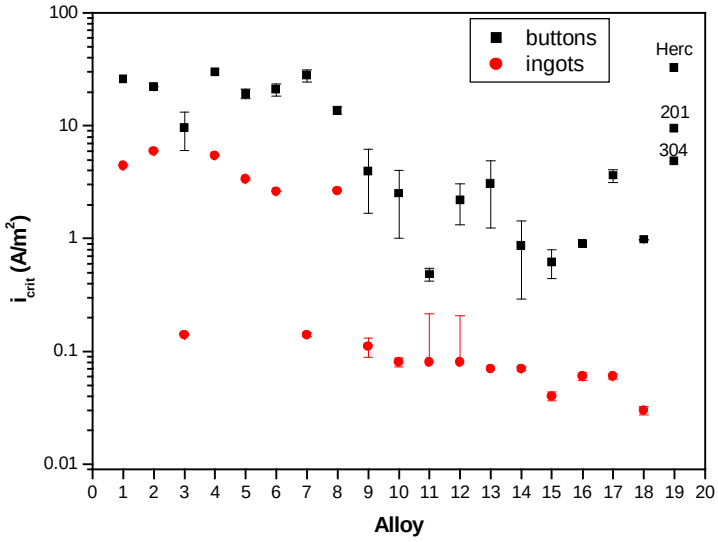

Figure 4. 8: i_{crit} for the buttons and ingots.

i_{crit} seems to decrease substantially at alloy 8 for both ingots and buttons. All ingots had a lower i_{crit} than the buttons. All the 5 wt% Mn buttons and ingots (alloys 1 to 6) had a higher i_{crit} than the rest of the alloys. The i_{crit} trends are not clear in Figure 4.8, further analysis of these samples' behaviour is thus analysed in Figures 4.9 and 4.10, where the i_{crit} values for these alloys are plotted as a function of Mo content.

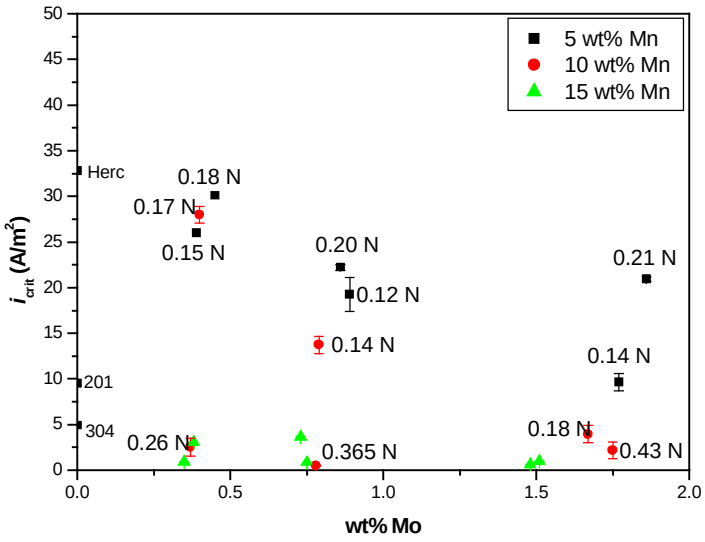

Figure 4. 9: i_{crit} for the buttons at 5, 10 and 15wt% Mn buttons.

The i_{crit} values for the 5 and 10 wt% Mn buttons, shown in Figure 4.9, seems to decrease as molybdenum increases but those of the 15 wt% Mn show no variation with changes in composition. An increase in molybdenum at 5 and 10 wt% Mn thus makes it easier for the buttons to passivate. For the 10 wt% Mn buttons an increase in nitrogen decreases i_{crit}, but the opposite effect occurs at the 5 wt% Mn. i_{crit} is higher fir the 5 wt% Mn buttons than the 10 or 15 wt% Mn ones.

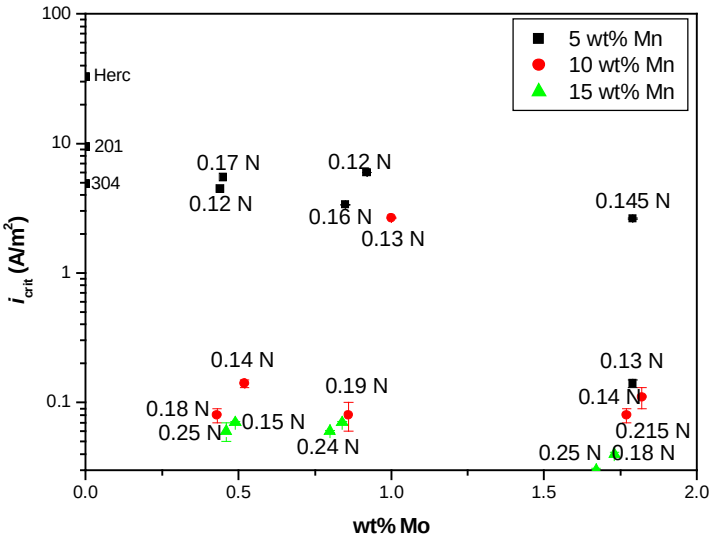

Figure 4. 10: Ingots 5 and 10 wt% Mn

For the ingots in Figure 4.10, there is again a decrease in i_{crit} as Mo increases at 5 wt% Mn. At 10 and 15 wt% Mn i_{crit} remains generally constant with an increase in molybdenum. i_{crit} is again higher at 5 wt% Mn than at 10 or 15 wt% Mn. The i_{crit} values for the ingots are much lower than those for the buttons.

4.3 Discussion and conclusions

The 50g buttons were difficult to work with because of their small size. Most of the buttons had porosity, probably due to the nitrogen content of the alloys. Nitrogen solubility in liquids decreases as the temperature increases, therefore during melting the liquid can become supersaturated with nitrogen, which then bubbles out as nitrogen gas, causing porosity. As discussed previously, once drillings had been taken for nitrogen analysis, most of the button was destroyed, leaving no material for further testing. This meant that nitrogen analysis had to be carried out after the corrosion tests so as to have material to work with. This was problematic in that the nitrogen content of the alloys was not up to target and this could only be determined after the corrosion tests had been done. Tests had thus been done on 50g buttons that did not have the desired composition. Nevertheless, important trends were noted from the corrosion testing results of the buttons such as:

- The decrease in corrosion rate with increasing manganese content (since the 5 wt% Mn buttons had the highest corrosion rate, while the 15 wt% Mn buttons had the lowest corrosion rate). Hercules has 9 wt% Mn.
- The decrease in corrosion rate with increasing molybdenum additions at 5 and 10 wt% Mn levels.

In view of the technical challenges encountered with the 50 g buttons it was decided to remake the alloys on a larger scale, in the hope of getting better homogeneity and stability. Larger ingots meant that more material was available for carrying out multiple tests, such as hardness and microstructural analysis. 5kg ingots were successfully made and were more homogenous and stable in terms of composition. Their nitrogen content did vary in some instances from target, but the variation was constant.

From the corrosion test results of the ingots similar conclusions as those drawn for the buttons could be made, such as a decrease in corrosion rate with increase in manganese and molybdenum content. At 10 wt% Mn, the ingots behaved differently from the buttons in that there was no change in corrosion behaviour with changes in chemical composition for the ingots. 10 wt% Mn seems optimum for the ingots since the 15 wt% Mn ingots behaved similarly.

Hercules™ (with no molybdenum and 0.25 wt% N) had a corrosion rate of 35 mm/y, it thus seems that any addition of molybdenum or nitrogen can improve the corrosion rate of Hercules™ since all the alloys tested (buttons and ingots) had lower corrosion rates. The effect of nitrogen on the alloys is not clear from the corrosion test results, but in the cases where it did lower corrosion rate, the decrease was not significant. It should be noted though the variation in nitrogen was not large, ranging from 0.15 to 0.30 wt%.

Overall, the ingots were much more stable than the buttons. For this reason and the fact that the current Hercules™ alloy has been developed for its mechanical properties and changing its composition would markedly alter these properties, it was decided to concentrate, in more detail on the 10 wt% Mn alloys, as discussed in the next chapter.

5. The 10wt% Manganese ingots

From the results in the previous chapter (covering the overall corrosion behaviour of the eighteen alloys) it was clear that the 10 wt% Mn alloys were of optimum composition, also from a mechanical point of view, as mentioned. This chapter therefore focuses solely on the 10 wt% Mn alloys with a detailed study of their corrosion behaviour, benchmarked against those of AISI 304, 201 and Hercules™. The 10 wt% Mn alloys (ingots 7 to 12) were tested for general and pitting corrosion using ASTM standards. Immersion tests were done, along with scanning electron microscopy (SEM) analysis on the corroded surfaces to determine the mechanism of corrosion. Results for reference alloys in this chapter are from actual tests done on alloys AISI 201, AISI 304 and Hercules™ .

5.1 General corrosion of 10 wt% Mn ingots

Ingots 7 to 12 were tested for general corrosion behaviour according to ASTM standard G5–94(2002) in a 5 wt% sulphuric acid solution at 30°C. The solution was purged with nitrogen for an hour prior to scanning and also during scanning. The alloys were ground to a 600-grit surface finish. A three-electrode corrosion cell was once again used with carbon as the counter electrode and a saturated calomel electrode (SCE) as the reference electrode. The scan was started at –200 mV vs. E_{corr} and ended at 1200 mV at a rate of 10mV/min. Two tests were performed per alloy. Figure 5.1 is an example of a typical scan obtained during testing showing reproducible results.

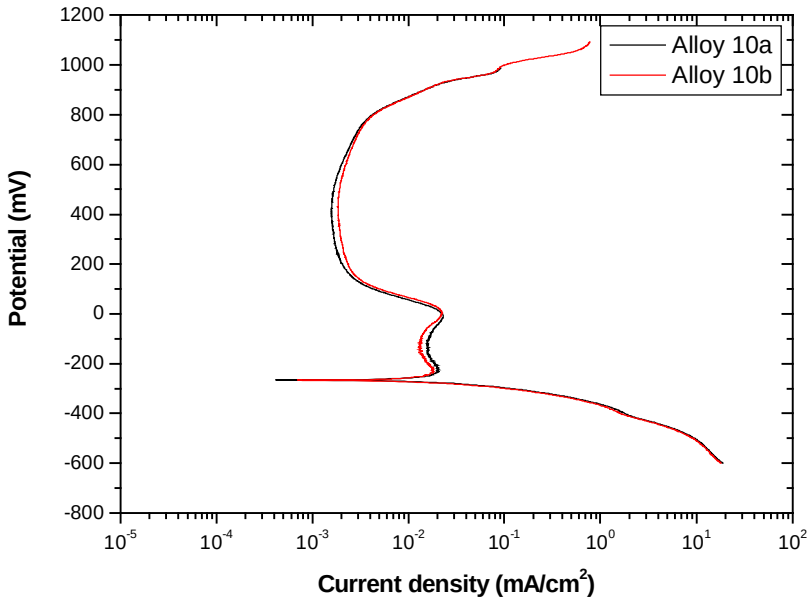

Figure 5. 1: A typical scan obtained during testing of ingots 7 to 12, showing very good reproducibility.

The scans obtained did not have three noses as in previous results. This was probably due to the ingots being stabilized before scanning and the samples having passivated to a large extent. The rest of the scans along with a table of the results obtained are given in Appendix F. The corrosion rate in mm/y was once again calculated directly from the potentiodynamic scan and the results are shown in Figure 5.2. Hercules, AISI 201 and 304 were also tested and are given as benchmark values.

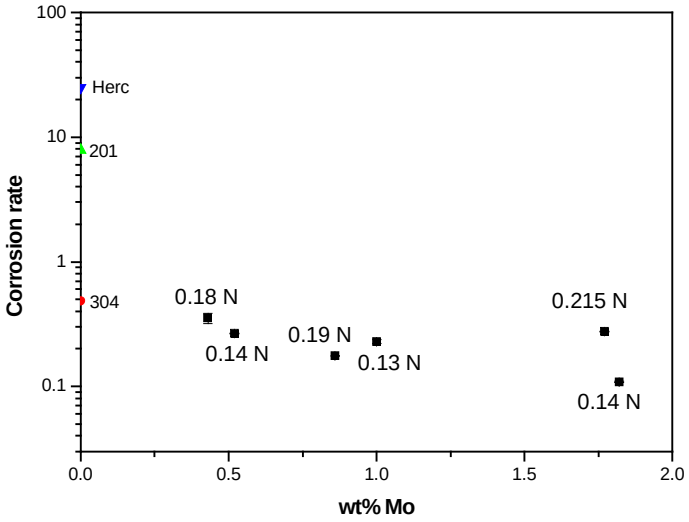

Figure 5. 2: Corrosion rate for ingots 7 to 12 as a function of Mo content.

The results verified what was found in previous tests, namely that no change in corrosion rate at the 10 wt% Mn alloys occurs with changes in chemical composition. The ingots had corrosion rates comparable to that of 304 and lower than Hercules™ and 201. The corrosion rate of the ingots was low, ranging form 0.1 to 0.5 mm/y. Hercules™ was found to have a corrosion rate of 24 mm/y (lower than in previous tests) , and 201 was found to have a corrosion rate of 8 mm/y. The ingots had nitrogen levels lower than Hercules™ (0.25 wt% N) but any combination of molybdenum and nitrogen in the ingots still resulted in a much lower corrosion rate than Hercules™

Figure 5.3 shows all the scans obtained for ingots 7 to 12 on one graph so that the effect of the alloying elements on the passivation and critical current densities of the alloys can be illustrated.

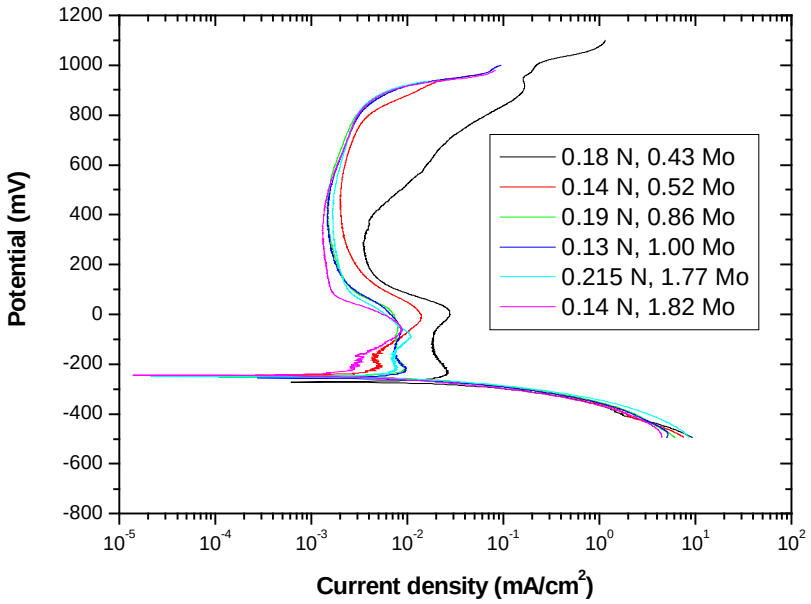

Figure 5. 3: Full potentiodynamic scans of ingots 7 to 12 in 5 wt% H_2SO_4.

The passivation and critical current densities of the 10 wt% Mn alloys (Figure 5.3) decreases as the molybdenum content increases. This is in agreement with literature (section 2.4.4) where researchers found that molybdenum improves passivation and general corrosion of stainless steel by decreasing these currents. Molybdenum thus makes it easier for the alloy to passivate. Variations in nitrogen does not seem to have a significant effect on the general corrosion of the 10 wt% Mn. No clear trend is evident with changes in nitrogen content. The effect of changes in nitrogen on the pitting potential of the 10 wt% Mn alloys was not clear. Actual pitting tests were done to clarify this result as is discussed in the next section.

5.2 Pitting corrosion tests of 10 wt% Mn ingots

5.2.1 Pitting resistance equivalent (PRE) for the 10 wt% alloys

The pitting resistance equivalent (PRE), as mentioned in section 2.2.2, is a guide used to predict the pitting resistance of stainless steel according to their chromium, molybdenum and nitrogen content as in equation 5.1 [Frankel, 1998, Peckner and Bernstein, 1977; Levey 1995]:

$$PRE = (\%Cr) + 3.3(\%Mo) + 16(\%N) \qquad \textbf{Equation 5. 1}$$

The higher the pitting resistance of an alloy, the more resistant it is to pitting corrosion [McEwan, 1994].

Figure 5.4 illustrates the PRE values for the six 10 wt% Mn alloys along with those of Hercules™, AISI 304 and 201.

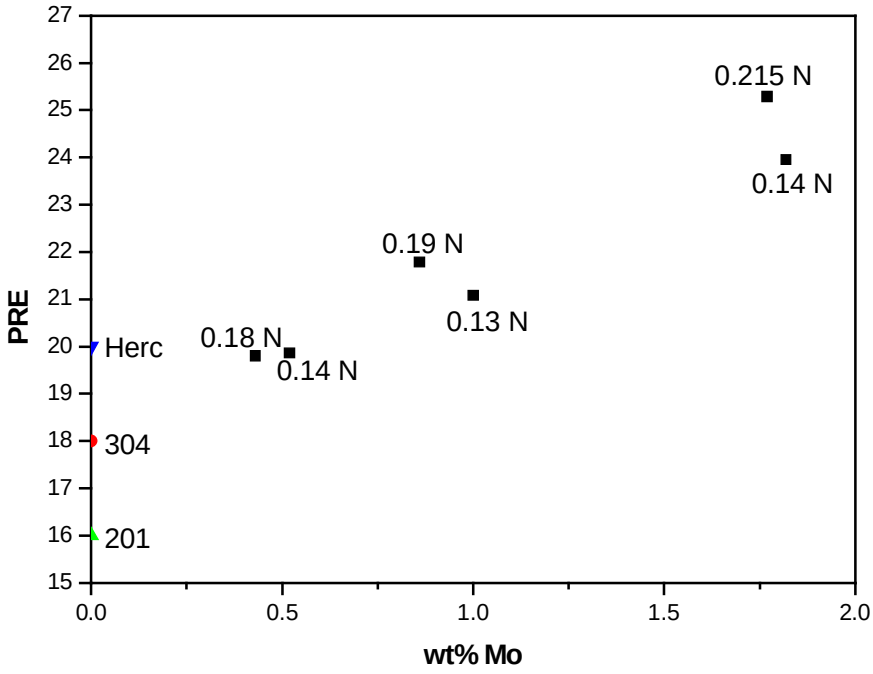

Figure 5. 4: PRE values for ingots 7to 12.

PRE values rank the alloys according to calculated pitting resistance. The pitting resistance of the alloys is predicted to increase as molybdenum increases. Hercules™ was predicted to have a higher pitting resistance than 304 and 201. Two of the ingots (0.18 N and 0.14 N) were predicted to have similar pitting resistances to Hercules™ while the rest were predicted to have a higher pitting resistance. None of the ingots were predicted to have a lower pitting resistance than Hercules™. These values were verified by actual pitting tests.

5.2.2 Cyclic potentiodynamic polarization testing of the 10 wt% Mn ingots

Cyclic potentiodynamic tests were done on ingots 7 to 12 according to ASTM standard G61-86 (2002) to determine the susceptibility of these alloys to pitting corrosion. The alloys were tested in a 3.56 wt% NaCl solution at 25 ºC. The solution was dearated for an hour prior to starting the scan and also during scanning. The alloy surface was ground to a 600-grit surface finish and the scan was started at –50

mV vs. E_{corr} up to 1200 mV. Duplicate scans were done per sample. An example of a typical scan is shown in Figure 5.5. The complete set of scans obtained is given in Appendix G. and table of results.

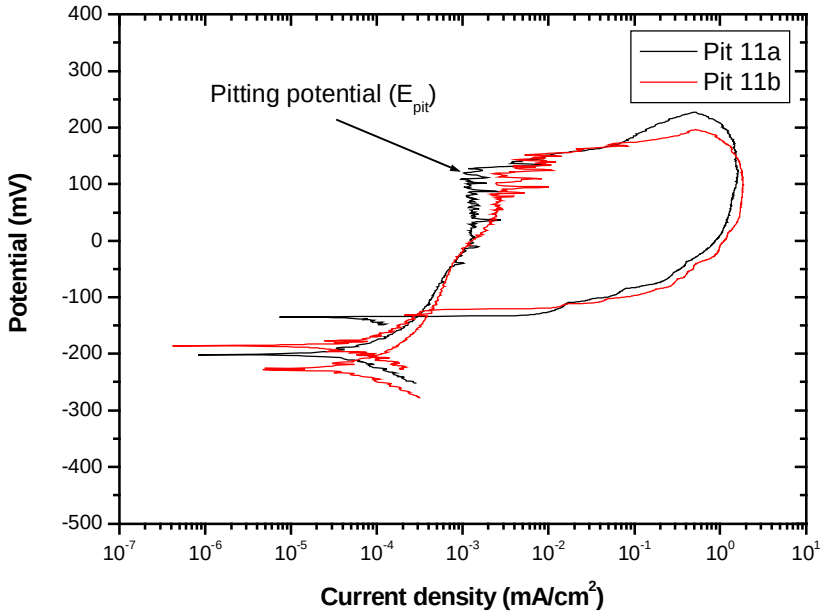

Figure 5. 5: Example of cyclic scan obtained from pitting tests

All scans were reversed at 5 mA and all formed a hysterisis loop, as shown in Figure 5.5. The pitting potentials were read directly from the scan. These values are represented graphically in Figure 5.6 as a function of Mo content.

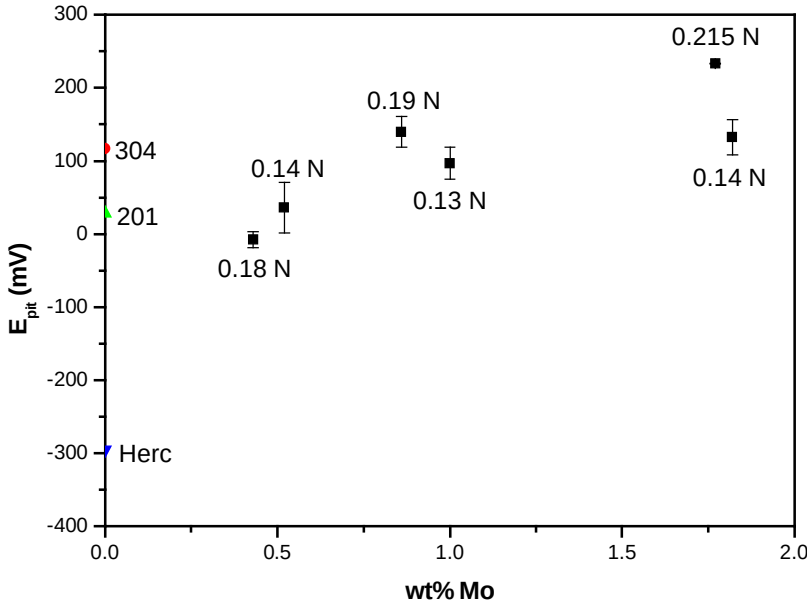

Figure 5. 6: Pitting potentials of alloys 7-12, as well as Hercules, AISI 304 and 201.

As predicted by the PRE numbers, there is an increase in pitting potential as molybdenum increases, and therefore resistance to pitting is increased. In terms of pitting potential, all the alloys are comparable to 304 and 201. Hercules™ has a low pitting potential of –295 mV, much lower than all the alloys tested and contrary to its PRE value. PRE values are theoretical and they will differ from actual test values since alloys are composed of more than just Cr, Mo and N. An increase in nitrogen seems to increase the pitting potential, except at the 0.5 wt% Mo level. It seems clear therefore that any addition of molybdenum with nitrogen, will improve the corrosion resistance of Hercules™.

5.3 Immersion tests of 10wt % Mn ingots

Immersion tests were performed to test the alloys in a closer simulation of actual exposure conditions and to verify electrochemical results. The 10 wt% Mn alloys

were thus tested in a 5 wt% sulphuric acid solution at room temperature in a naturally aerated environment. The alloys were ground to a 120-grit surface finish, weighed and measured before immersing in the solution on sample holders. The alloys were weighed every 24 hours. After 14 days, the alloys were cleaned with a wire brush and weighed again. The corrosion rate was then calculated with equation 5.2 [ASTM standard G31-72 (2002)]

$$\text{corrosion rate (mm/y)} = \frac{K \times W}{D \times A \times t} \qquad \textbf{Equation 5. 2}$$

Where K =8.76 x 10^4, W = mass loss (g), D = density (g/cm^3), A = surface area (cm^2), t = time (hrs)

5.3.1 Results of immersion tests

Figure 5.7 illustrates the mass loss experienced for the different ingots over the 14-day immersion period. Readings were taken every 24 hours.

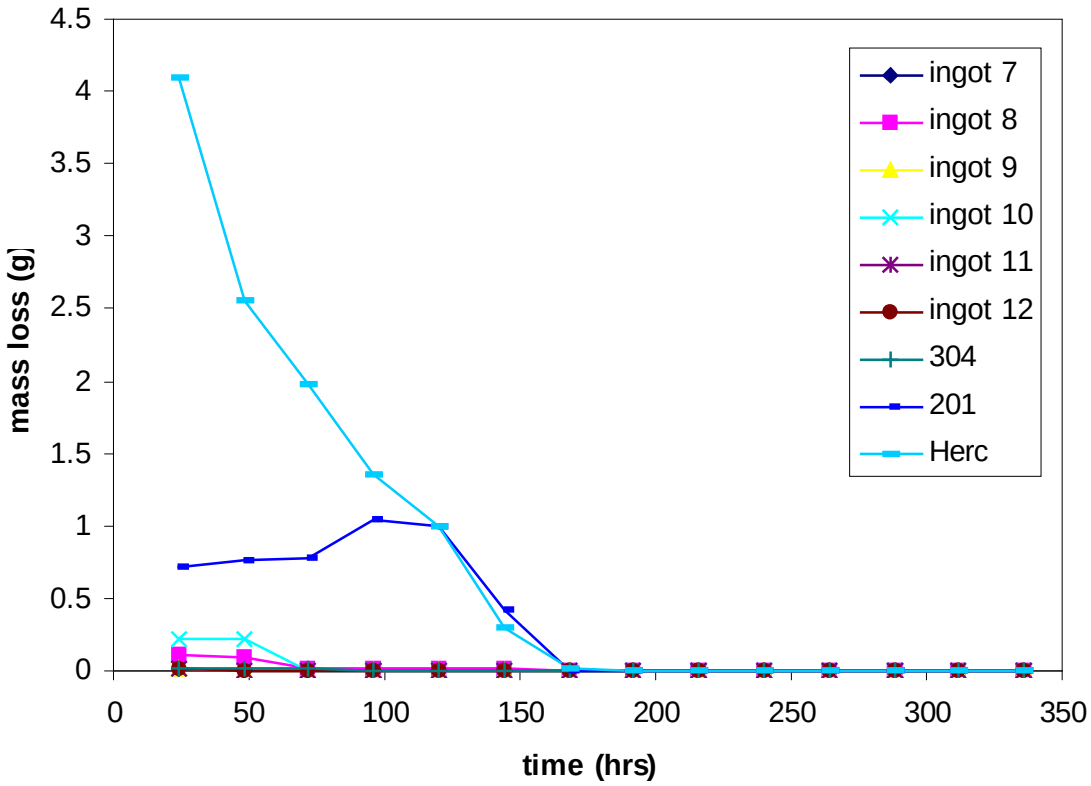

Figure 5. 7: Massloss vs. time graph for ingots 7-12.

After 24 hours, Hercules™ was corroding and losing mass rapidly. It formed an adherent black corrosion product after the first day. Ingots 8 and 10 tarnished slightly, while the rest of the ingots showed no change in colour or mass over the testing period. AISI 201 and 304 were also tested and used as benchmark alloys. Figure 5.8 illustrates the corrosion rates obtained for the ingots after 14 days of immersion.

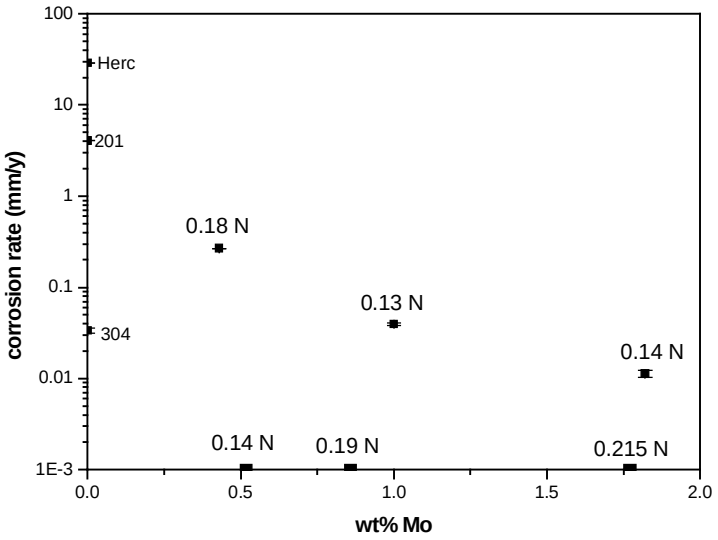

Figure 5. 8: Corrosion rate of ingots 7-12 after immersion tests.

At 10 wt% Mn, the ingots showed a low corrosion rate that seemed to decrease with an increase in molybednum. AISI 304 was found to corrode at 0.03 mm/y and AISI 201 at 4.05 mm/y. These figures fall within the range reported in literature (section 2.2.3). Hercules™ was found to corrode at 29 mm/y, which is slightly higher than the 24 mm/y found potentiodynamically. The ingots had a corrosion rate again comparable with 304.

5.3.2 SEM analysis of ingots 7-9

SEM analysis revealed no evidence of corrosion for alloys 7, 9, 11 and 12 after cleaning. The SEM images were taken as both Secondary Electron Images (SEI) and Backscattered Electron Images (BEI) all at the same magnification of 1100 (X1100). The complete set of micrographs is given in Appendix H. The SEM image for ingot 9 (figure 5.9) is shown here as an example of the type of images obtained with the SEM analysis.

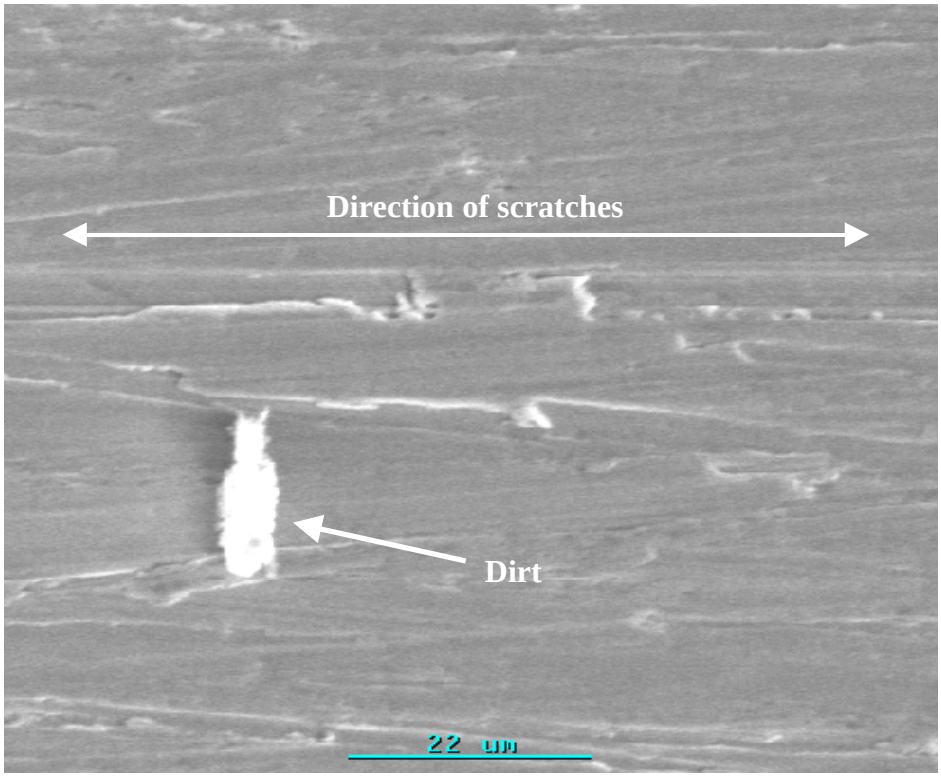

Figure 5. 9: SEM (SEI) image of ingot 9 at X1100.

Ingot 9 showed no evidence of corrosion. There seemed to be some etching, however, along the grinding lines (direction of scratches).

From the SEM analysis it can be concluded that the 10 wt% Mn alloys are generally passive in a 5 wt% sulphuric acid solution at room temperature. In the cases where

they do corrode, the mechanism is general corrosion, except for ingot 8 (Appendix H) which pitted. AISI 304 also showed pitting.

5.4 Discussion and Conclusions

From the potentiodynamic tests, it was found yet again that the 10 wt% Mn alloys have low corrosion rates that are comparable to AISI 304. Potentiodynamic tests showed Hercules™ to have a high corrosion rate of 24 mm/y. There was again no change in corrosion rate as either molybdenum or nitrogen varied. This confirms results obtained in previous tests. Immersion tests revealed that the mechanism of corrosion in most instances was general corrosion, even though ingot 8 pitted. The exposure time, however, was too short to make firm conclusions. More tests would have to be done to determine when each type of corrosion occurs.

The 10 wt% ingots pitted in a 3.5 wt% NaCl solution at 25ºC, which is an environment in which the alloys are susceptible to pitting. The tests revealed that the higher the molybdenum content the more resistant the alloy was to pitting, as predicted by the PRE values. An increase in nitrogen also increased resistance to pitting.

Hercules™ again had a higher corrosion rate and a lower pitting resistance than the rest of the alloys. Any addition of molybdenum with nitrogen therefore seems to improve the corrosion resistance of this alloy.

6. Summary and Conclusions

The aim of this project was to establish the effect of nitrogen, manganese and molybdenum on the corrosion behaviour of low nickel austenitic stainless steels, such as Hercules^{TM}, developed by Mintek. A further aim was to find a combination of these elements that will give a more corrosion resistant version of Hercules^{TM}. Preliminary tests were done on buttons and standard corrosion tests on ingots. The alloys were made with a Hercules^{TM} base composition with variations in manganese, nitrogen and molybdenum. Manganese was varied in three levels (5, 10 and 15 wt%), nitrogen in two levels (0.15 and 0.30 wt%) and molybdenum in three levels (0.5, 1 and 2 wt%). Eighteen alloys were tested. Compositional and microstructural analyses were done on the alloys along with hardness, general corrosion, immersion and pitting tests. SEM analysis was done after immersion testing.

From literature (Chapter 2) it was found that manganese can be used as a cheaper substitute for nickel and that it aids nitrogen solubility. Researchers, however, found manganese to weaken the passive film and form manganese sulphides which assist in pit formation. Molybdenum and nitrogen were found by researchers to improve both the general and pitting corrosion resistance of stainless steels by decreasing the passivation current density and increasing the pitting potential. Contrary to literature, actual potentiodynamic tests carried out on the different buttons and ingots (Figure 4.4-4.6), showed that an increase in manganese decreased the general corrosion rate of Hercules ^{TM}. In all alloys tested the 15 wt% Mn alloys had the lowest corrosion rate while the 5 wt% Mn alloys had the highest corrosion rate. Ferritescope readings (Figure 3.12) illustrated that an increase in manganese generally decreased the ferrite content of the alloys.

.

This is to be expected since manganese is an austenite former and an increase in this element would decrease the ferrite content of the alloys. Manganese also aids nitrogen solubility, which in turn stabilises the austenite and thus decreases the ferrite content of the alloys. Additions of manganese beyond 5 wt% thus decreases the corrosion rate due to an increased austenite stability. 10 wt% Mn, was the optimum in achieving significantly low corrosion rates of Hercules^{TM}, even with 0.5 wt% Mo.

It can thus be concluded that reducing the manganese content below 10 wt% would produce alloys that have higher corrosion rates. Increasing the manganese content beyond 10 wt% has no significant effect in reducing the corrosion rate of Hercules^{TM} since the 15 wt% Mn alloys behaved similarly to the 10 wt% Mn ones.

The current Hercules^{TM} alloy has no molybdenum addition. Molybdenum proved, however very effective in decreasing the corrosion rate of Hercules^{TM} especially at 5 wt% Mn (Figure 4.4-4.6). At this level of Mn an increase in molybdenum, decreased the corrosion rate of Hercules^{TM} from values around 20 mm/y down to about 5 mm/y and lower, with the larger molybdenum contents (2 wt% Mo) resulting in the lowest corrosion rate.

Any addition of molybdenum to the 10 and 15 wt% Mn alloys reduced the corrosion rate significantly. Varying the amount of Mo added at these levels of Mn did not however vary the corrosion rate behaviour which remained low and constant irrespective of the increasing molybdenum contents. The buttons differed from the ingots at the 10 wt% Mn level (Figure 4.5) by having a higher corrosion rate. The corrosion rate of the buttons at 10 wt% Mn decreased with increasing molybdenum whereas that for the ingots remained low and constant. .

Additions of molybdenum affected the ferrite content of the ingots. An increase in molybdenum additions generally increased the ferrite content of the alloys (Figure 3.13) as is to be expected since molybdenum is a strong ferrite former. Results further showed that molybdenum decreased the passivation and critical

current densities of the 10 wt% Mn ingots (Figure 5.3), as is found in literature. Molybdenum thus improves corrosion rate by aiding the alloys to passivate easier and lowering the passivation current, and leads to increased pitting potentials (Figure 5.6). Molybdenum was more effective in improving the pitting resistance of Hercules^{TM} than the general corrosion resistance of the alloy, which did not vary significantly with change in Mo content (Figure 5.2). Pitting potentials were improved in such a way that the values were compatible with AISI 304, one of the benchmark alloys in this project.

The addition of molybdenum thus improves the corrosion and pitting resistance of Hercules^{TM}, since at 10 wt% Mn, all alloys tested had a lower corrosion rate than Hercules^{TM}. Low corrosion rates can be attained with as little as 0.5 wt% Mo at the 10 wt% Mn level (Figure 5.2).

Hercules^{TM} has 0.25 wt% N, but all the ingots tested had lower nitrogen levels (Figure 3.6). At 10 wt% Mn, increasing the nitrogen content of the ingots from 0.13 to 0.215 wt% had no effect on the corrosion rate (Figures 4.5 and 5.2). The corrosion rate remained low and constant as both nitrogen and molybdenum increased. The same behaviour is observed at the 15 wt% Mn level (Figure 4.6). At 5 wt% Mn (Figure 4.4), however, higher nitrogen levels resulted in a lower corrosion rate only at the 1 wt% Mo level.

Nitrogen levels greater than 0.25 wt% could only be attained with the buttons (Figure 3.6) at the 10 and 15 wt% Mn levels. This is probably due to the manganese aiding nitrogen solubility at these levels. At 10 wt% Mn (Figure 4.5) an increase in nitrogen content resulted in a lower corrosion rate at molybdenum contents less than 1.5 wt%. This is probably due to the nitrogen being an austenite former and stabiliser. At higher molybdenum contents, however, increasing the nitrogen content to 0.43 wt% increased the corrosion rate of the buttons. This could be due to the nitrogen solubilty limit being reached, causing nitrides to form in the microstructures and thus decreasing the corrosion resistance of the button. At 15 wt% Mn (Figure 4.6), however, low corrosion rates could be

obtained in the buttons with 0.47 wt% N and molybdenum contents less than 0.5 wt%. There is thus a synergism between nitrogen, molybdenum and manganese in reducing the corrosion rate of Hercules™.

Hercules™ with constant Mo and Mn values, but varying nitrogen levels, would need to be made and tested to clarify the effect of nitrogen on corrosion rate. The nitrogen range would perhaps have to be increased to include levels beyond those of the present range if there was an interest in determining the actual effect of N on the corrosion rate of Hercules™. Nitrogen values between 0.1 and 0.5 wt% could possibly be used to determine the solubility limit of nitrogen at the 10 wt% Mn level.

No changes in passivation current densities were observed with changes in nitrogen content (Figures 4.7). Critical current density decreased with increasing Mo content at the 5 wt% Mn level for both buttons and ingots (Figures 4.8 to 4.10). There was a general decrease in i_{crit} with an increase in Mo at the 10 wt% Mn level for the buttons but not the ingots. Both the buttons and ingots showed to changes in i_{crit} with changes in Mo at 15 wt% Mn. It can thus again be said that 10 wt% Mn is optimum in decreasing the corrosion rate of Hercules™ significantly through a decrease in i_{crit} which aids passivation.

An increase in nitrogen decreased the ferrite content of the Hercules™ alloys (Figure 3.11). This is to be expected since nitrogen is an austenite former that stabilises austenite and reduces the tendency for ferrite formation. An increasing nitrogen content, increased the pitting resistance of the 10 wt% ingots at molybdenum levels greater than 0.5 wt% (Figure 5.6). All alloys, however, had higher pitting resistances than Hercules™.

Immersion tests done on the 10 wt% Mn ingots confirmed that Hercules™ has a high corrosion rate and that all other alloys tested had a much lower corrosion rate. At 10 wt% Mn the ingots tested had low corrosion rates that decreased with

increasing Mo content (Figure 5.8). SEM analysis revealed that in 5 wt% sulphuric acid, the alloys corroded mostly by general corrosion.

In tests performed thus far no changes in composition caused a change in hardness in any of the low nickel austenitic stainless steels. All alloys tested had a similar average hardness of about 200 Hv (Figure 3.14).

Hercules^{TM} was found to have an average corrosion rate ranging from 24 mm/y-29 mm/y. This was much higher than that of any of the other alloys tested. It can thus be said that any addition of Mo can improve the corrosion rate of Hercules^{TM}. Varying the amount of molybdenum added however has no effect on the corrosion rate. Low corrosion rates at 10 wt% Mn can be attained with nitrogen levels lower than those of Hercules^{TM} (0.25 wt%) with a molybdenum addition of less than 0.5 wt%, provided the nitrogen content is below the nitrogen solubility limit. An alloy with a Hercules^{TM} base composition, a minimum additions of 0.5 wt% Mo, 10 wt% Mn and 0.15 N would thus be a more corrosion resistant version of Hercules^{TM}.

The development of Hercules^{TM} aimed at producing an alloy that was 25 % cheaper than AISI 304. It has been calculated that Hercules^{TM} would cost R14.50/kg in bar form [White, 2005] which is 21% less than the cost of AISI 304 in bar form. The current Hercules^{TM} composition does not contain molybdenum and any additions of molybdenum will thus increase its cost. Molybdenum prices are currently higher than nickel prices and just as unpredictable [Adanac, 2005], see Appendix I, and it could therefore be more cost effective to find another alloying addition or method to reduce the corrosion rate of Hercules^{TM}.

7. References

Adanac-Moly-Corp (November, 2005), http://www.adanacmoly.com/,

Angel, T. (1954). Formation of Martensite in Austenitic Stainless steels: Effects of Deformation, Temperature and Composition, *Journal of The Iron and Steel Institute*, May 1954, pp. 165-174.

Audouard, J.P. (1993). Stainless Steels, Les Editions de Physique Les Ulis, France, .pp. 254-301.

ASTM G65, pp 370-373

Avesta Sheffield. (1994). Corrosion Handbook for Stainless Steels: Corrosion Tables, Sandvikens Tryckeri, Sweden pp. 59-62.

Baba, H., Kodama, T., and Katada, Y. (2002). Role of Nitrogen on the Corrosion Behaviour of Austenitic Stainless steels, *Corrosion Science*, Vol. 44, Issue 10, Oct, pp. 2393-2407.

Banerjee, M.K., Mukherjee, A.N.and Mukherjee, K.P. (1990). Potentiokinetic Behaviour of Copper and Manganese Bearing Stainless steels, *NML Technical Journal*, Vol. 32, Feb-Nov, pp. 11-17.

Bastidas, J.M., Torres, C.L., Cano, E. and Polo, J.L.(2002). Influence of Molybdenum on Passivation of Polarised Stainless Steels in a Chloride Environment, *Corrosion Science*, Vol. 44, Issue 3, Mar., pp. 625-633.

Blom, K.J and Degerbeck, J. (1983). Low Manganese Austenitic Stainless Steels has Improved resistance to Pitting and Crevice Corrosion, *Materials Performance*, July, pp. 52-54.

Brigham, R.J. and Tozer, E.W. (1974). Effect of Alloying Additions on the Pitting Resistance of 18% Chromium Austenitic Stainless Steels, *Corrosion,* Vol. 30, May 1974, pp. 161-166.

-

Callister, Jr. W.D (1994). Materials Science and Engineering, An Introduction, John Wiley and Sons, Inc.,USA, pp. 242, 361.

Colombier, L. and Hochman, J. (1965). Stainless and Heat Resisting Steels, Edward Arnold (Publishers) Ltd, pp 65-106, 134.

Cortie M.B. (1995). Low Nickel Austenitic Stainless Steel, Mintek Patent (P 12500 Za/MVS MINTEK), November, pp. 1-35.

Fontana, M.G. and Greene, N.D. (1982). Corrosion Engineering, Second Edition, Mc Graw Hill Publishers, pp. 51-54.

Frankel, G.S. (1998). Pitting Corrosion of Metals, *J. Electrochem. Soc*., Vol. 145, No. 6., June, pp. 2186-2197.

Gross, C.J. and Robinson, F.P.A. (1981). Effect of the Addition of up to 18% Manganese on the Microstructure and Corrosion Properties of a 14.5% Chromium

Stainless Steel, *Metallic Corrosion*, Proceedings-31st International Congress on Metallic Corrosion, South Africa,Vol. 1, pp. 114.

Gross, C. J. (1980). The Effect of Manganese on the Structure and Corrosion Properties of 14.5% Chromium Stainless Steels, MSc Dissertation, January, University of the Witwatersrand, Department f Metallurgy,pp. 14, 61, 62.

Hajjaji, S.E., Aries, L., Audouard, J.P. and Dabosi, F. (1995). The Influence of Alloying Elements on the Corrosion Resistance of Stainless Steels in Phosphoric Acid Medium Polluted by Sulphide Ions, *Corrosion Science*, Vol. 37, No. 6, pp. 927-939.

Harvey, P.D. (1982). Engineering Properties of Steel, American Society For Metals, U.S.A, pp. 246-281.

Hashmito, K. and Asami, K. (1979). An X-ray Photoelectron Spectroscopic Study of the Passivity of Ferritic 19Cr-Stainless Steels in HCL, *Corrosion Science*, Vol. 19, pp. 251, 1979.

Ilevbare, G.O. and Burstein, G.T. (2001). The Role of Alloyed Molybdenum in the Inhibition of Pitting Corrosion in Stainless Steels, *Corrosion Science*, Vol. 43, pp. 485-513.

Iorio, L., Cortie, M. and Jones, R. (1994). Technical Data: Solubility of Nitrogen in Experimental low-nickel Austenitic Stainless Steels, *The Journal of The South African Institute of Mining and Metallurgy*, Vol. 94, no. 7, july, pp. 173-177.

Jargelius-Patterson, R.F.A. (1999). Electrochemical Investigation of the Influence of Nitrogen on Pitting Corrosion of Austenitic Stainless Steels, *Corrosion Science*, Vol. 41, pp. 1639-1664.

Jargelius-Patterson, R.F.A. (1994). Phase Transformations in Manganese-Alloyed Austenitic Stainless steel, *Scripta Metallurgica et Materialia*, Vol. 30, No. 9, pp. 1233-1238.

Jones, D.A., *Principles and Prevention of Corrosion*, Prentice-Hall, Inc., U.S.A., pp. 75-80, 143-153.

Kerr, J. (2003). New Generation Low-Nickel (≤2%) Austenitic Stainless Steels for Structural Application, *MINTEK Annual Report (C3785M)*, pp. 1-2, 42-57.

Kincer, M.U and McEwan, J.J. (1993). Corrosion Testing of Stainless Steel, *Chemical Technology*, Oct. 1993, pp. 7-9.

Levey, P.R.. (1995), The Mechanistic Involvement of Alloyed Nitrogen In The Corrosion of Stainless Steel, MSc Dissertation, University of the Witwatersrand, pp. 3-30.

Lula, R.A. (1986), Manganese Stainless Steels, The Manganese Centre, France, pp. 22.43, 51-57.

McEwan, J.J. (1994). Corrosion Control in Southern Africa, Corrosion Institute of Southern Africa, South Africa, pp. 25-26.

Moema, J.S., Paton, R. and Papo, M.J. (2005). On the Development of a New Low-Nickel Stainless Steel for Structural and Long Product Application, *Mintek Publication (C4076M)*, Mintek, Randburg, South Africa, p. 1.

Newman, R.C. (2001). Understanding the Corrosion of Stainless Steel, *Corrosion*, Vol. 57, No.12, pp. 1030-1041.

Paton, R., Oliver, D., McEwan, J.J.and Kerr, J. (2004). “AlphaGamma” Estimating Microstructures and Properties in Stainless Steel Alloys, Revision 6, Advanced Materials Division- January 1994, Mintek, Randburg, South Africa.

Peckner, D. and Bernstein, I.M. (1977). Handbook of Stainless Steels, Mc-Graw–Hill Company, pp. 1-2, 4-3, 15-1-15-6.

Pickering, F.B. (1979). The Metallurgical Evolution of Stainless Steels, American Society for Metals: The metals Society, pp. 23-39.

Raja, V.S., Davasenapathi, A., Veluchamy, P. and Minoura, H. (1999). Electron Spectroscopy for Chemical Analysis Study of Corrosion Films Formed on Manganese Stainless Steels, *Corrosion*, Vol. 55, No. 12, pp. 1119-1125.

Rama Rao, P. and Kutumbarao, V. (1989). Developments in Austenitic Steels Containing Manganese, *International Materials Reviews*, Vol. 34, No. 2, pp. 69-85.

Rondelli, G., Vicentini, B. and Cigada, A. (1995). Influence of Nitrogen and Manganese on Localised Corrosion Behaviour of Stainless Steels in Chloride Environments, *Materials and Corrosion*, Vol. 46, pp. 628-632.

Schollenberger, H.J. (1995). The Effects of Delta Ferrite and Sigma Phase on the Mechanical Properties and Corrosion Behaviour of 300 Series Austenitic Stainless Steels, MSc Dissertation. March, Faculty of Engineering, University of The Witwatersrand, Johannesburg, pp. 2-20.

Sedriks, A.J. (1979). Corrosion of Stainless Steels, John Wiley and Sons, Inc., Canada, pp. 9-21.

Sedriks, A.J. (1983). Role of sulphide Inclusions in Pitting and Crevice Corrosion of Stainless Steels, *International Metals Reviews,* Vol. 28, No. 5, pp. 295-306.

Sedriks, A.J. (1986). *National Association of Corrosion Engineers,* vol. 42, July,No. 7, pp. 376-389.

Shams, A.M., Din, E.L., Badran, M.M. and Khalil, S.E. (1999) *Corrosion Behaviour of Manganese-Containing stainless Steels*, Werkstoff und Korrosion, pp.50-56.

Simpson, J. (1990). Guideline on Electrochemical Corrosion Measurement, European Federation of Corrosion, The Institute of Metals, London, pp. 37-39.

Sibanda, M, Vismer, S.L. and Knutsen, R.D. (1994). Consideration of Reduced Nickel Containing Austenitic Stainless Steels for Forming Application, *Materials Letters 21*, pp. 203-207.

Sumita, M., Hanawa T and Teoh, S.H. (2004). Development of Nitrogen- Containing Nickel-Free Austenitic Stainless steels for Metallic Biomaterials, *Materials Science and Engineering:C*, Vol. 24, issues 6-8, December, pp. 753-760.

Tretheway and Chamberlain (2002) Corrosion for Science and Engineering, 2nd Edition, Longman, Harlow Essex.

Turan, Y.N. (1991). Effect on Nitrogen on the Structure and Properties of Type AISI 310 Austenitic stainless Steels, MSc Dissertation, University of the Witwatersrand, Johannesburg.

Vismer, S.L. (1997). The Influence of Copper Addition on the Corrosion Behaviour of Low-Nickel Austenitic Stainless Steels, MSc, University of Cape Town, Cape Town.

Wellbeloved, D. and Stanko, J. (1990). Manganese – A Substitute for Nickel, *Metals Bulletin Monthly*, January, pp. 61- 63.

White, R. (2005). Mintek Commercialisation plan-Project 32434, pp. 2-43.

Appendices

Appendix A:Ferritescope readings and chemical composition of alloys made.

Table A. 1: Ferritescope readings for the buttons and ingots.

	magnetism (%)		
Alloy	**50g buttons**	**50g buttons after reheating at 1050°C**	**5 kg ingots**
1	41.65	28.18	6.8
2	37.02	24.91	2.2
3	47.07	38.2	14.17
4	4.44	19.71	0.81
5	11.43	6.1	0.89
6	29.41	23.56	11.93
7	19.64	12.65	0.38
8	17.68	12.27	2.7
9	30.54	20.53	8.5
10	1.29	*	0
11	0.4	*	0
12	0.21	*	0.61
13	0.48	*	1.01
14	0.79	*	3.8
15	13.52	*	5.2
16	4.06	*	0
17	0.91	*	0
18	0.85	*	0.26

Table A. 2: Composition of 50g buttons

Alloy	C	Mn	Ni	Mo	N	Cr
1	0.023	4.78	1.89	0.39	0.17	15.9
2	0.019	4.51	1.84	0.86	0.2	16.3
3	0.029	3.74	1.88	1.77	0.14	16.1
4	0.026	4.34	1.92	0.45	0.18	16.3
5	0.027	5.21	2.2	0.89	0.12	17
6	0.026	4.08	1.88	1.86	0.21	16.4
7	0.026	8.08	1.92	0.4	0.15	16.4
8	0.03	9.42	1.87	0.79	0.14	16
9	0.027	9.05	1.85	1.67	0.18	16.1
10	0.03	9.55	1.91	0.37	0.26	16.1
11	0.031	9.09	1.89	0.78	0.365	16.1
12	0.016	9.2	1.9	1.75	0.43	16.4
13	0.033	11	1.89	0.38	0.47	16.6
14	0.037	14.8	1.78	0.75	0.6	15.8
15	0.03	13.5	1.79	1.48	0.21	16.1
16	0.02	13.3	1.85	0.35	0.36	16
17	0.034	14.2	1.8	0.73	0.39	16
18	0.027	14.4	1.74	1.51	0.44	15.8
***201**	0.1	6.5	5	-	0.15	17
***304**	0.04	1.5	8.5	-	0.05	18.3
***Hercules™**	0.05	9	2	-	0.25	16.5

* Values for the reference alloys as cited on the Hercules™ data sheet [Moema and Papo, 2005, Mintek].
- Typically no Mo in these alloys

Table A. 3: Composition of 5 kg ingots

Alloy	C	Mn	Ni	Mo	N	Cr
1	0.036	5.02	2.19	0.44	0.12	15.4
2	0.036	4.89	2.21	0.92	0.12	15.6
3	0.03	5.02	2.09	1.79	0.13	15.7
4	0.031	4.91	2.22	0.45	0.17	15.6
5	0.034	4.92	2.1	0.85	0.16	15.7
6	0.036	5.42	1.98	1.79	0.145	15.8
7	0.027	9.33	2.1	0.52	0.14	15.9
8	0.019	9.12	2.09	1	0.13	15.7
9	0.028	9.36	2.11	1.82	0.14	15.7
10	0.032	8.93	2.24	0.43	0.18	15.5
11	0.028	9.04	2.19	0.86	0.19	15.9
12	0.043	9.09	2.21	1.77	0.215	16
13	0.019	14.7	2.12	0.49	0.15	16
14	0.021	15	2.15	0.84	0.15	16.2
15	0.024	15	2.23	1.73	0.18	15.8
16	0.029	15.4	2.23	0.46	0.25	15.9
17	0.028	15.8	2.2	0.8	0.24	15.9
18	0.038	15.5	2.21	1.67	0.25	16
***201**	0.1	6.5	5	-	0.15	17
***304**	0.04	1.5	8.5	-	0.05	18.3
***Hrecules™**	0.05	9	2	-	0.25	16.5

* Values for the reference alloys as cited on the Hercules™ data sheet[Moema and Papo, 2005, Mintek].
- Typically no Mo in these alloys

Graphs of the chemical composition

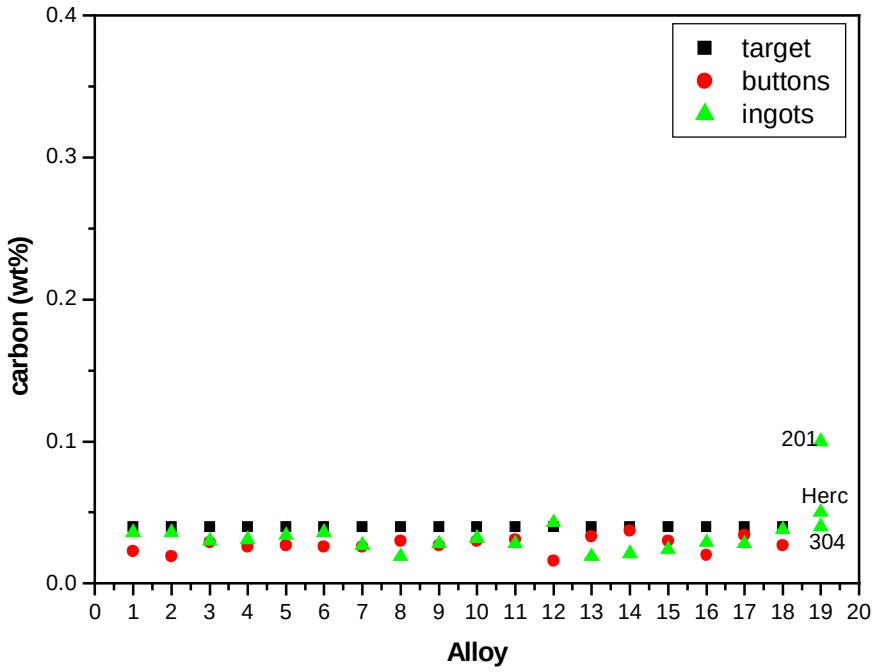

Figure A. 1: Carbon content of alloys made.

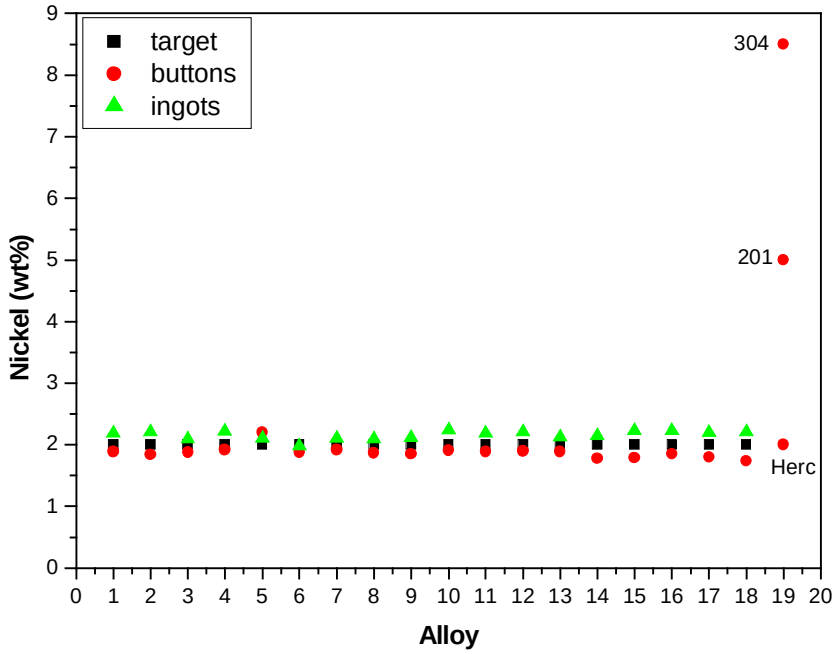

Figure A. 2: Nickel content of alloys made.

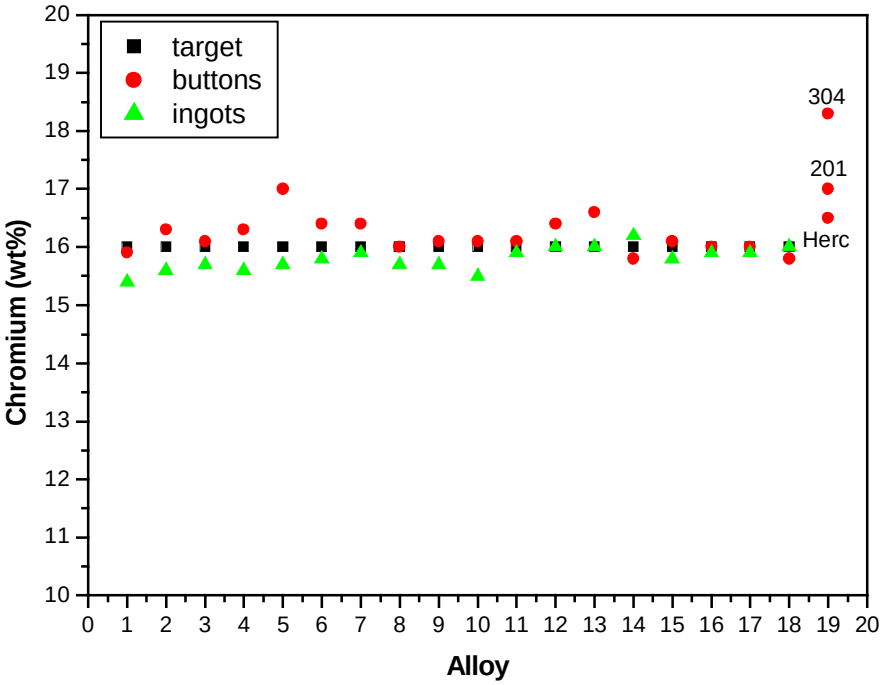

Figure A. 3: Chromium content of alloys made.

Appendix B: Rolling history of alloys.

Table B. 1: Rolling history of 50g buttons.

alloy	thickness	ferrite%	alloy	thickness	Magnetism (%)
alloy 1	6.86-->6.55(annealed-4hrs-furnace cool)	27.4	alloy 11	6.86-->6.46	0.56
	6.55 -->6.09	37.13		6.46--->5.90	1.24
				5.90--->4.48	4.41
alloy 2	7.40-->6.50	39.99			
	6.50-->4.49	64.94	alloy 12	7.69-->6.55	0.84
				6.55-->5.96	1.28
alloy 3	7.93-->6.91	54.12		5.96-->4.44	1.96
	6.91-->4.42	66.33			
			alloy 13	7.16-->6.40	0.59
alloy 4	10.99-->8.25	24.85		6.40-->5.88	0.28
	8.25-->6.41	28.9		5.88-->4.46	0.46
	6.41-->5.45-cracked-annealed at 1050-1hr	54.06			
	5.45-->4.66	36.21	alloy 14	7.06-->6.42	0.7
				6.42-->5.93	0.76
alloy 5	8.78-->6.44	10.6		5.93-->4.49	0.41
	6.44-->4.50	37.16	alloy 15	7.39-->6.67	8.85
				6.67-->6.01	10.23
alloy 6	7.50-->6.47	38.9		6.01-->4.49	10.83
	6.47-->4.84 cracked+annealed @1050 for 1 hr	57.49			
	4.84-->4.76	17.21	alloy 16	7.13-->6.55	3.36
				6.55-->6.03	3.49
alloy 7	7.63-->6.46	18.53		6.03-->4.49	4.3
	6.46-->4.46	49.5			
			alloy 17	8.26-->6.68	1
alloy 8	7.58-->6.45	14.73		6.68-->6.03	1.12
	6.45-->4.49	35.09		6.03-->4.50	2.29
alloy 9	7.18-->6.44	20.24	alloy 18	7.99-->6.35	1.53
	6.44-->4.47	33.52		6.35-->4.49	1.55
alloy 10	7.84 -->6.62	3.89			
	6.62 --->6.04	13.15			
	6.04 --->4.50	24.1			

Table B. 2: Hardness of 5 kg ingots

Alloy	hardness (Hv)
1	239
2	207.3
3	216.4
4	215.6
5	214.7
6	223.4
7	188
8	204.2
9	202.6
10	228
11	196.6
12	200.3
13	170
14	173
15	185.9
16	184.6
17	181.9
18	190.1
***201**	210
***304**	176
***Hercules ™**	260

*Values as cited in MINTEK communication C4105M pp. 50 [Moema and Papo, 2005].

Appendix C: Microstructural analysis of the ingots.

Alloy	Microstructure obtained using 10% oxalic acid	Microstructure obtained using KOH
Alloy 1	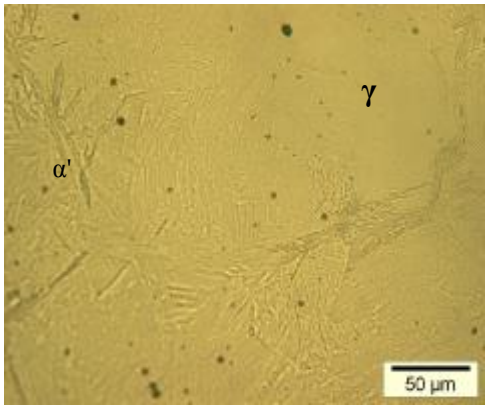	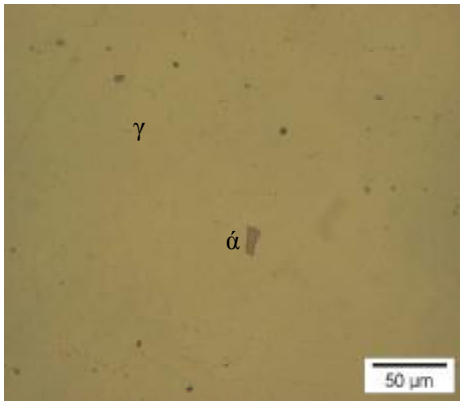
Alloy 2	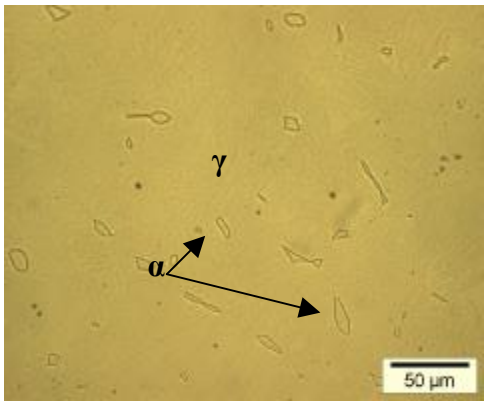	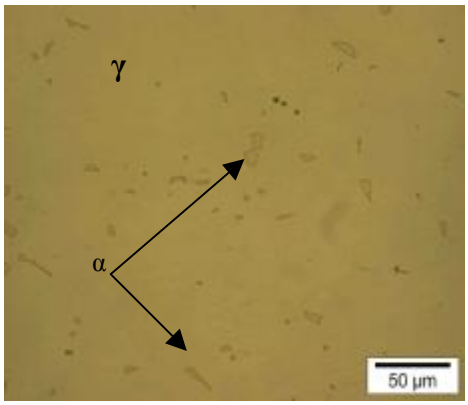
Alloy 3	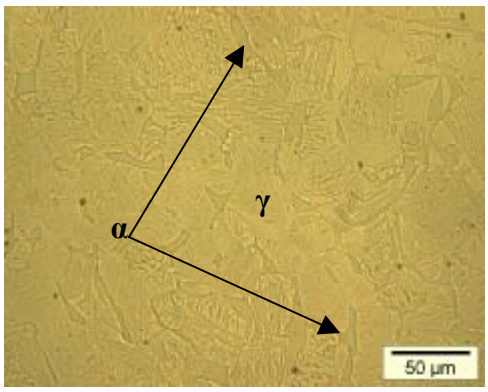	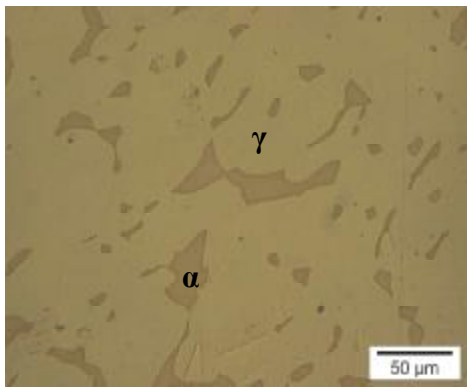

Alloy 4	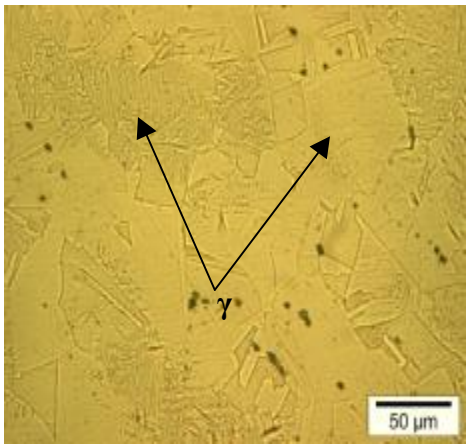	No ferrite was detected with KOH.
Alloy 5	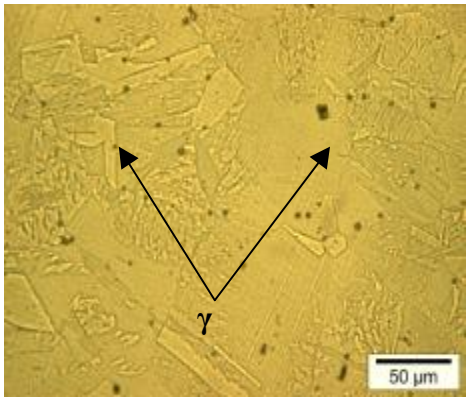	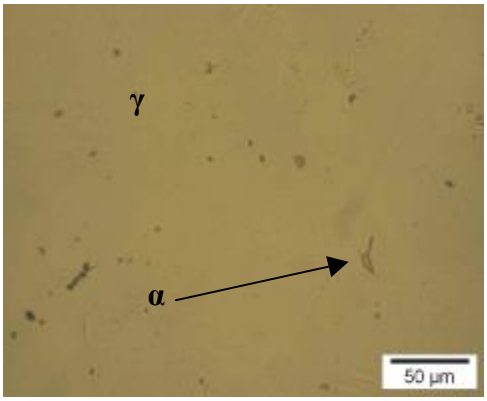
Alloy 6	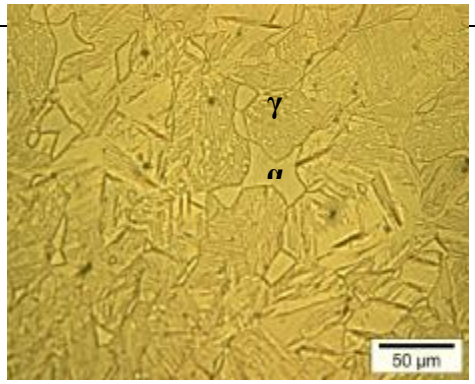	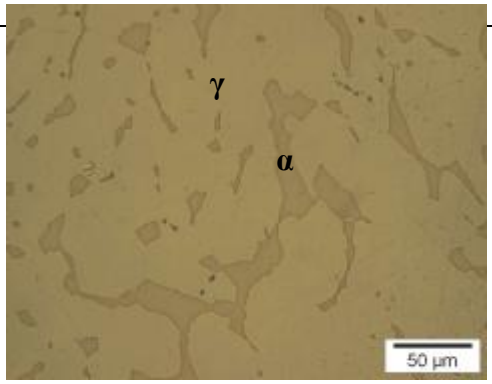

Alloy 7	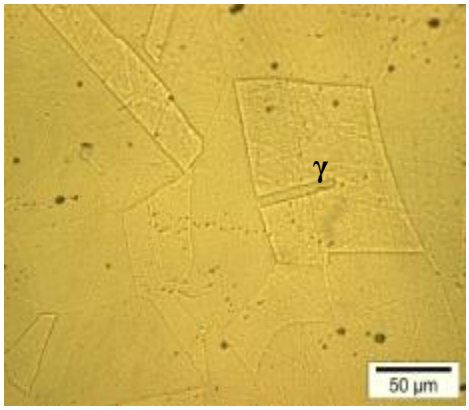	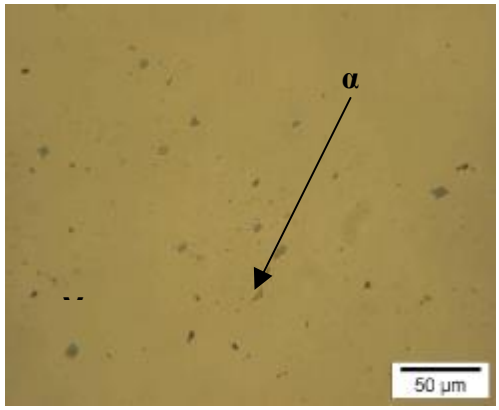
Alloy 8	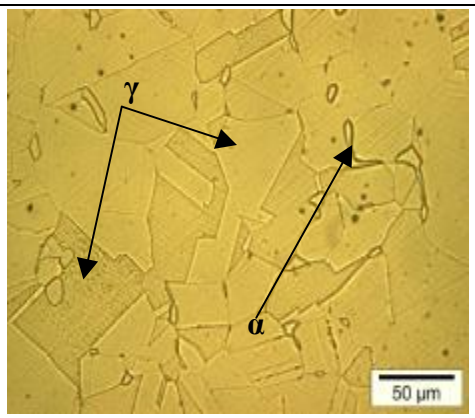	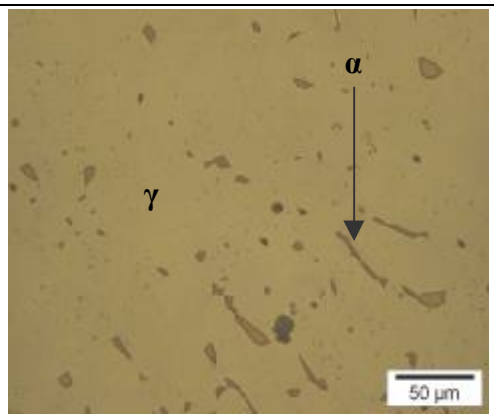
Alloy 9	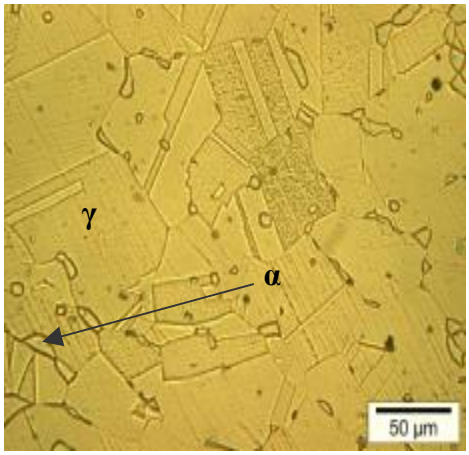	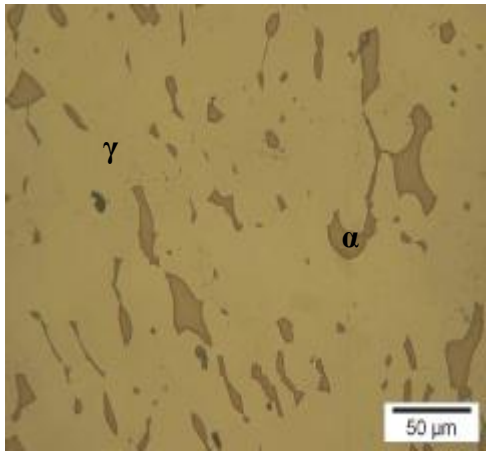

Alloy 10	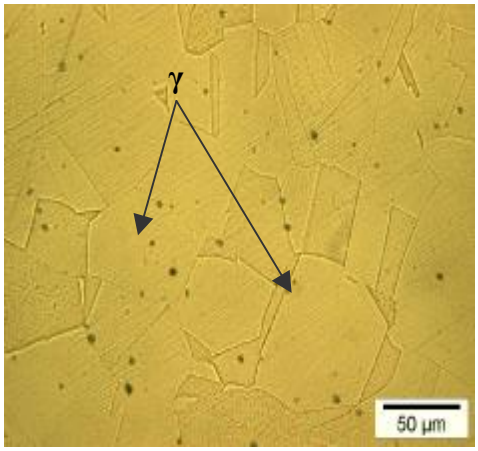	**No ferrite was detected with KOH**
Alloy 11	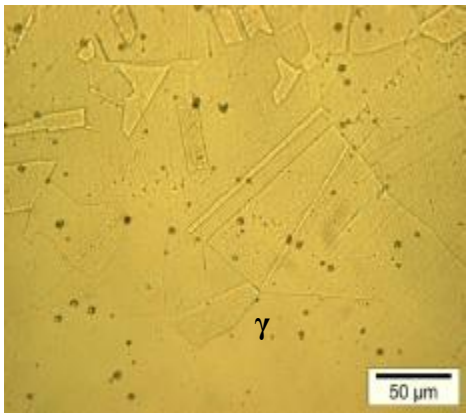	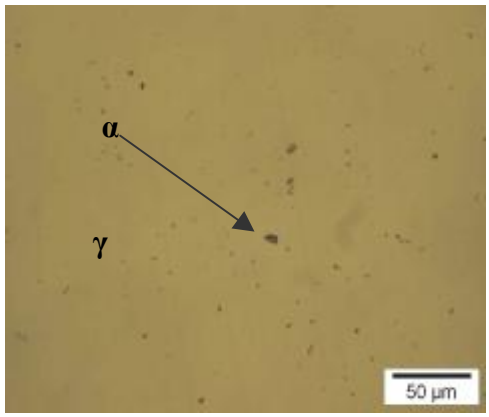
Alloy 12	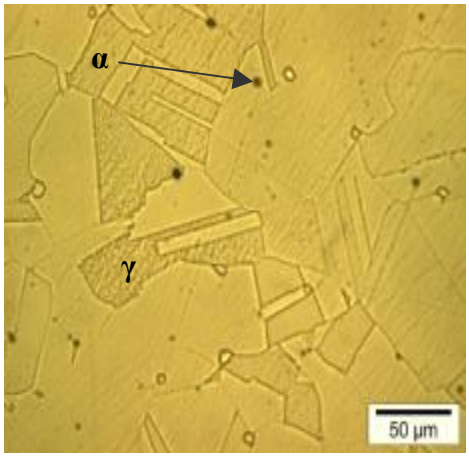	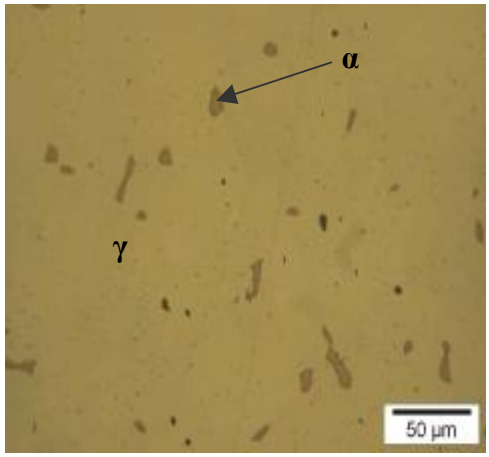

Alloy 13	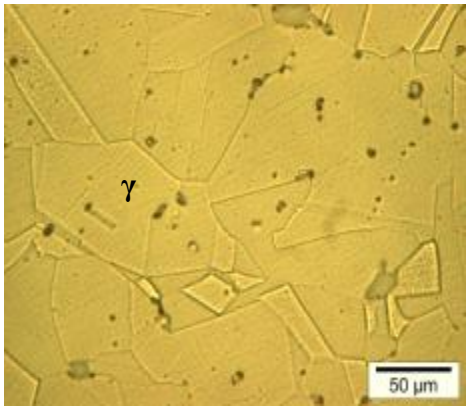	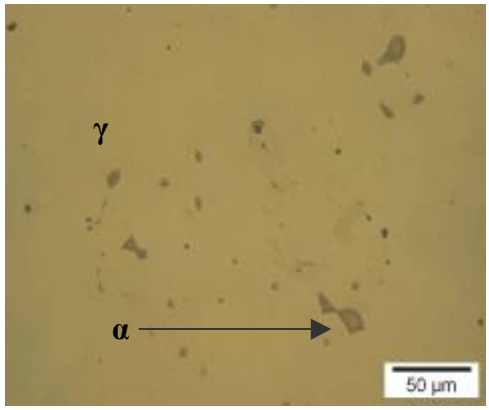
Alloy 14	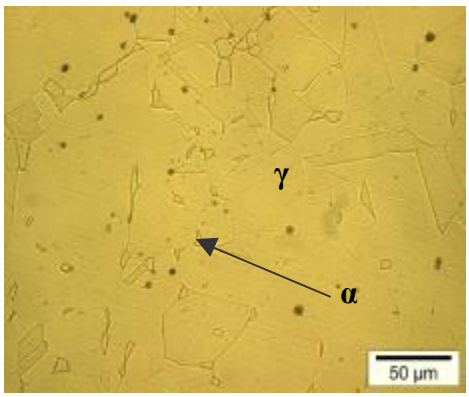	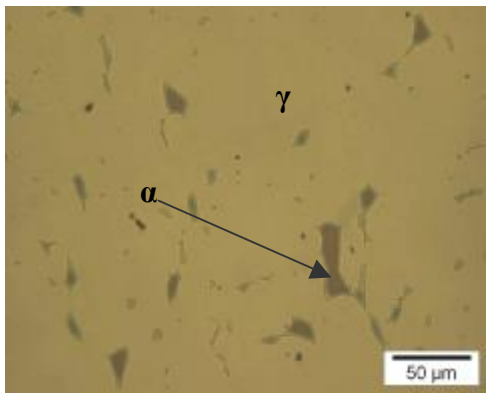
Alloy 15	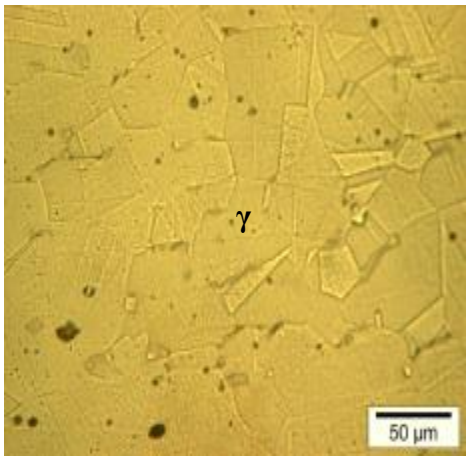	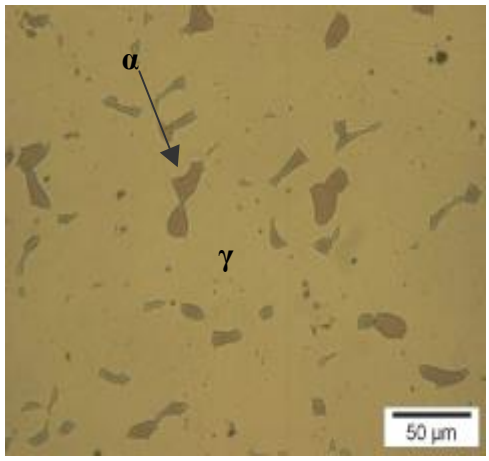

Alloy 16	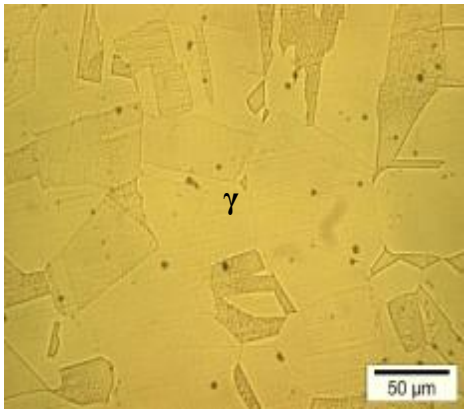	No ferrite detected with KOH
Alloy 17	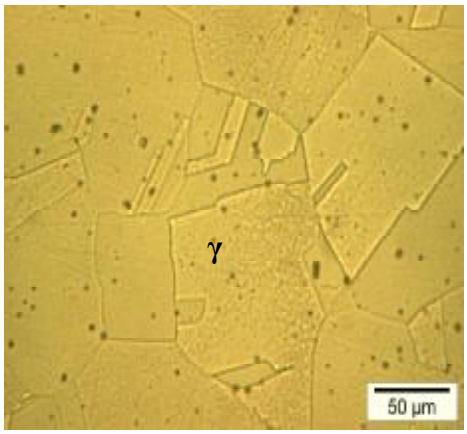	No ferrite detected with KOH.
Alloy 18	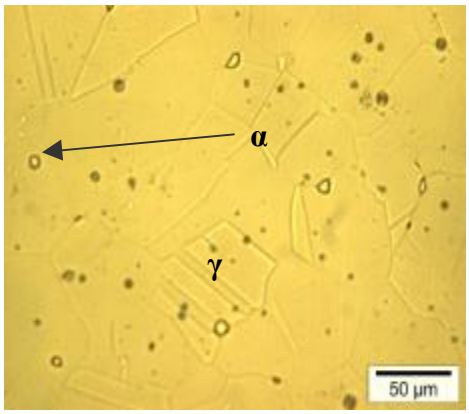	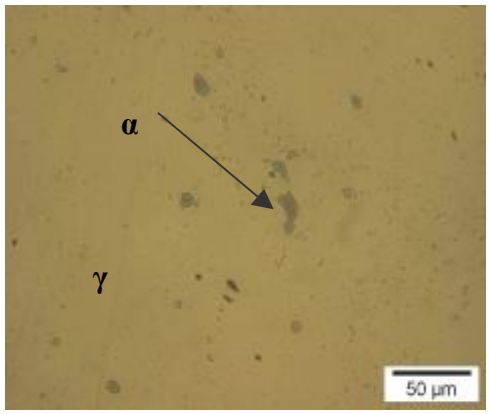

Appendix D: Results of potentiodynamic scans obtained for the buttons.

Table D. 1: Corrosion results for the 50g buttons.

alloy	corrosion rate (mm/y)	I_{corr}(A/m^2)	I_{pass} (A/m^2)	i_{crit} (A/m^2)
1	13.25	12.45	0.21	25.99
2	12.34	11.58	0.18	22.22
3	8.14	7.55	0.20	9.63
4	18.94	17.83	0.42	30.10
5	16.63	15.65	4.56	19.26
6	5.38	5.00	0.41	20.92
7	18.56	17.50	0.35	28.00
8	13.86	12.99	0.57	13.72
9	5.90	5.49	0.40	3.94
10	14.09	13.26	0.40	2.52
11	10.63	9.89	0.24	0.48
12	1.70	1.58	0.55	2.20
13	1.56	1.63	0.37	3.09
14	0.89	0.95	0.17	0.86
15	0.55	0.58	0.30	0.62
16	1.17	1.23	0.19	0.90
17	2.22	2.36	0.32	3.62
18	0.91	0.96	0.16	0.98
*201	8.30	8.02	0.090	9.5
*304	2.80	2.71	0.077	4.9
*herc	35.0	33.82	0.085	32.8

* Values for the reference alloys as cited in Mintek Communication C4105M [Moema and Papo, 2005, Mintek, pp. 54].

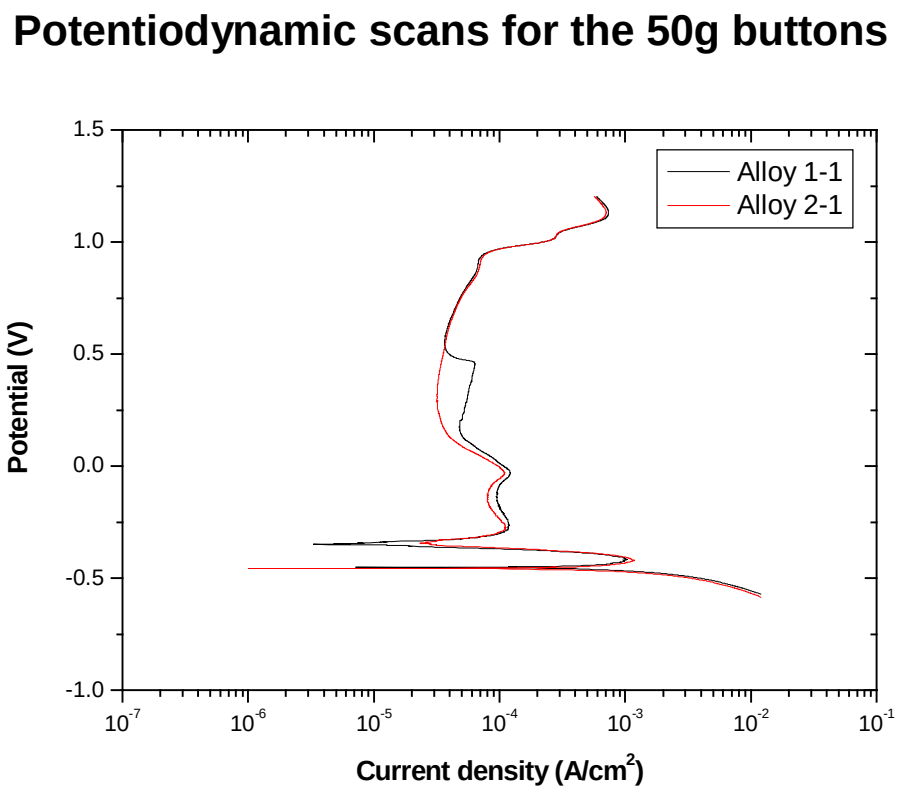

Figure D. 1: Scan obtained for button 1.

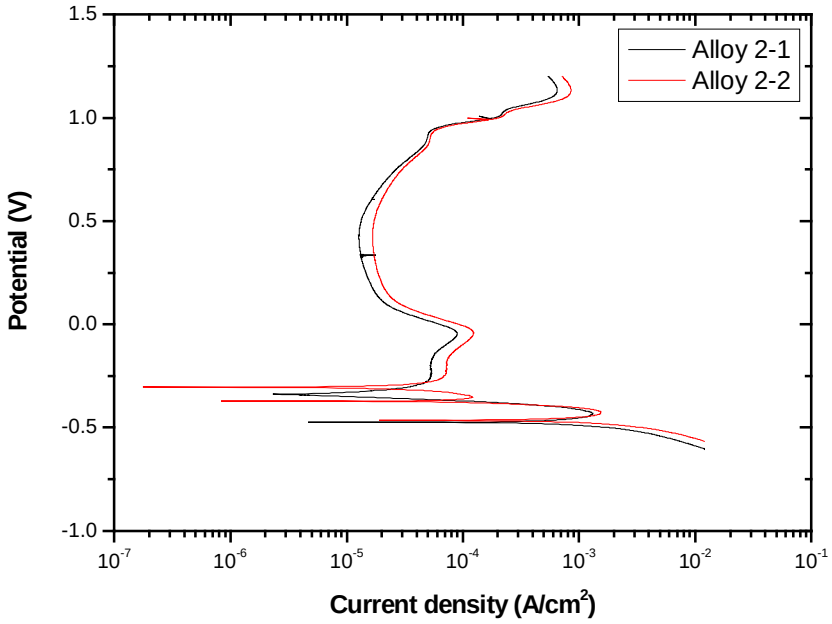

Figure D. 2: Scans obtained for button 2.

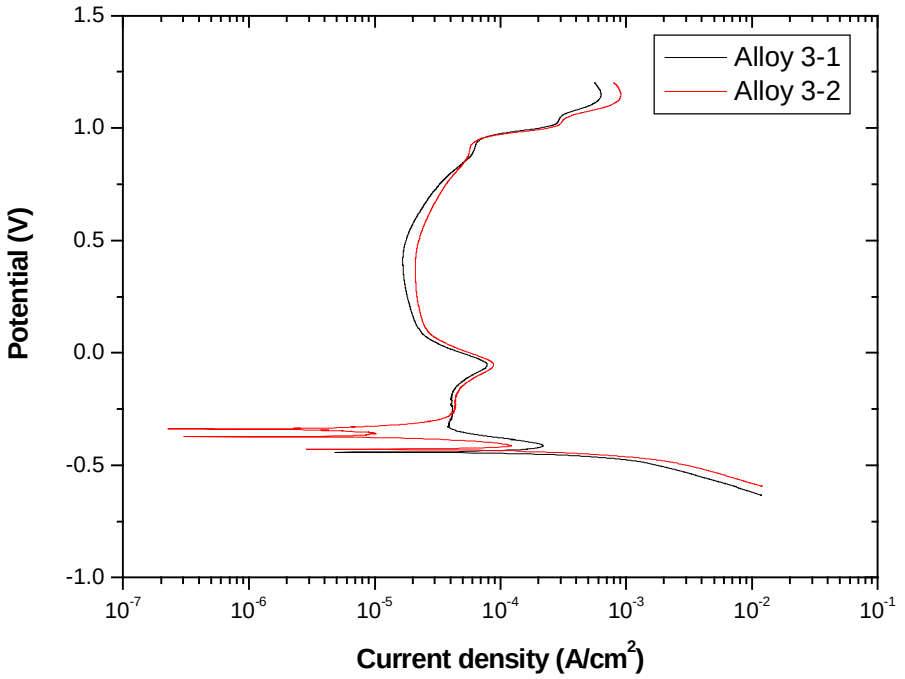

Figure D. 3: Scans obtained for button 3.

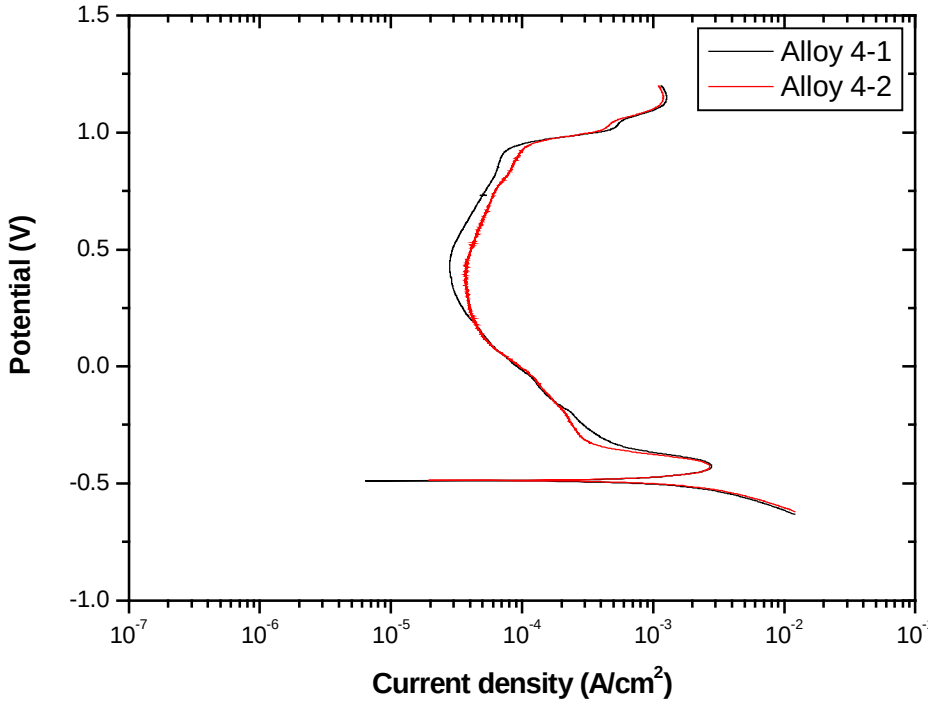

Figure D. 4: Scans obtained for button 4.

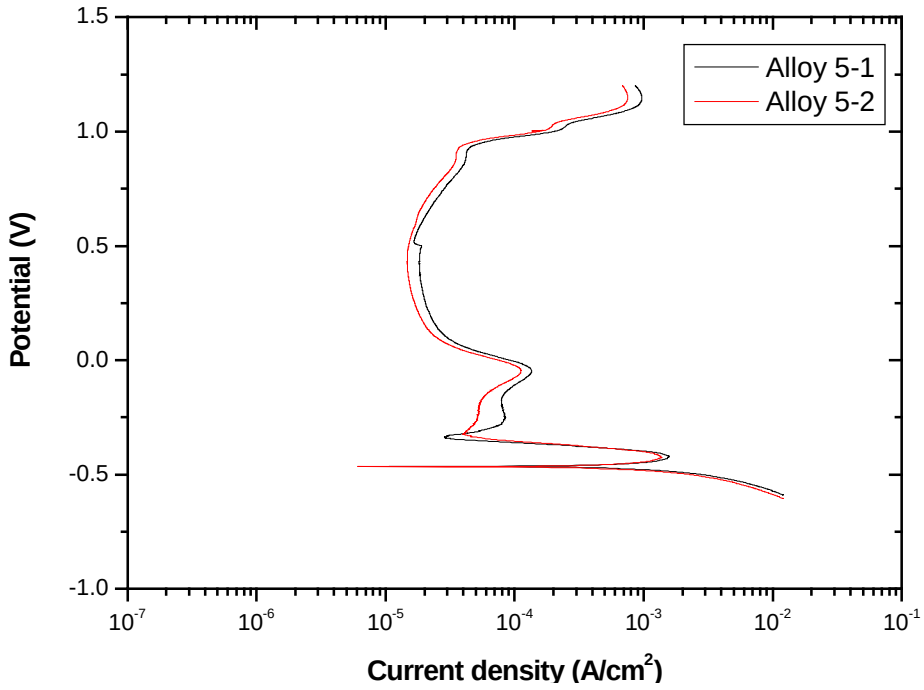

Figure D. 5: Scans obtained for button 5.

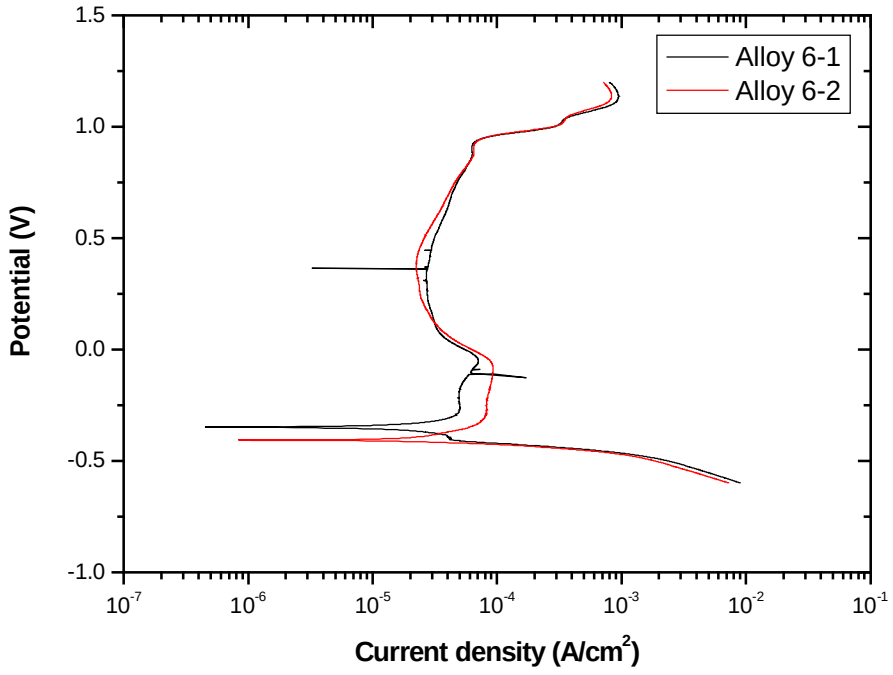

Figure D. 6: Scans obtained for button 6.

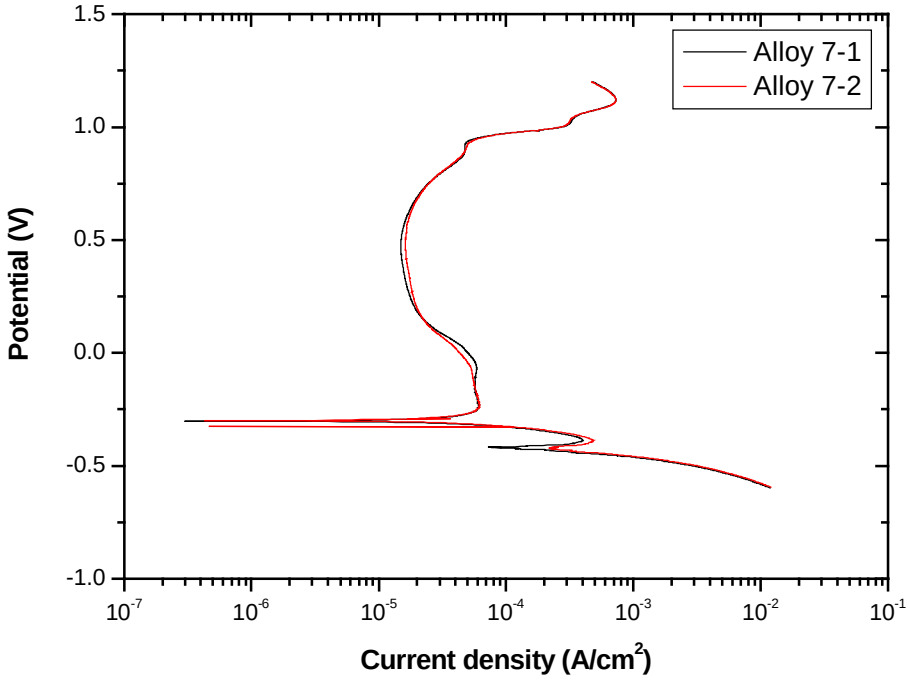

Figure D. 7: Scans obtained for button 7.

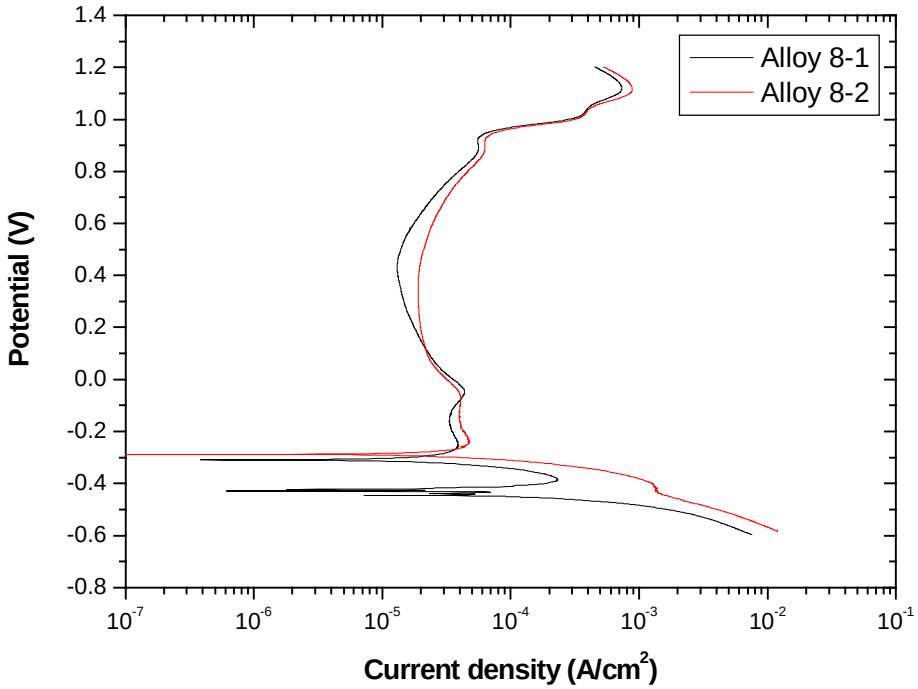

Figure D. 8: Scans obtained for button 8.

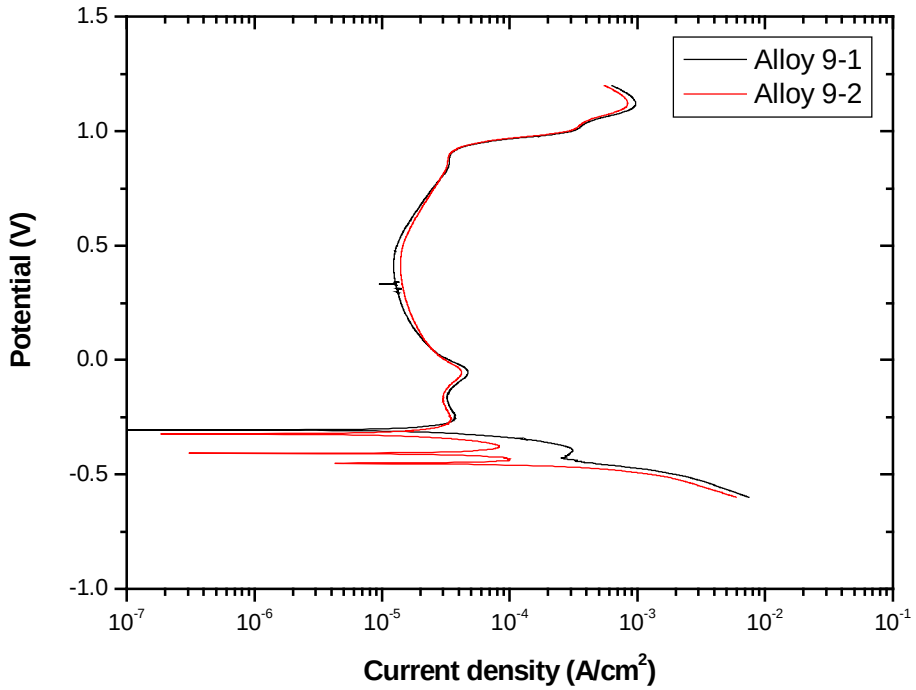

Figure D. 9: Scans obtained for button 9.

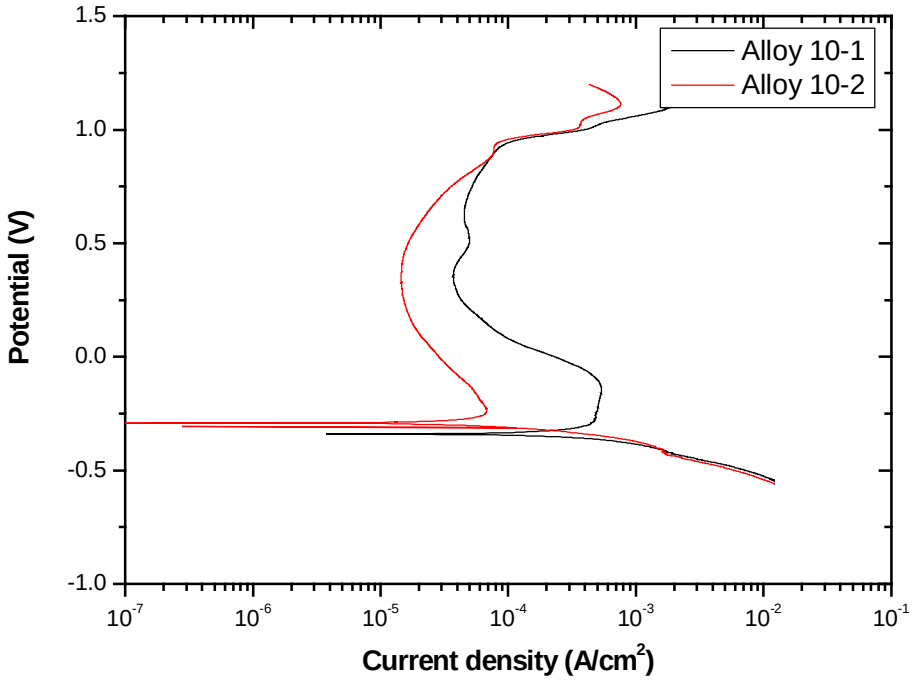

Figure D. 10: Scans obtained for button 10.

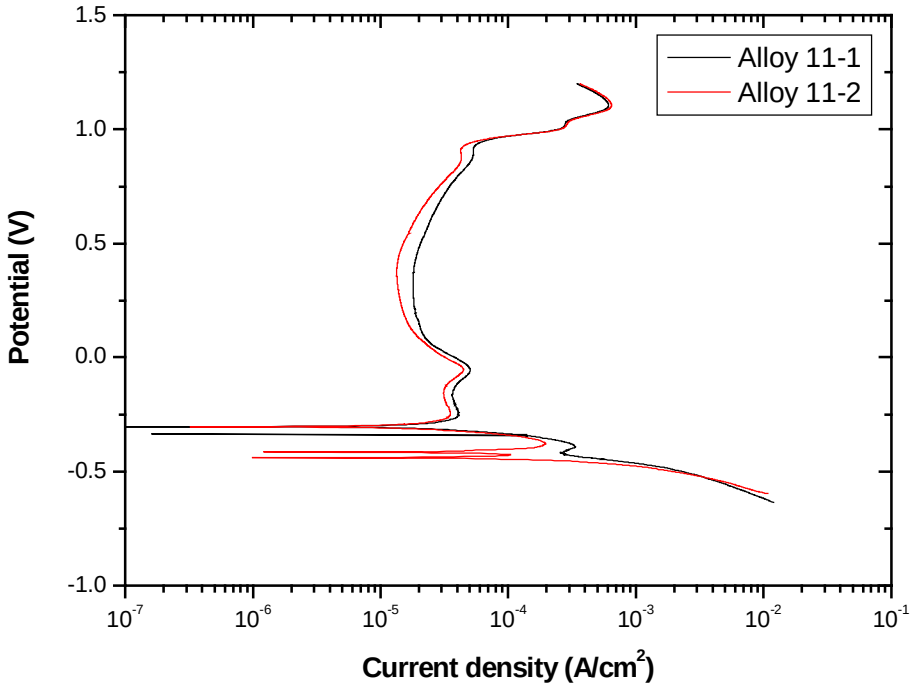

Figure D. 11: Scans obtained for button 11.

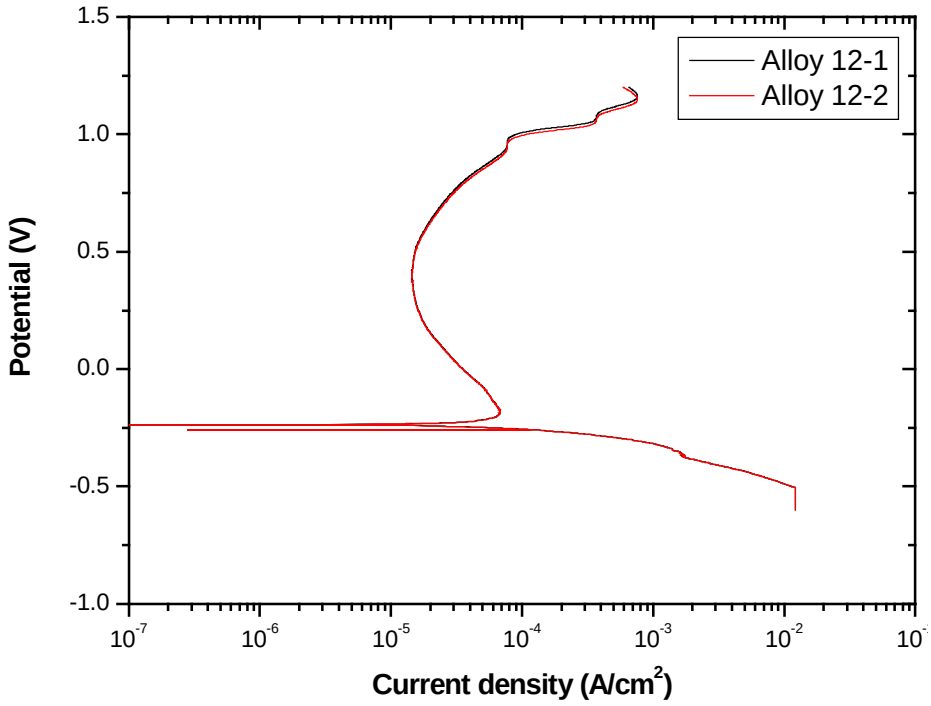

Figure D. 12: Scans obtained for button 12.

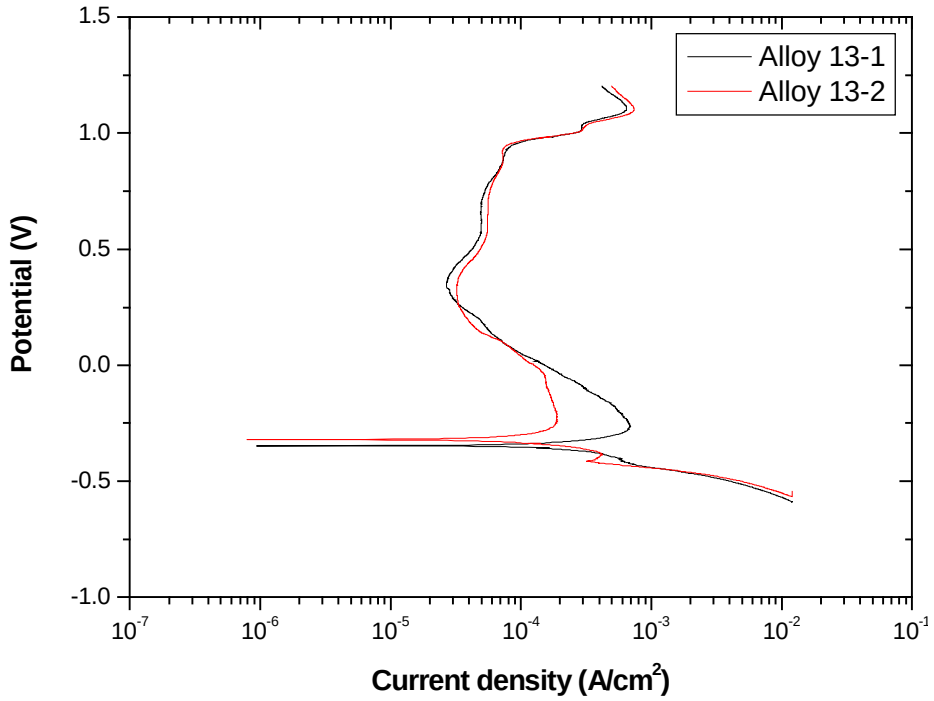

Figure D. 13: Scans obtained for button 13.

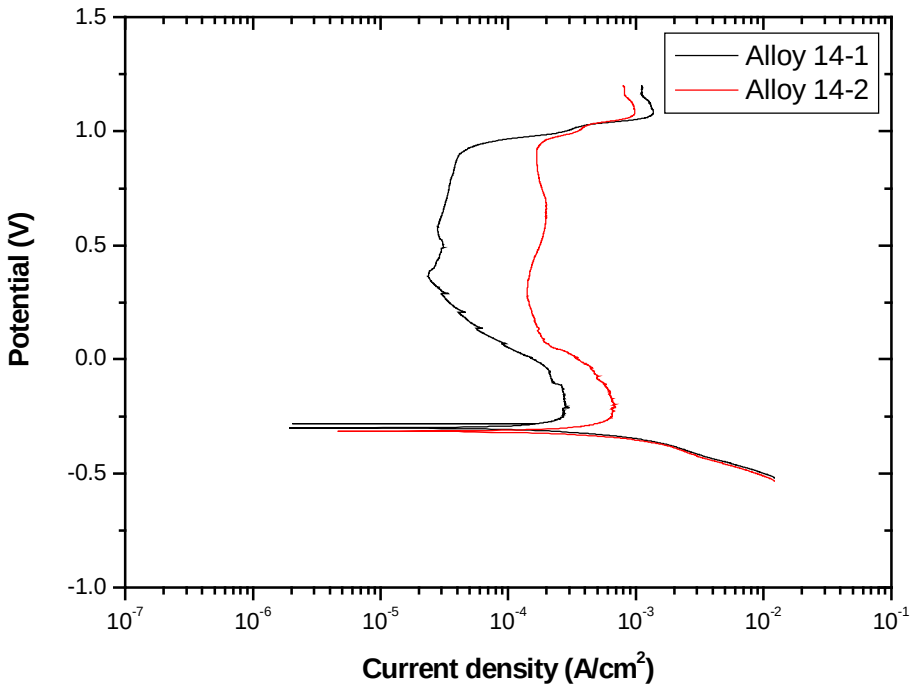

Figure D. 14: Scans obtained for button 14.

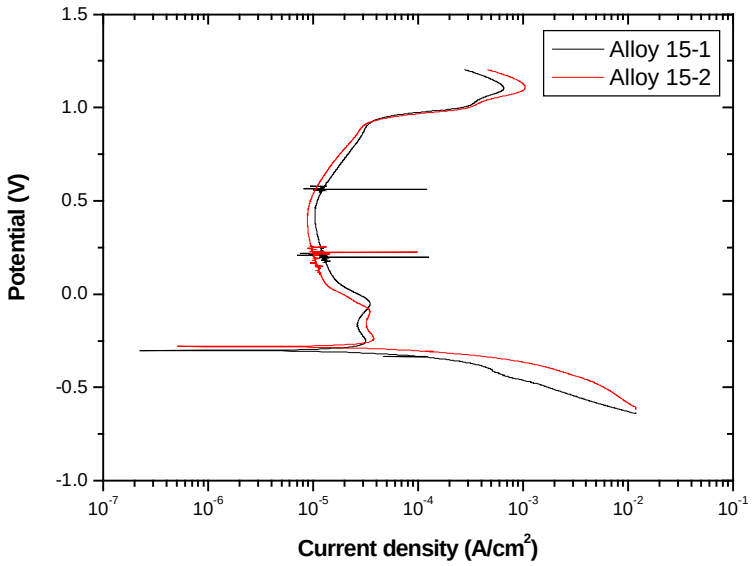

Figure D. 15: Scans obtained for button 15.

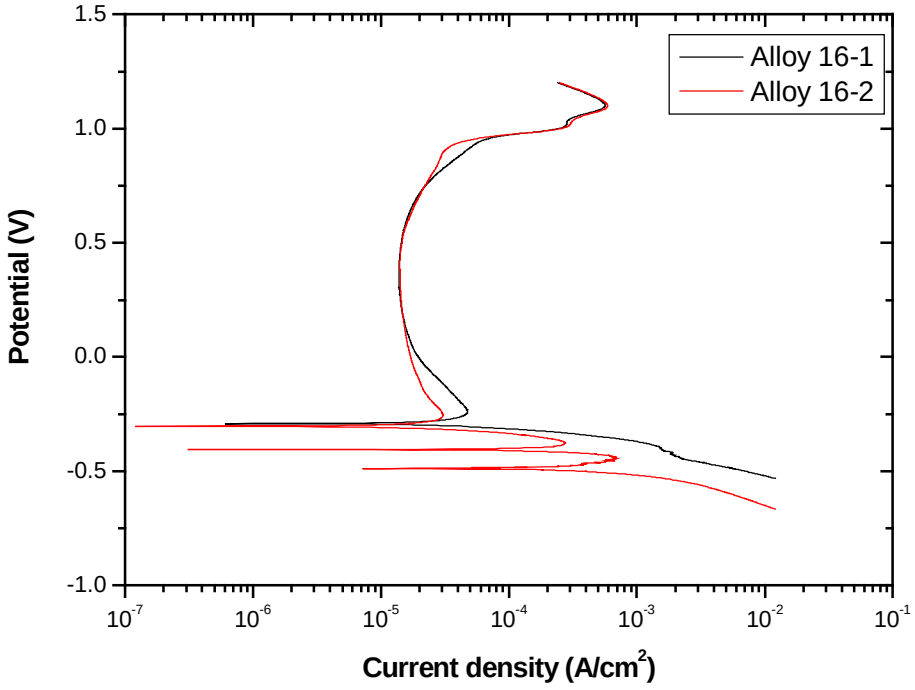

Figure D. 16: Scans obtained for button 16.

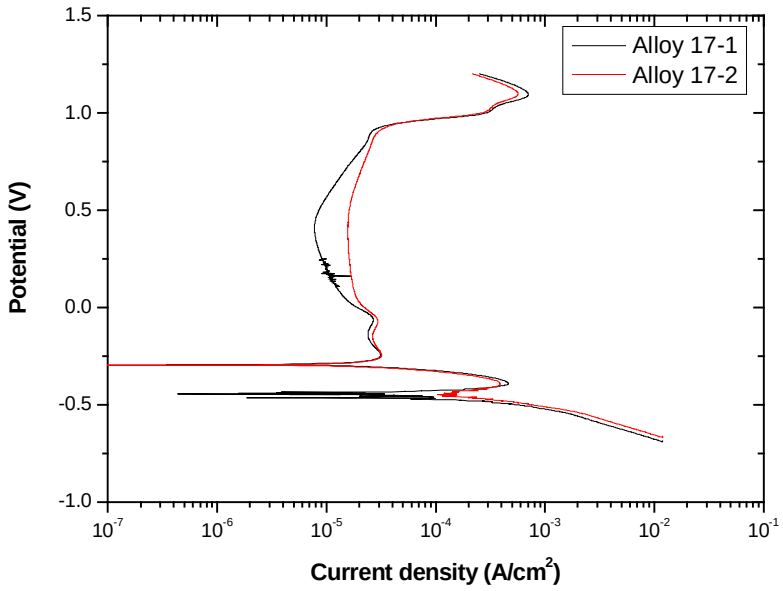

Figure D. 17: Scans obtained for button 17.

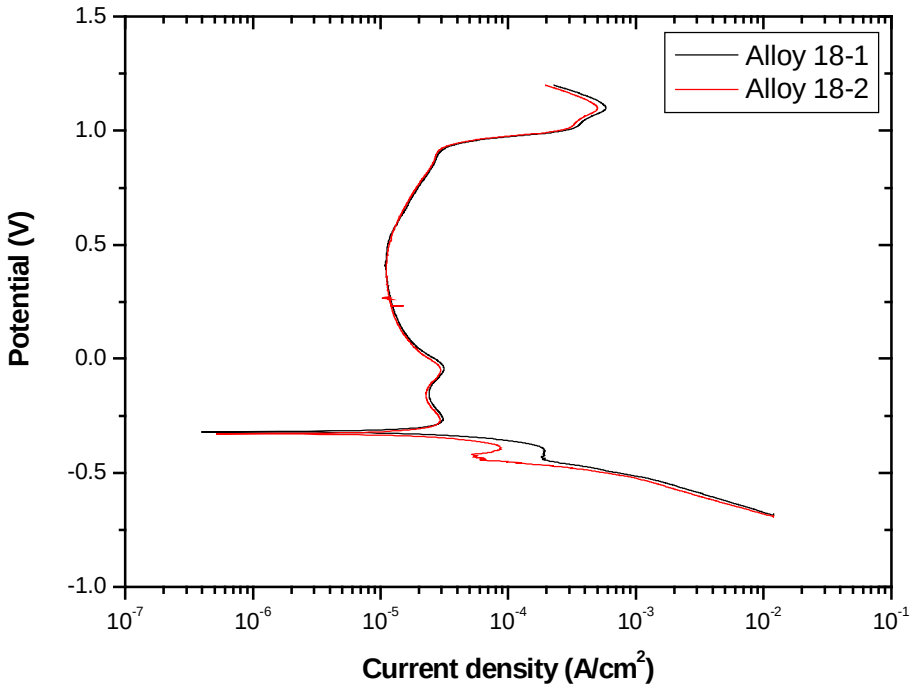

Figure D. 18: Scans obtained for button 18.

Appendix E: Results of potentiodynamic scans obtained for the ingots.

Table E. 1: Corrosion results for the 5 kg ingots.

alloy	corrosion rate (mm/y)	i_{corr}(A/m^2)	i_{pass} (A/m^2)	i_{crit} (A/m^2)
1	9.47	8.89	0.01	4.45
2	12.71	11.92	0.01	5.96
3	0.30	0.28	0.01	0.14
4	11.61	10.93	0.01	5.47
5	7.16	6.73	0.01	3.37
6	5.61	5.21	0.05	2.63
7	0.29	0.27	0.02	0.14
8	5.64	5.29	0.01	2.65
9	0.22	0.21	0.01	0.11
10	0.17	0.16	0.01	0.08
11	0.17	0.15	0.01	0.08
12	0.16	0.14	0.01	0.08
13	0.12	0.12	0.01	0.07
14	0.11	0.12	0.01	0.07
15	0.07	0.08	0.01	0.04
16	0.10	0.11	0.01	0.06
17	0.11	0.12	0.01	0.06
18	0.05	0.05	0.01	0.03
***201**	8.30	8.02	0.090	9.5
***304**	2.80	2.71	0.077	4.9
***Herc**	35.0	33.82	0.085	32

* Values for the reference alloys as cited in Mintek Communication C4105M [Moema and Papo, 2005, Mintek, pp. 54].

Potentiodynamic scans for the 5kg ingots

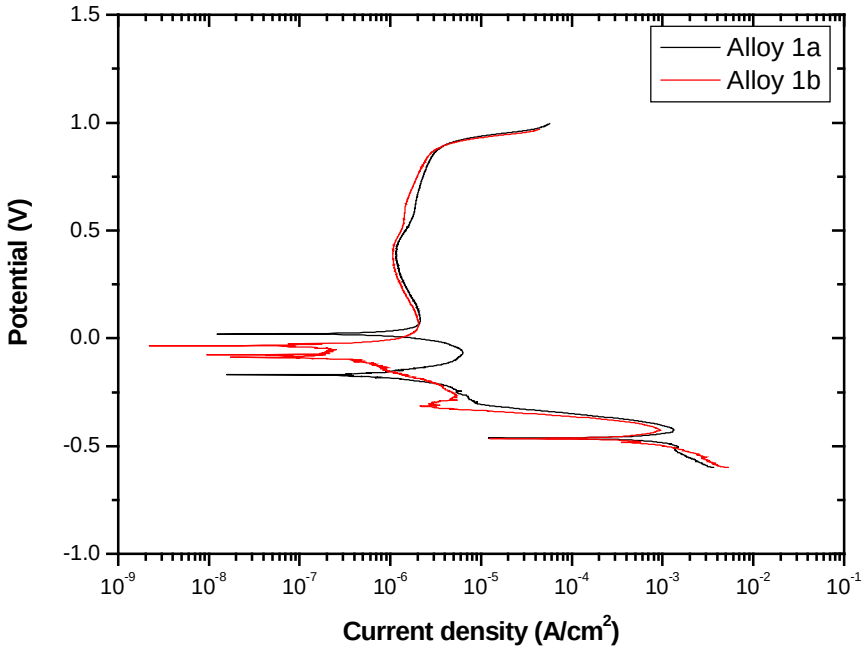

Figure E. 1: Scans obtained for ingot 1..

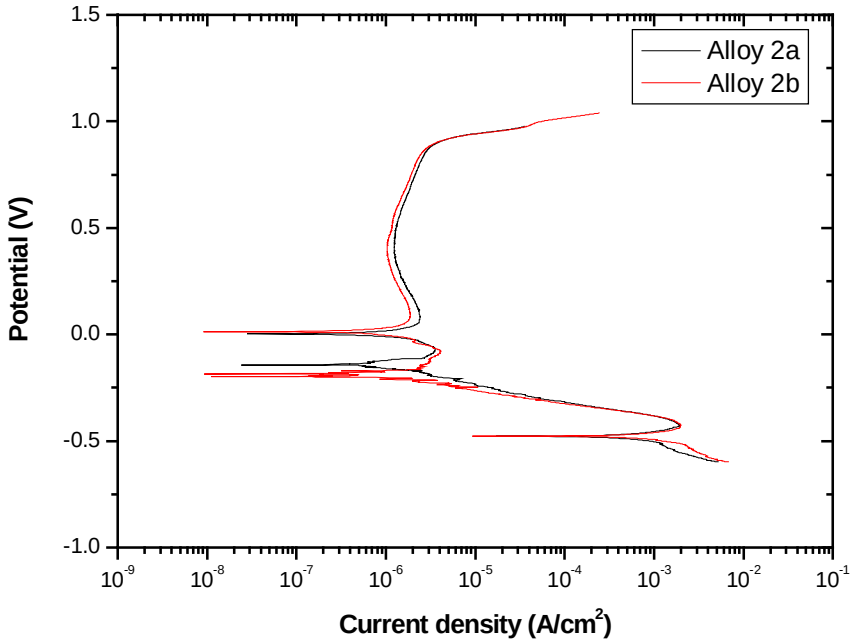

Figure E. 2: Scans obtained for ingot 2.

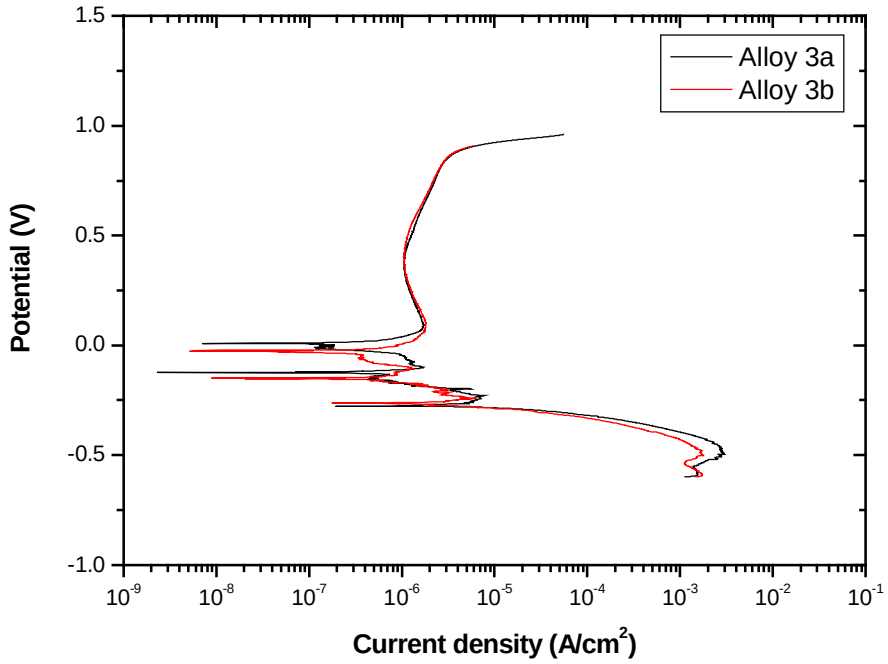

Figure E. 3: Scans obtained for ingot 3.

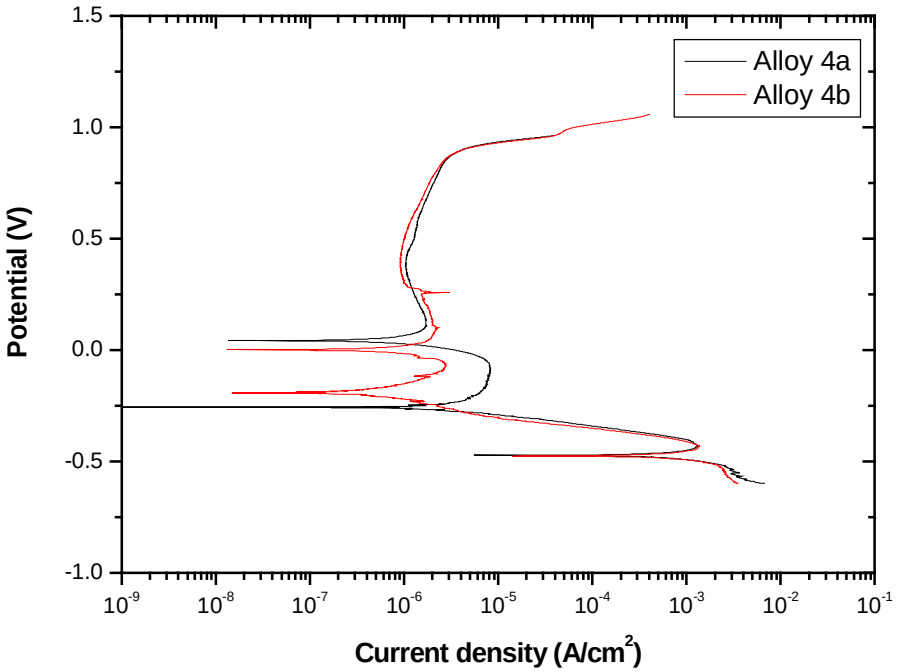

Figure E. 4: Scans obtained for ingot 4.

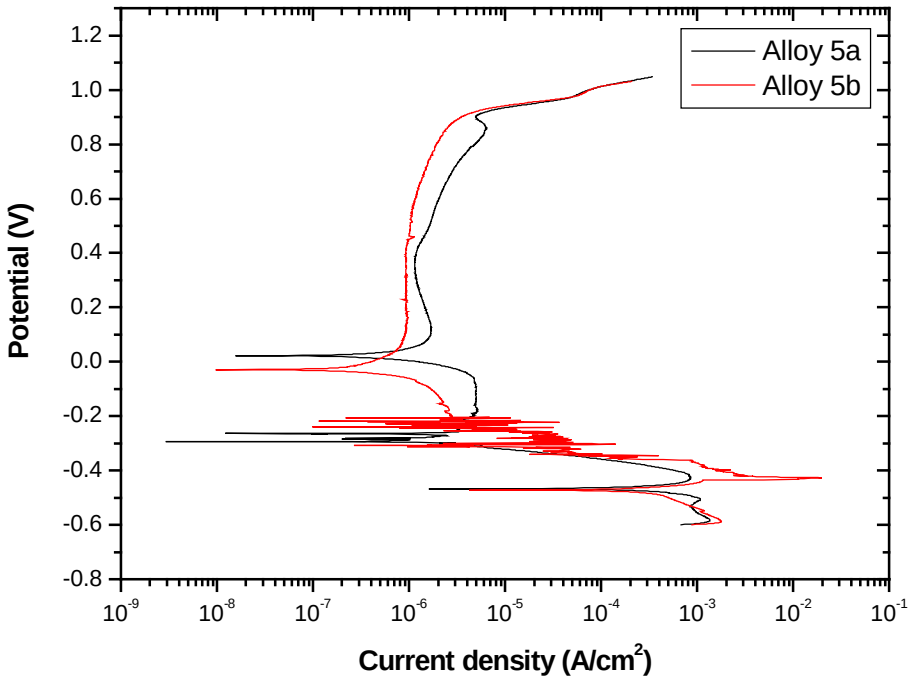

Figure E. 5: Scans obtained for ingot 5.

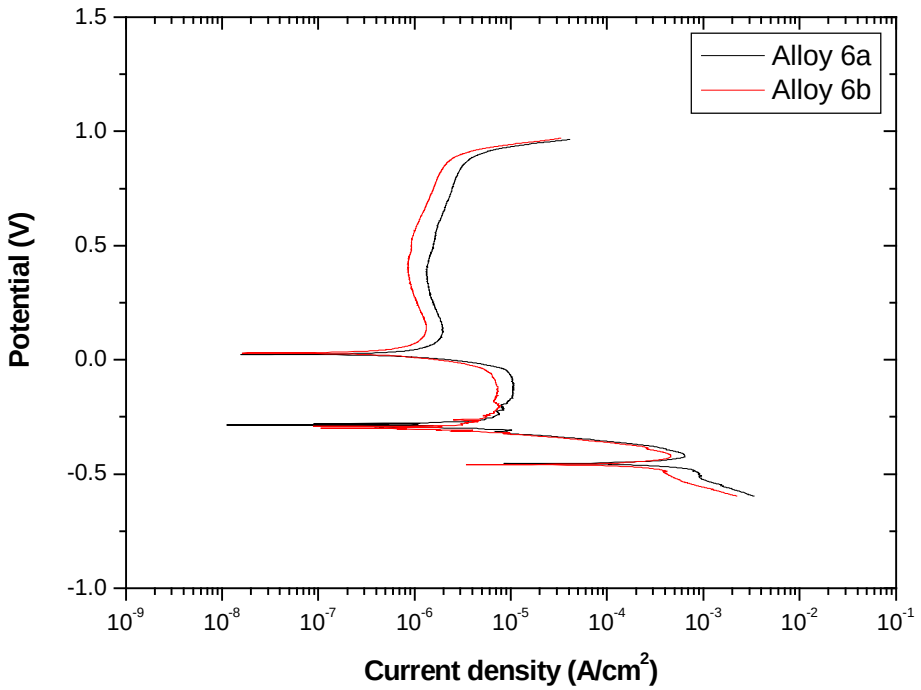

Figure E. 6: Scans obtained for ingot 6.

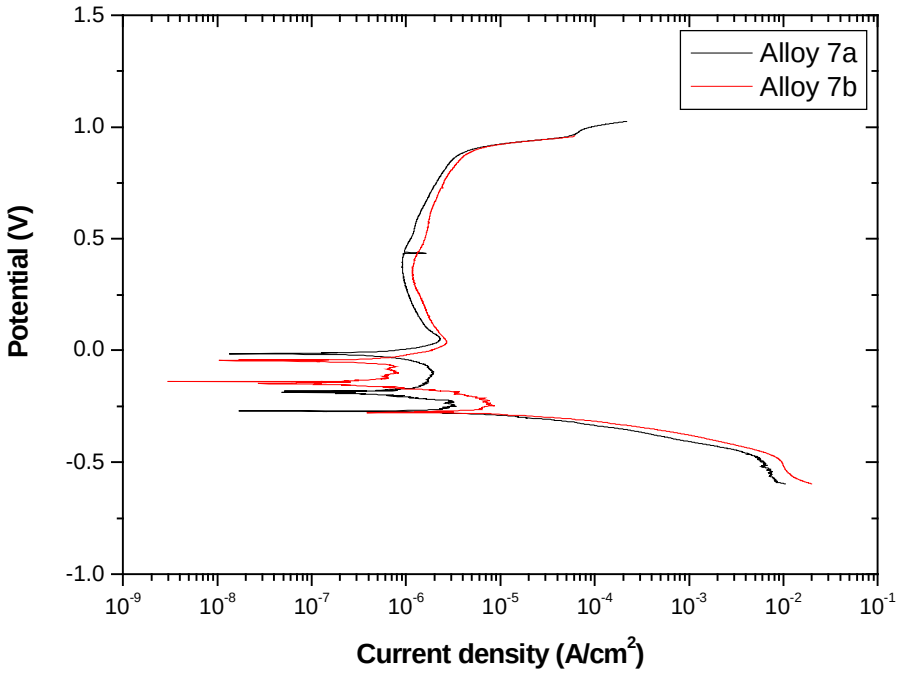

Figure E. 7: Scans obtained for ingot 7.

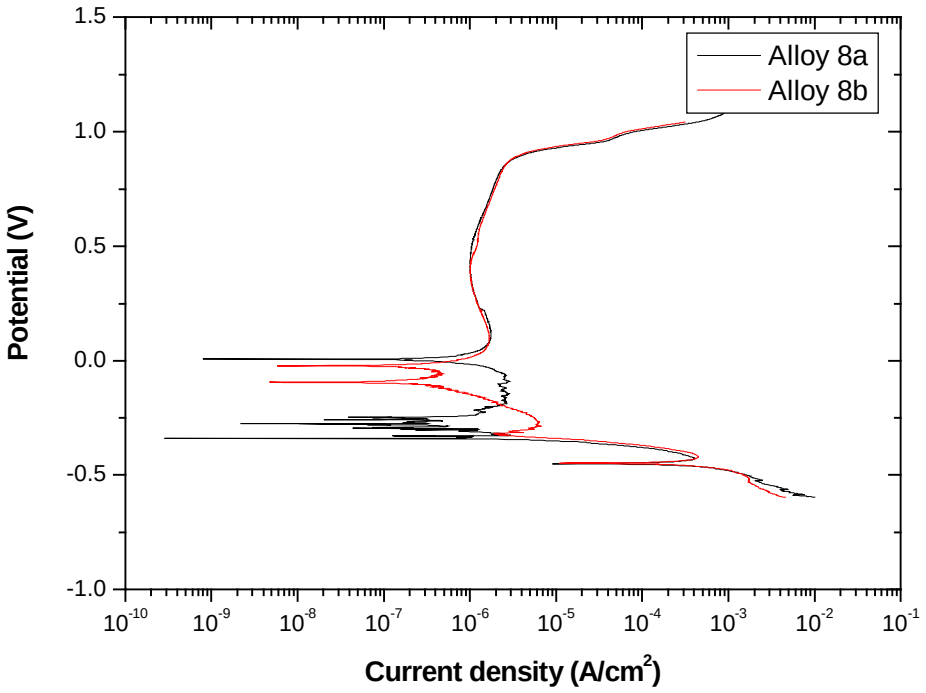

Figure E. 8: scans obtained for ingot 8.

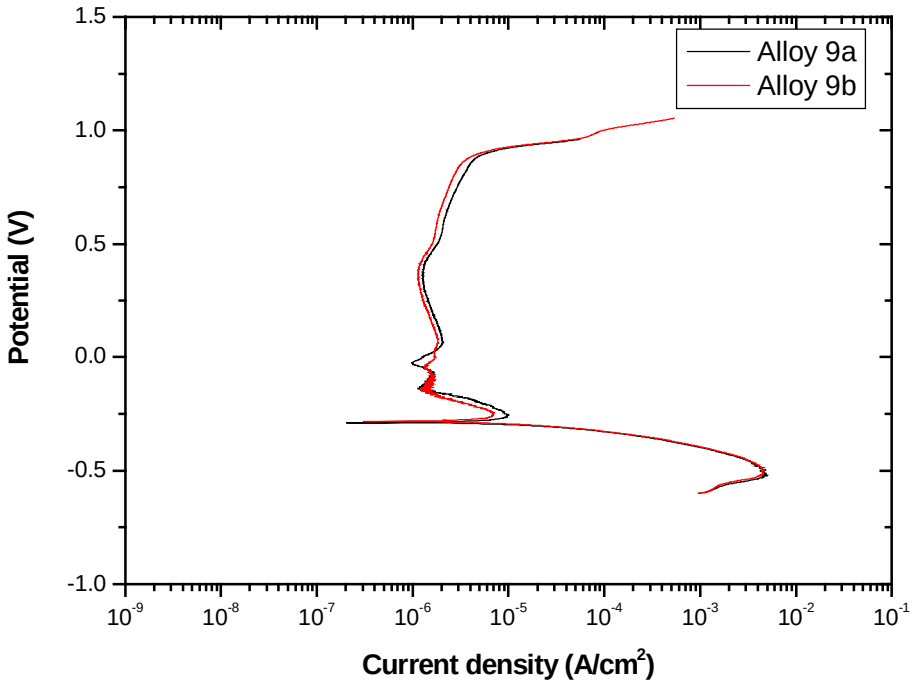

Figure E. 9: Scans obtained for ingot 9.

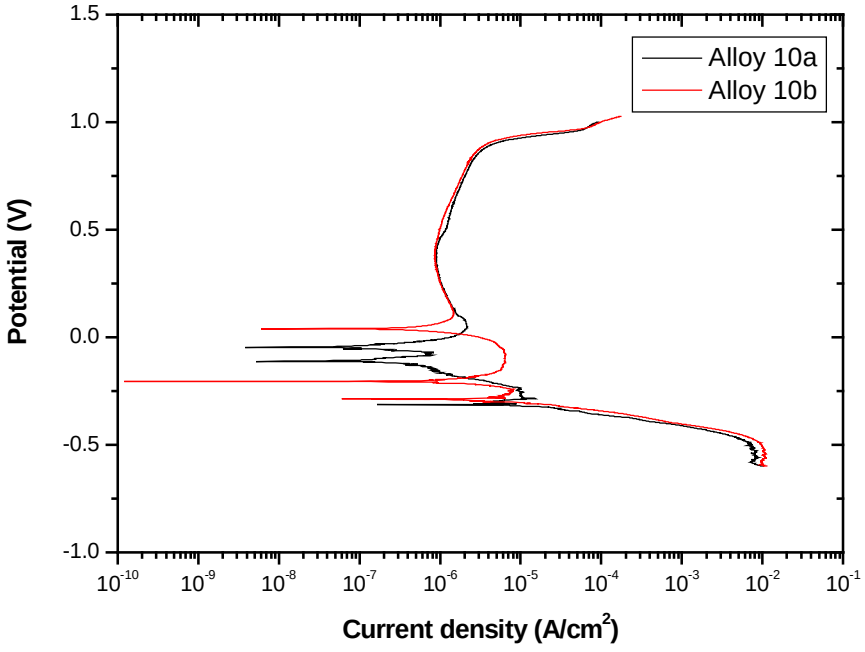

Figure E. 10: Scans obtained for ingot 10.

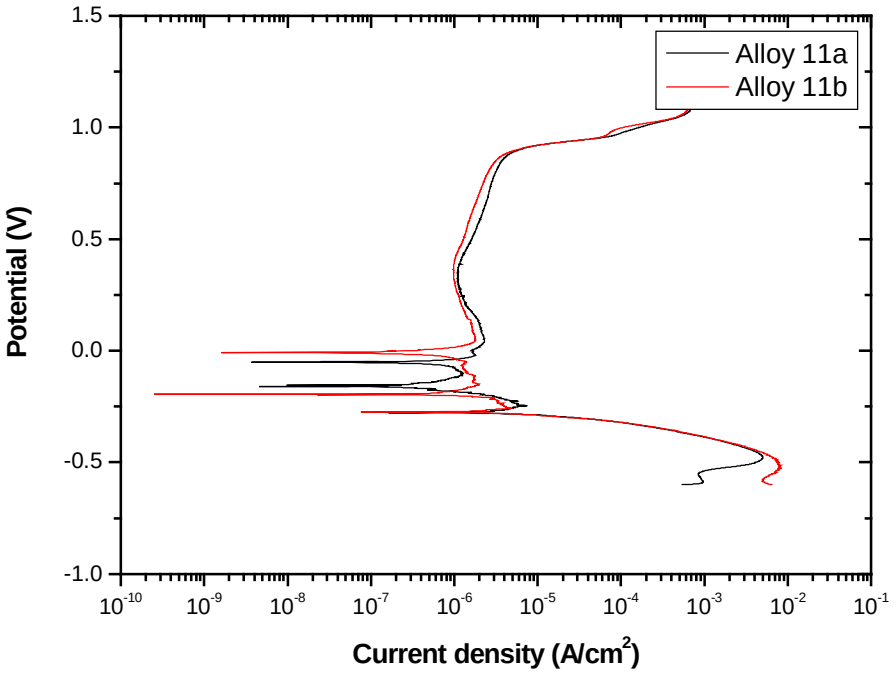

Figure E. 11: Scans obtained for alloy 11.

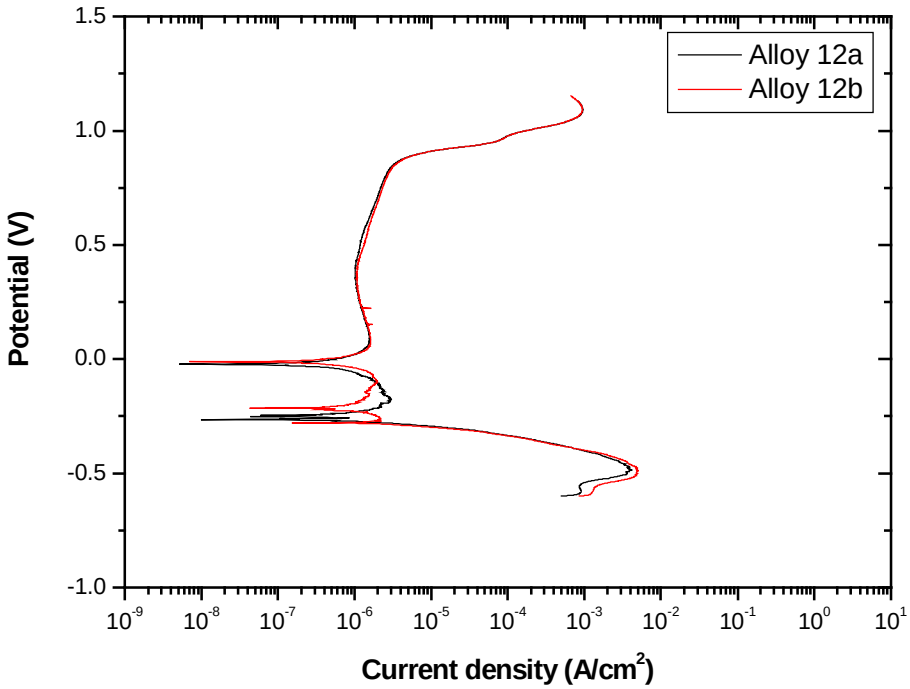

Figure E. 12: Scans obtained for ingot 12.

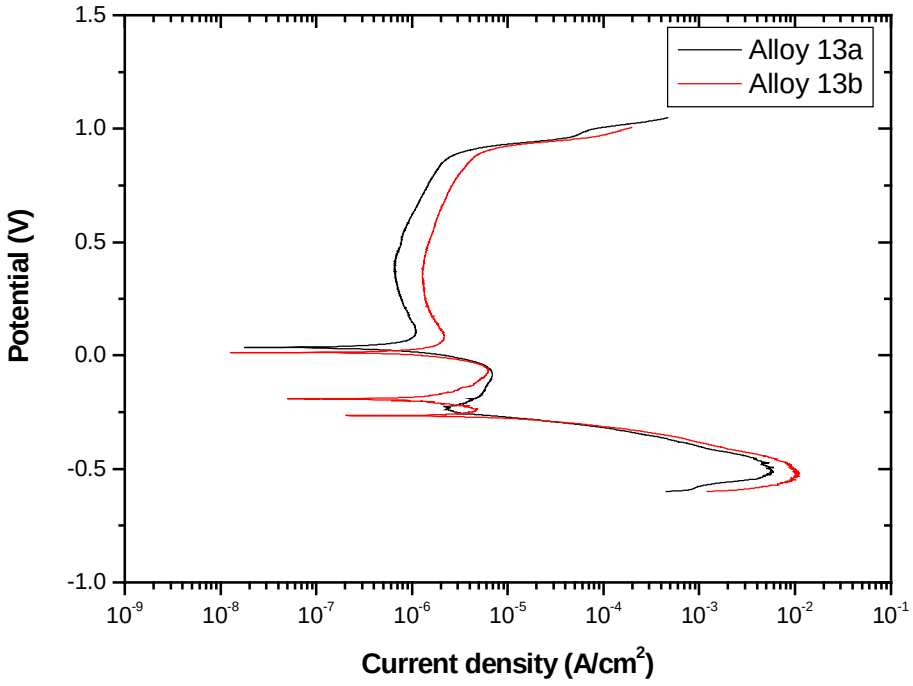

Figure E. 13: Scans obtained for ingot 13.

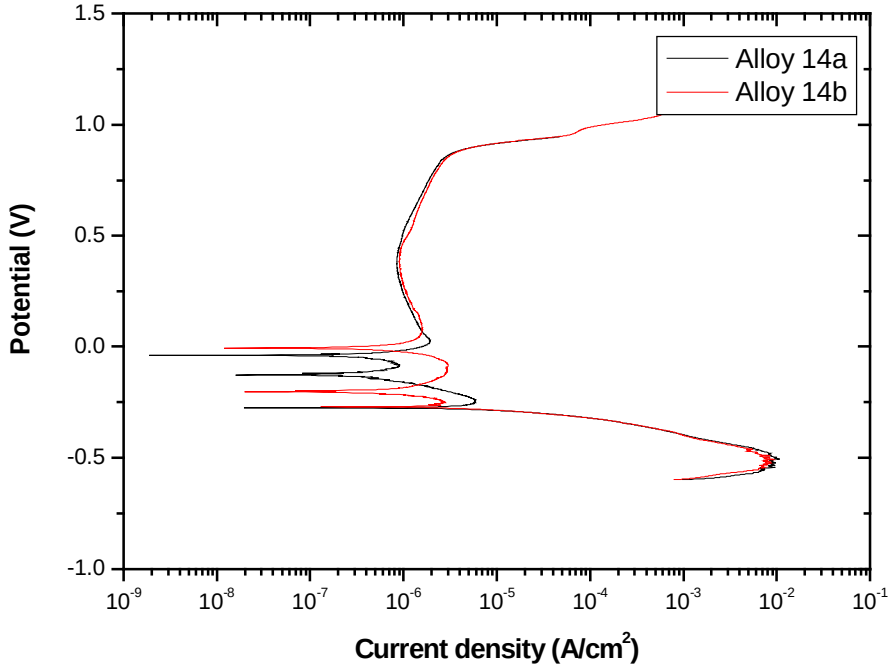

Figure E. 14: Scans obtained for ingot 14.

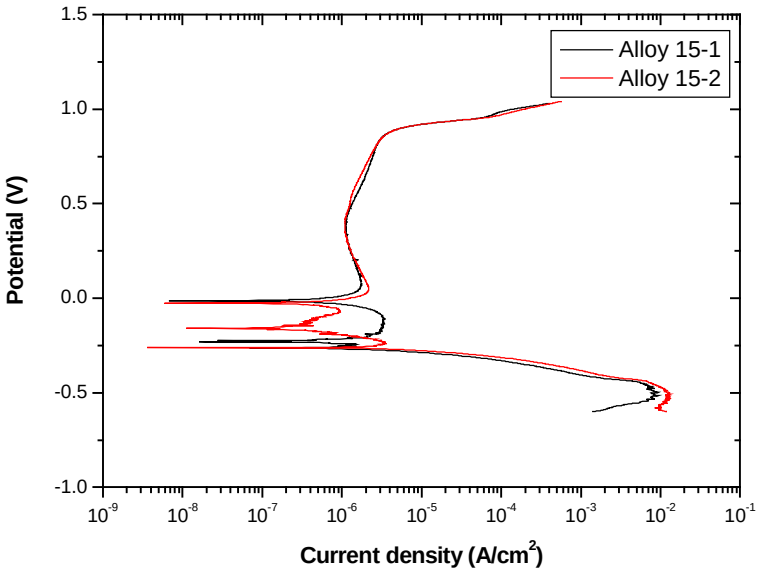

Figure E. 15: Scans obtained for ingot 15.

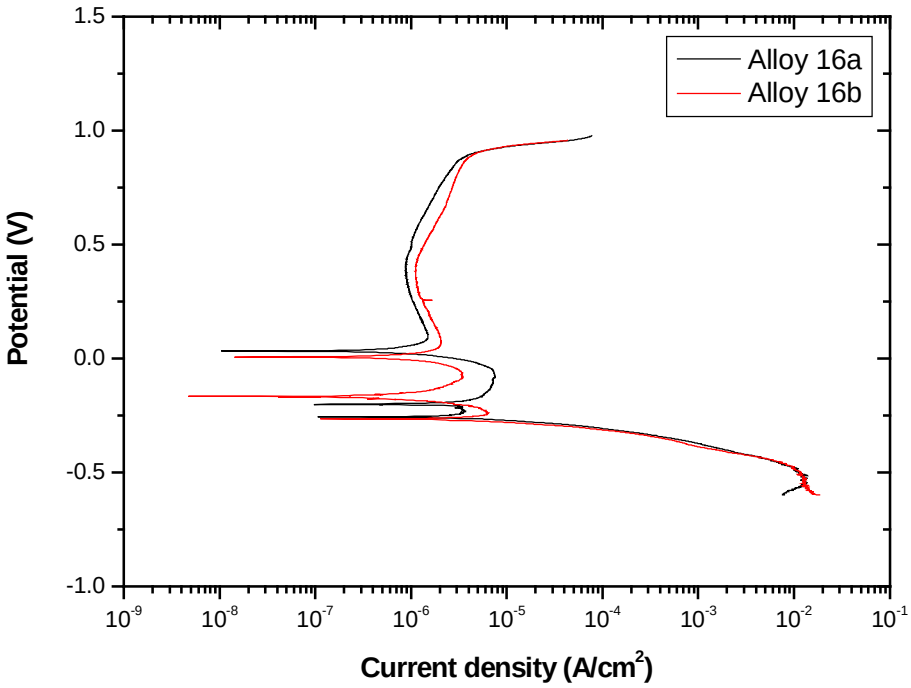

Figure E. 16: Scans obtained for ingot 16.

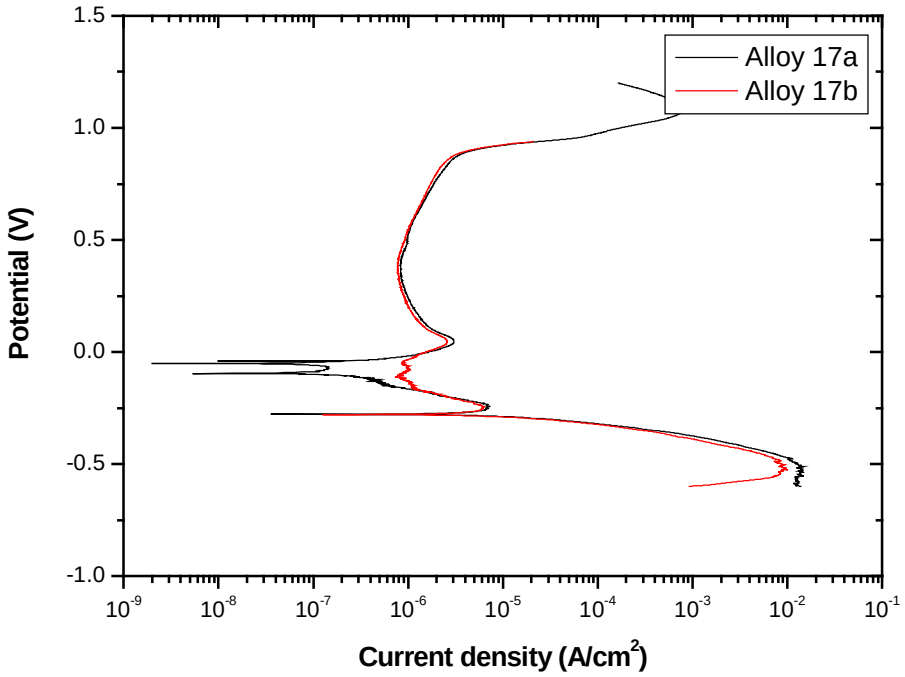

Figure E. 17: Scans obtained for ingot 17.

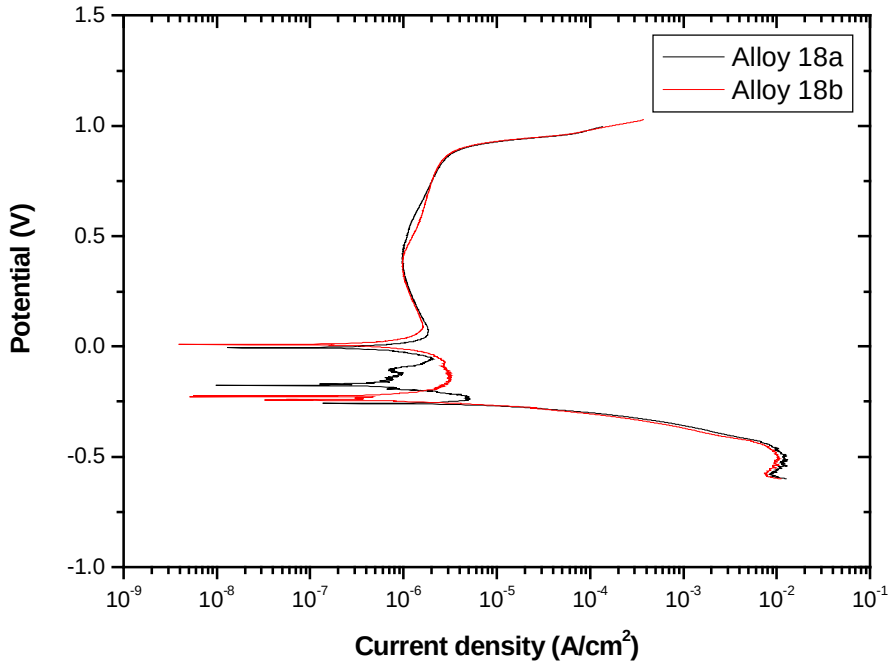

Figure E. 18: Scans obtained for ingot 18.

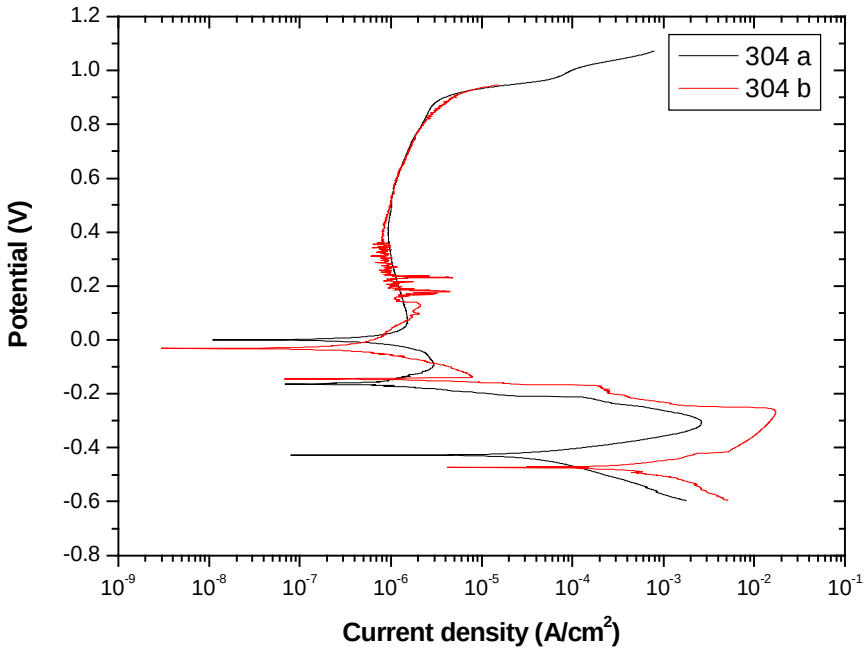

Figure E. 19: Scans obtained for ingot 304.

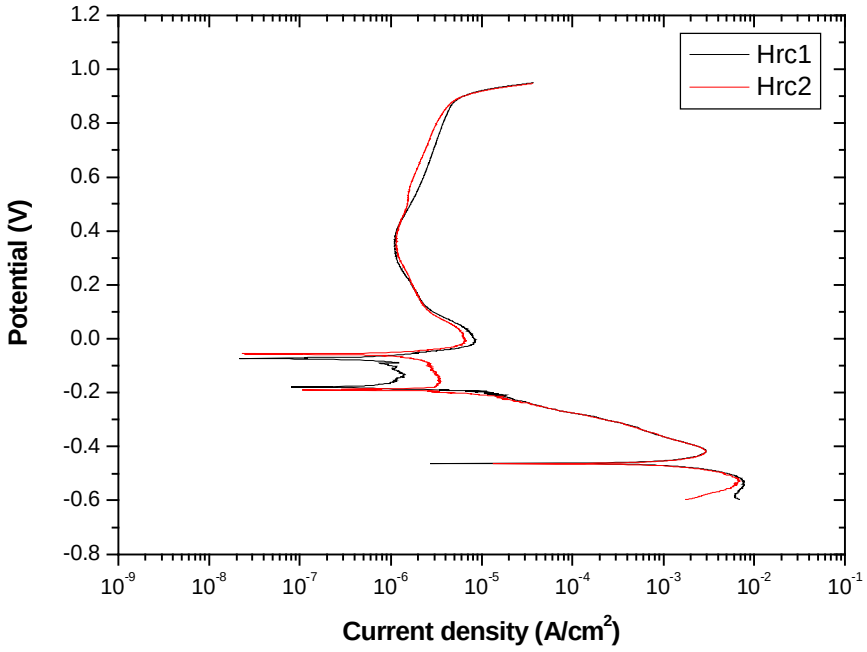

Figure E. 20: Scans obtained for ingot Hercules™.

Appendix F: Results of potentiodynamic scans for the 10 wt% Mn ingots according to ASTM standard G5-94 (2002).

Table F. 1: Corrosion results for the 10 wt% Mn alloys

alloy	corrosion rate (mm/y)	i_{corr} (A/m^2)
7	0.27	0.24
8	0.23	0.21
9	0.11	0.10
10	0.35	0.32
11	0.18	0.16
12	0.28	0.25
201	7.83	22.73
304	0.48	7.12
Herc	25.00	0.44

Potentiodynamic scans for the 10 wt% Mn alloys

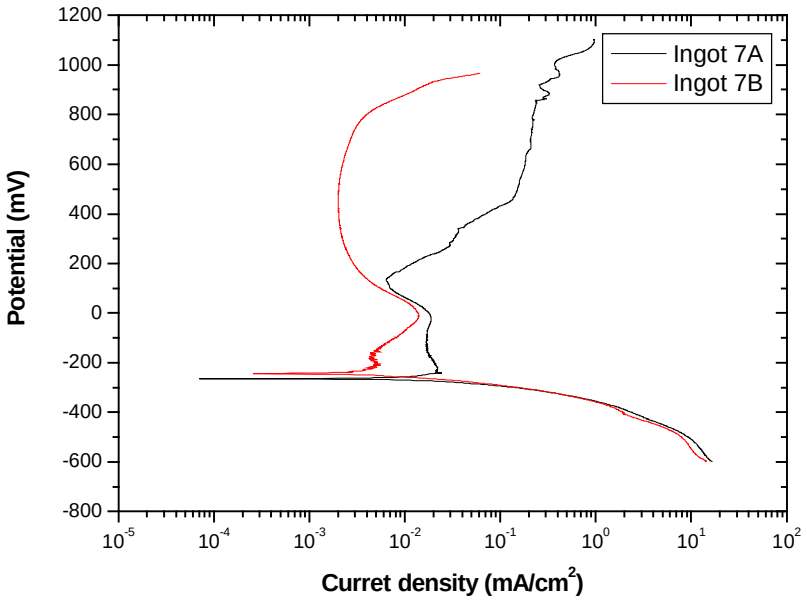

Figure F. 1: Scans obtained for ingot 7.

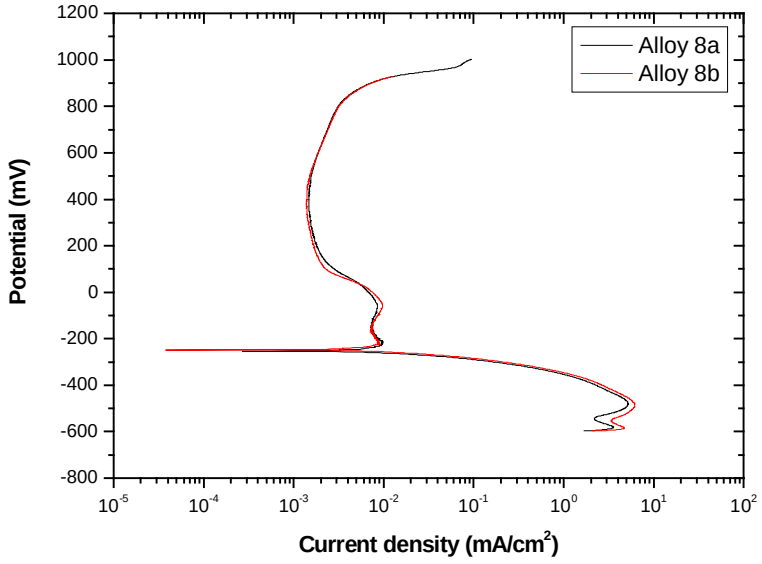

Figure F. 2: Scans obtained for ingot 8.

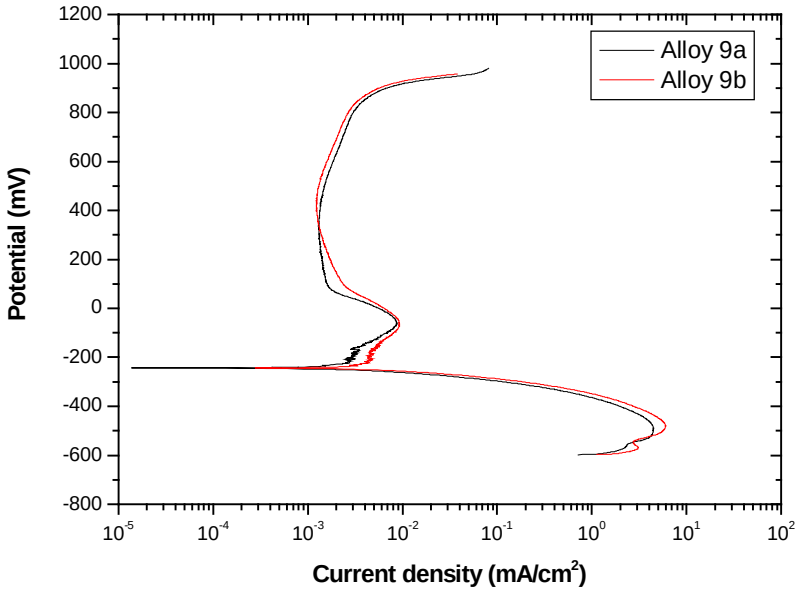

Figure F. 3: Scans obtained for ingot 9.

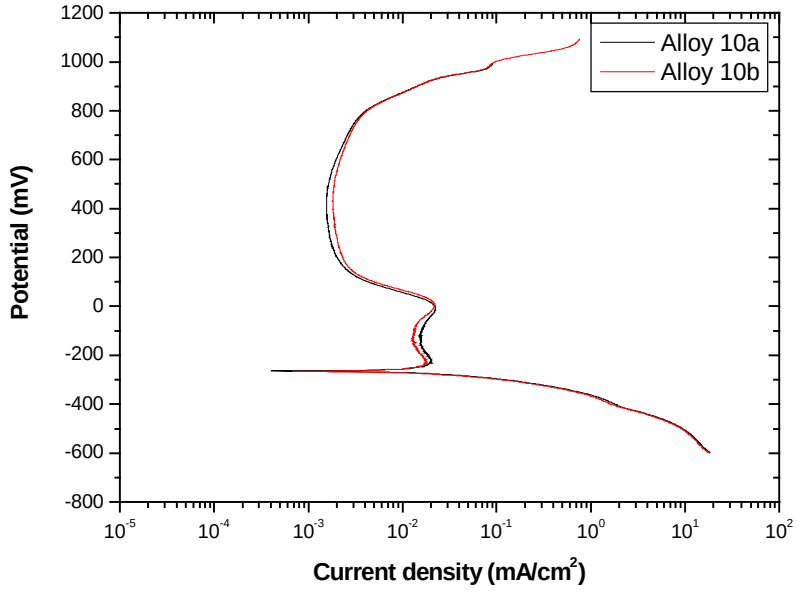

Figure F. 4: Scans obtained for ingot 10.

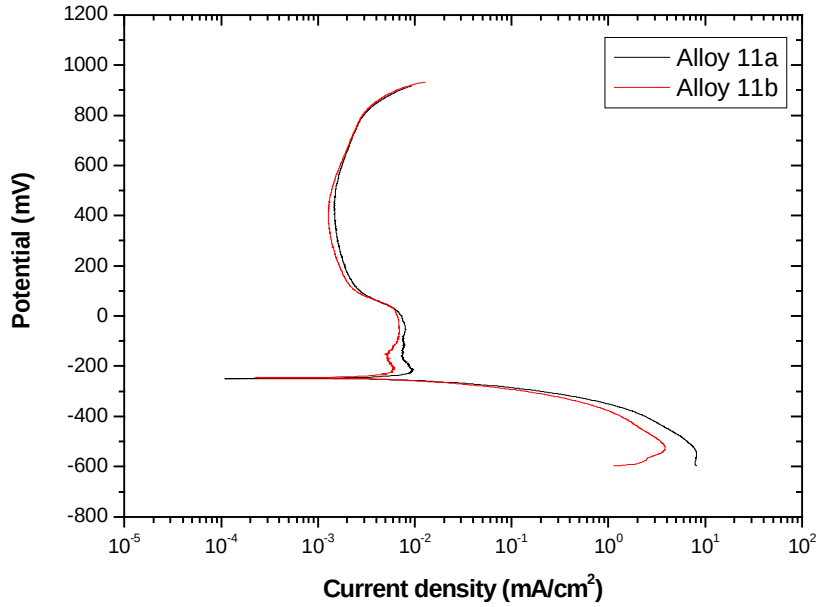

Figure F. 5: Scans obtained for ingot 11.

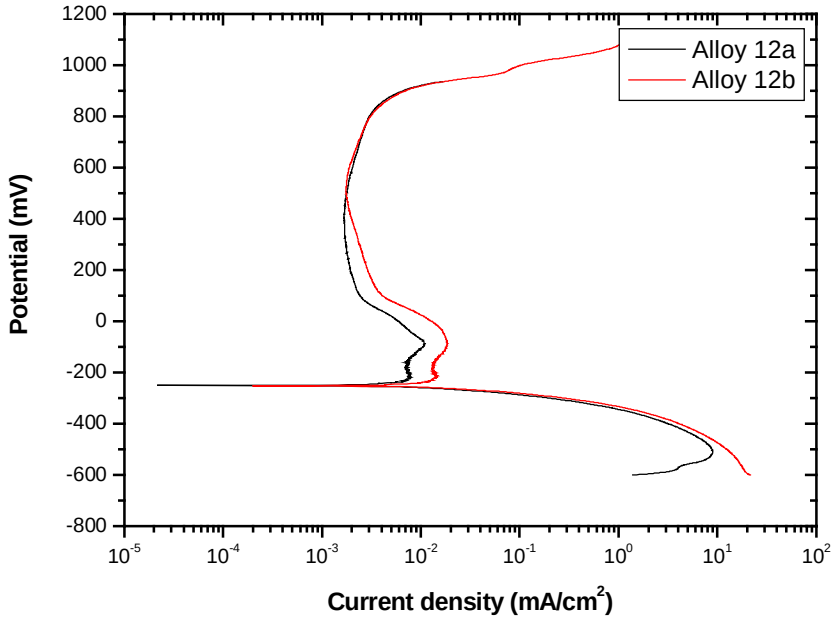

Figure F. 6: Scans obtained for ingot 12.

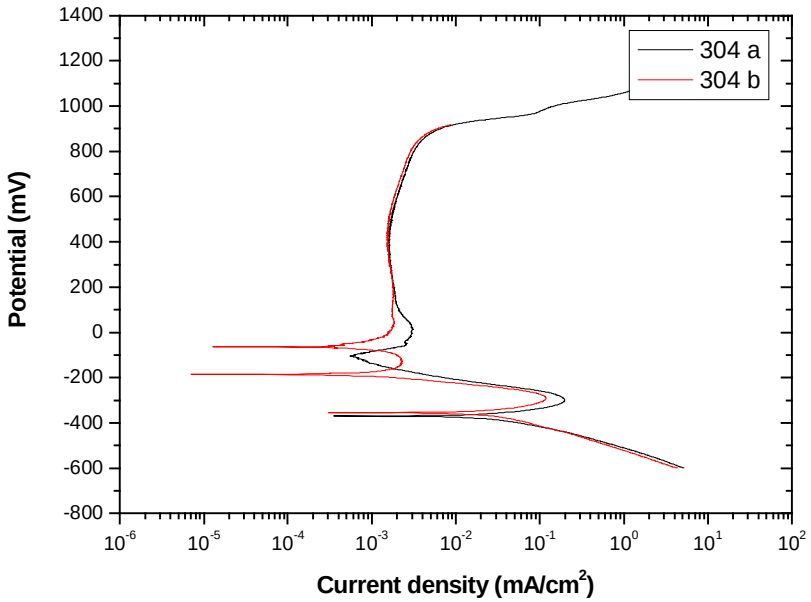

Figure F. 7: Scans obtained for ingot 304.

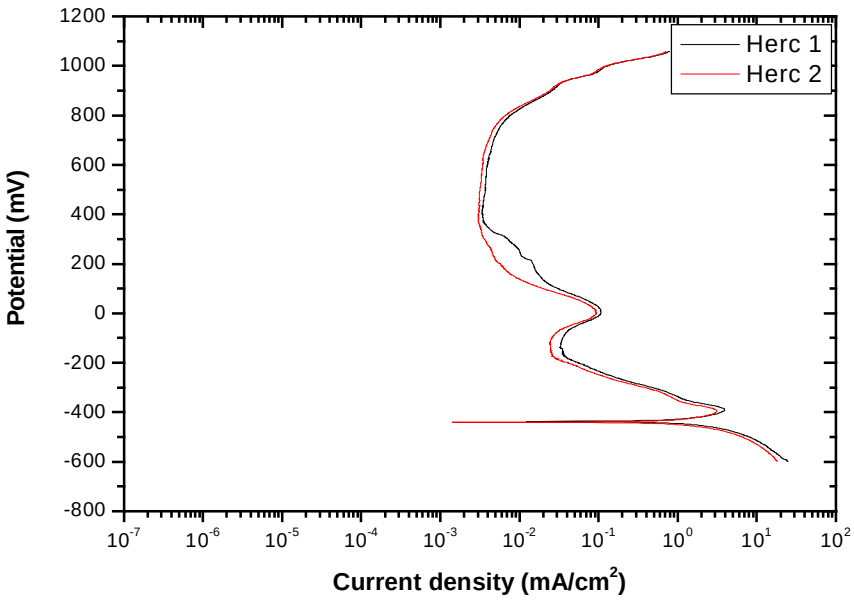

Figure F. 8: Scans obtained for ingot Hercules ™.

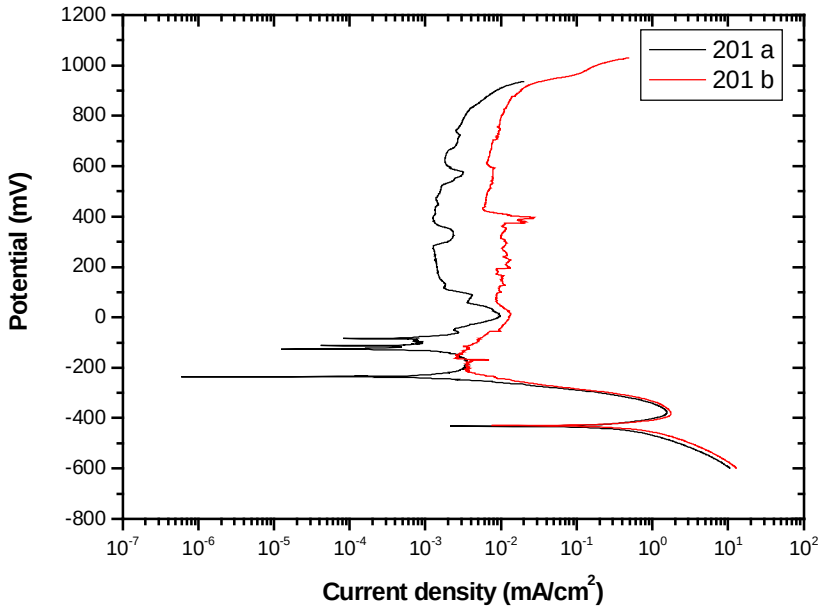

Figure F. 9: Scans obtained for ingot 201.

Appendix G: Pitting corrosion results for 10 wt% Mn ingots.

Table G. 1: Pitting potentials for 10 wt% Mn alloys

alloy	E_{pit}(mV)
7	36.05
8	96.77
9	132.70
10	-7.24
11	139.78
12	233.41
201	28.06
304	116.93
herc	-295.00

Pitting scans for the 10 wt% Mn alloys

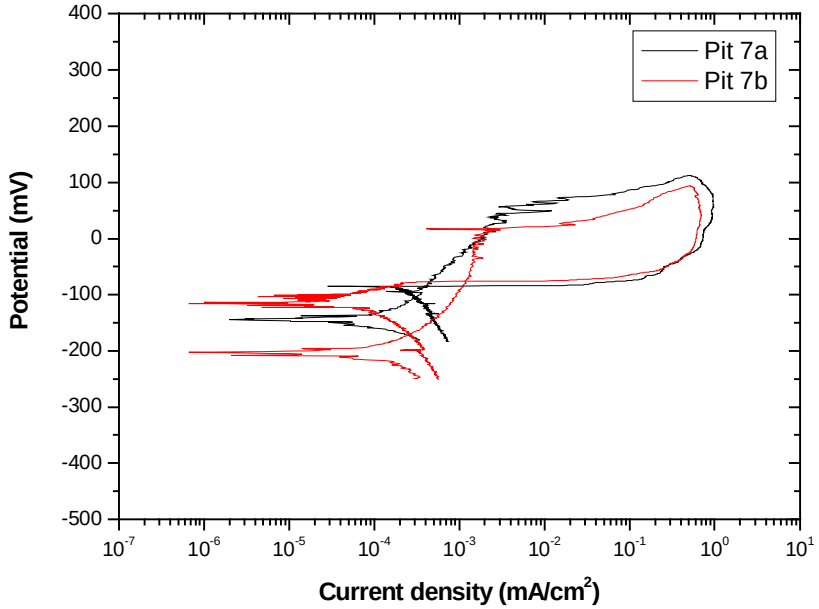

Figure G. 1: Cyclic potentiodynamic scans for ingot 7.

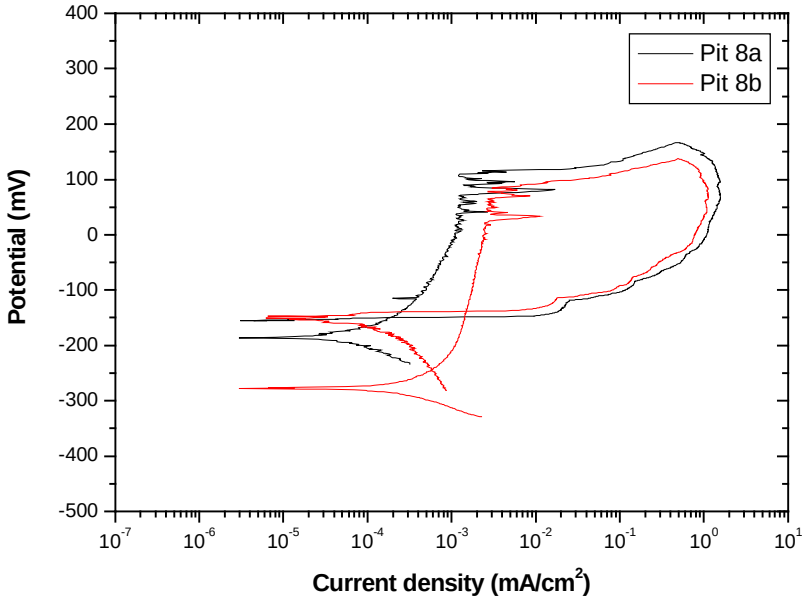

Figure G. 2: Cyclic potentiodynamic scan for ingot 8.

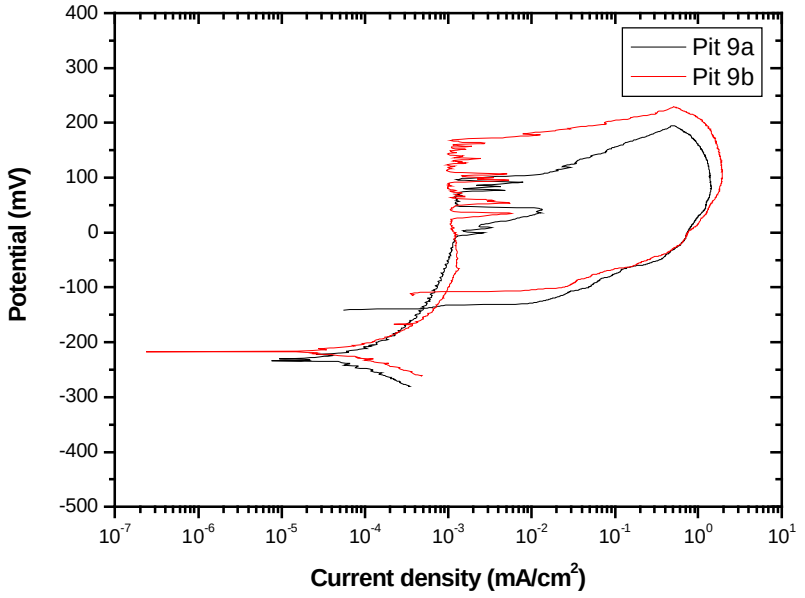

Figure G. 3: Cyclic potentiodynamic scans for ingot 9.

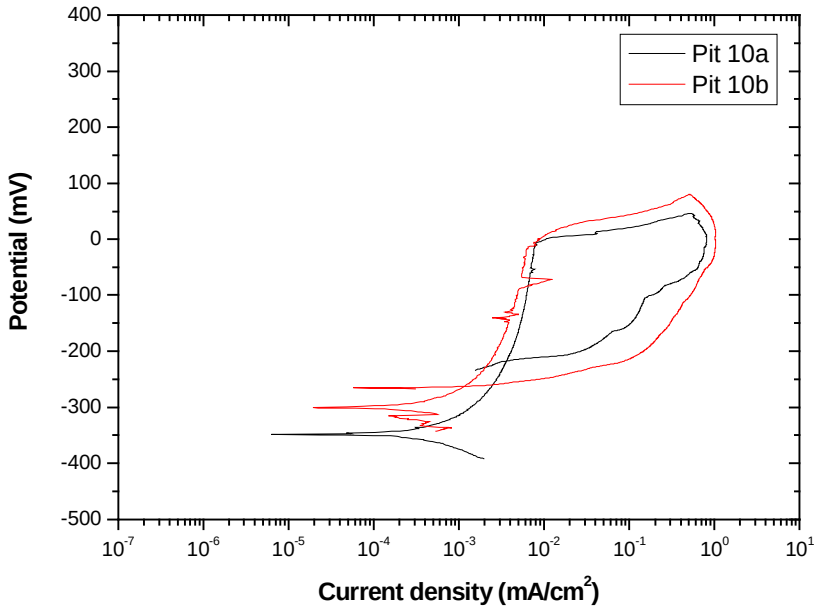

Figure G. 4: Cyclic potentiodynamic scans for ingot 10.

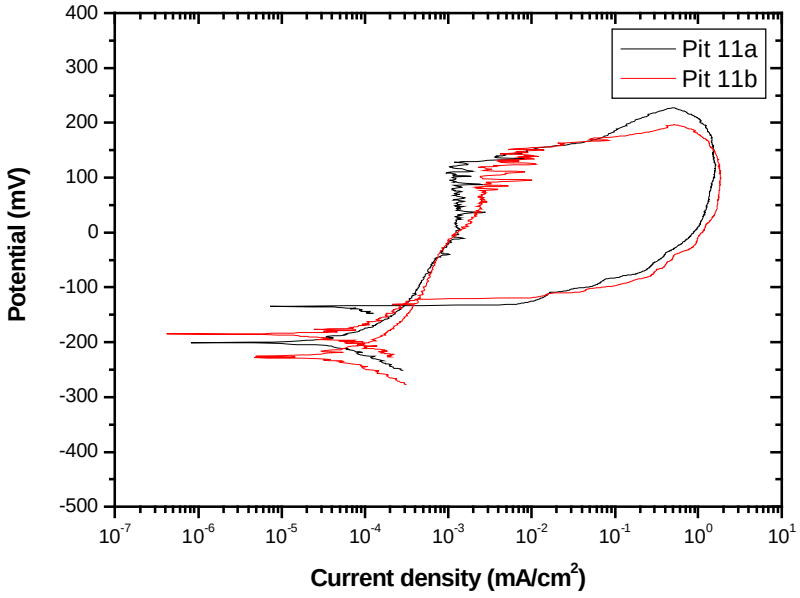

Figure G. 5: Cyclic potentiodynamic scans for ingot 11.

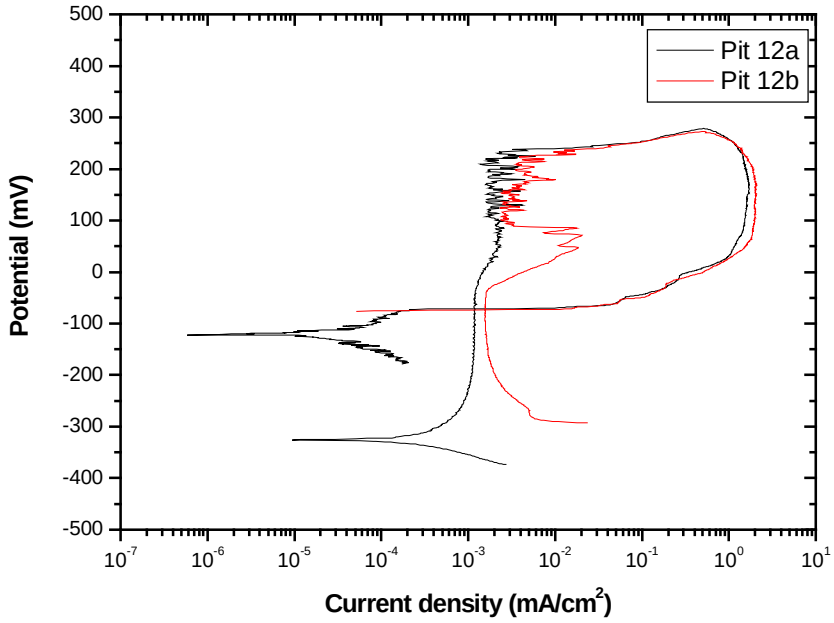

Figure G. 6: Cyclic potentiodynamic scans for ingot 12.

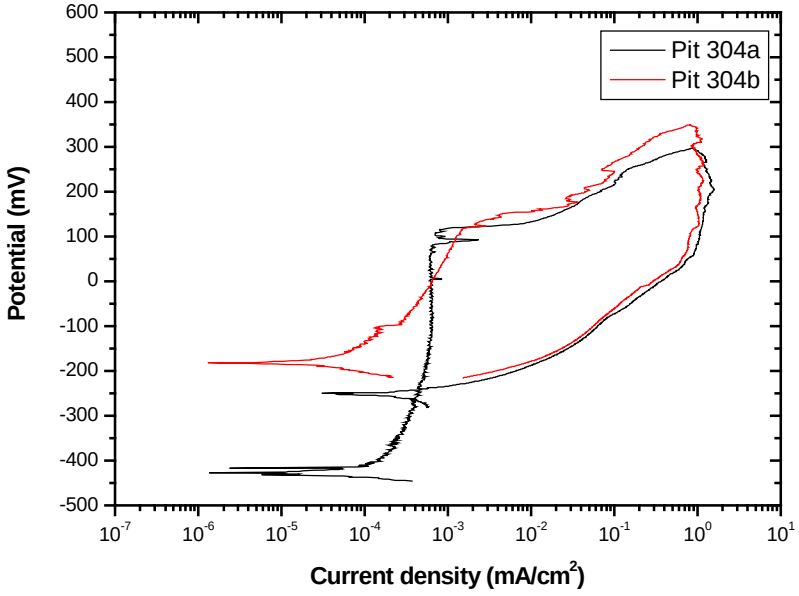

Figure G. 7: Cyclic potentiodynamic scans for ingot 304.

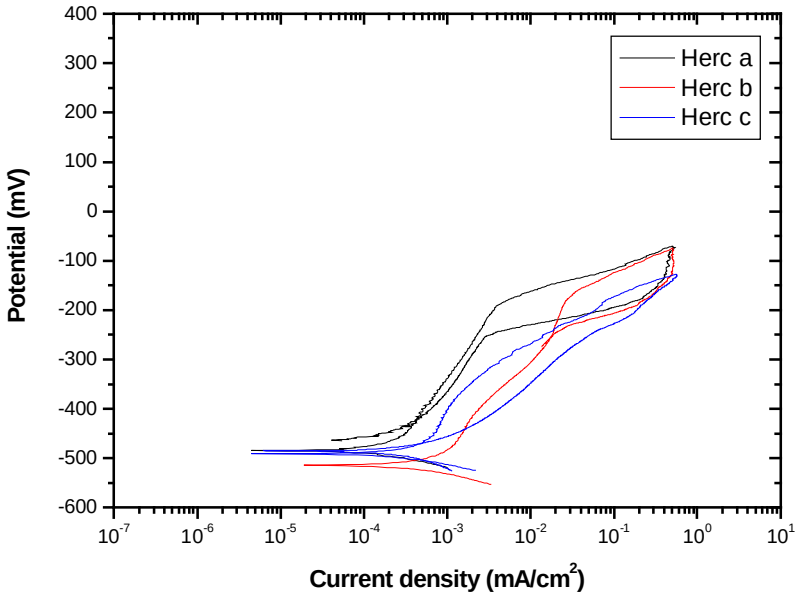

Figure G. 8: Cyclic potentiodynamic scans for ingot Hercules™.

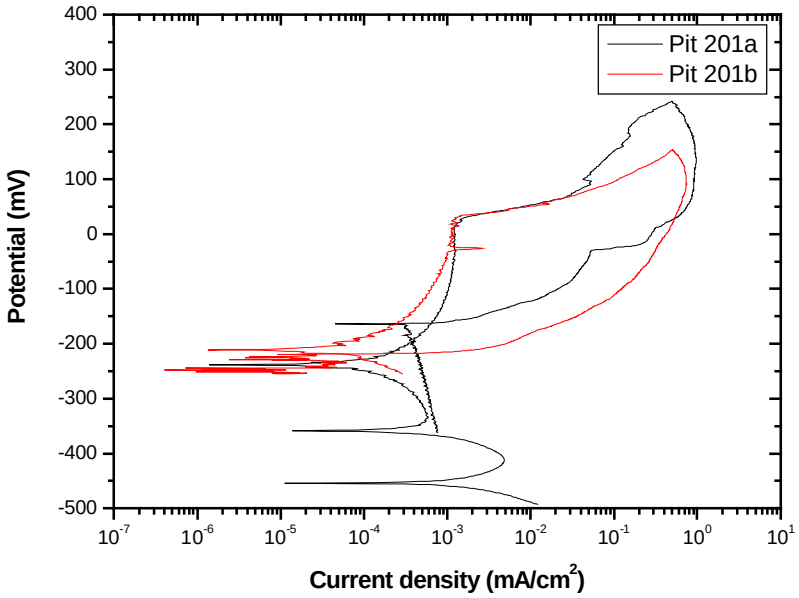

Figure G. 9: Cyclic potentiodynamic scans obtained for ingot 201.

Appendix H: SEM analysis of the 10 wt% Mn ingots.

Ingot	**Before corrosion.** **Secondary Electron Image (SEI)** **at X1100**	**After corrosion.** **(SEI at X1100)**	**After corrosion.** Backscattred Electron Image (BEI) **at X1100**
Ingot 7	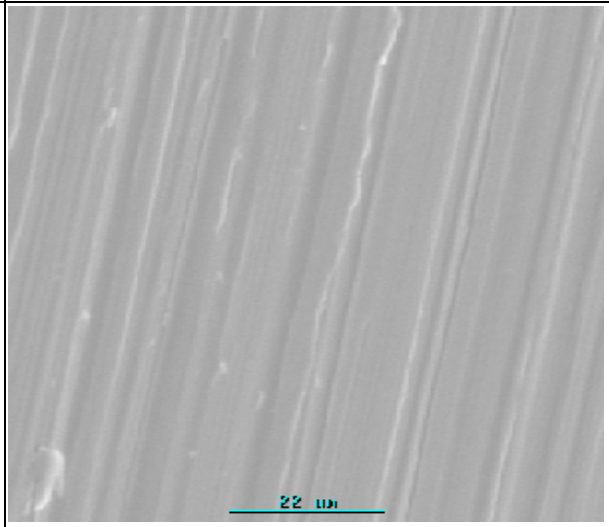	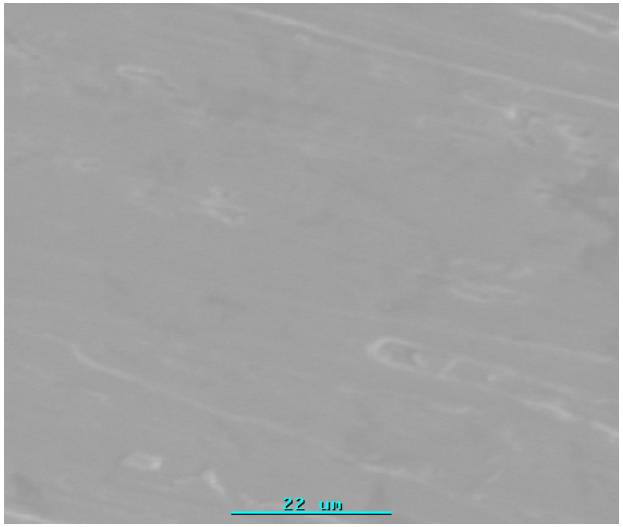	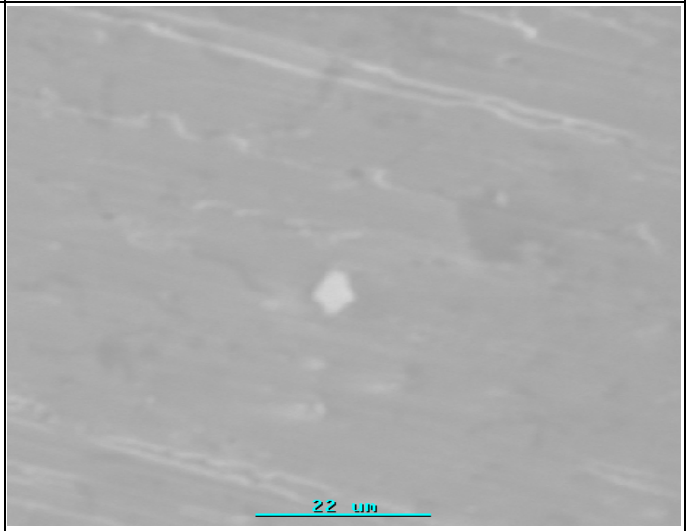
	Only scratches are visible	There was no evidence of corrosion	No evidence of corrosion

Ingot 8	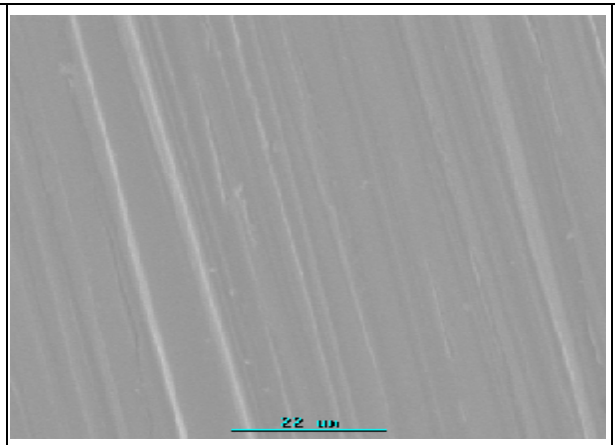	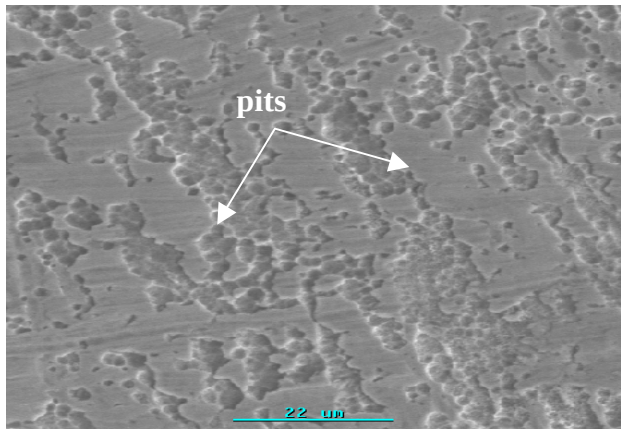	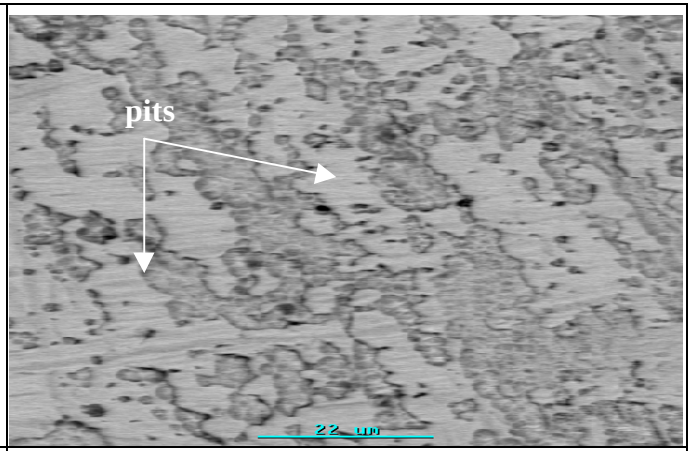
	Only scratches are visible	Pits distributed evenly across the whole surface. Pits seem to follow contour of scratch lines.	Pits distributed evenly across the whole surface. Pits seem to follow contour of scratch lines.

Ingot 9	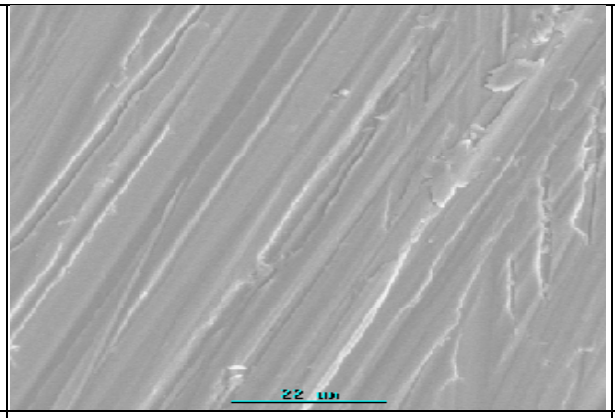	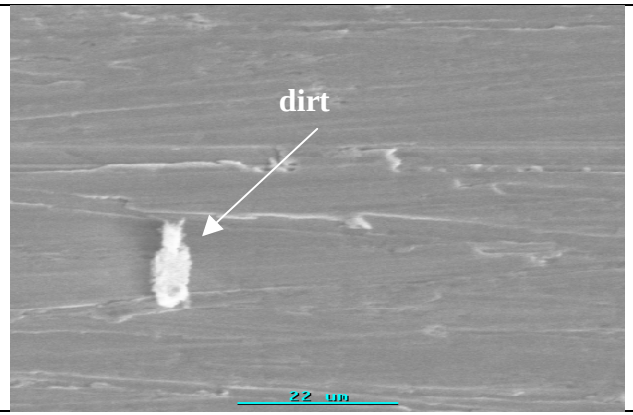	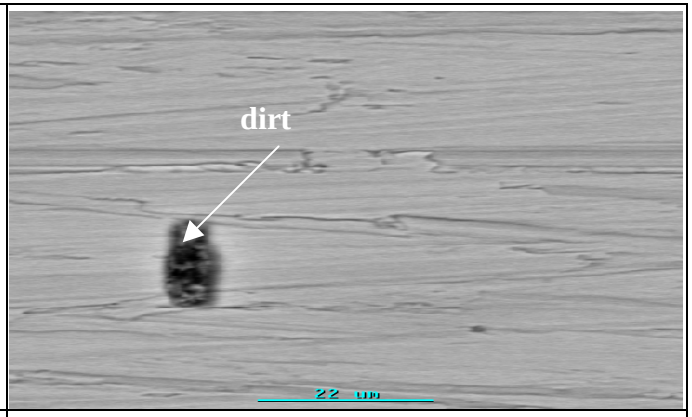
	Only scratches are visible	No evidence of corrosion.	No evidence of corrosion

Ingot 10	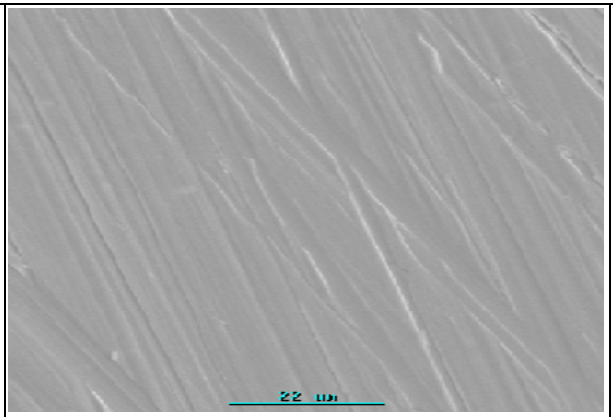	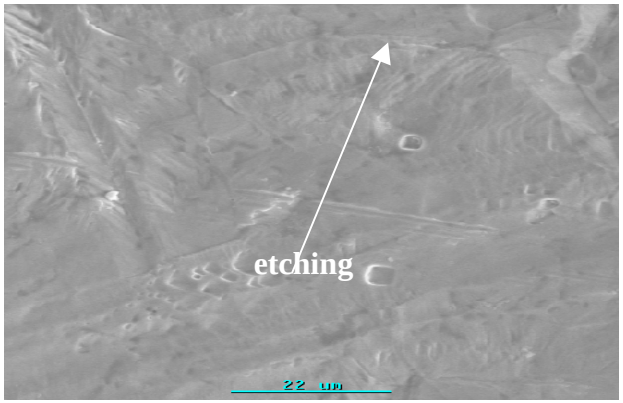	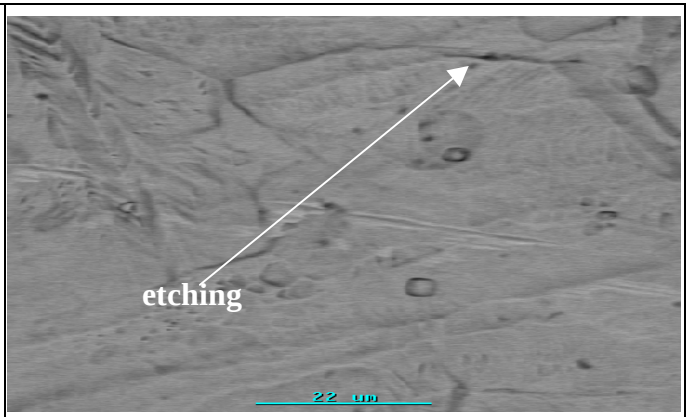
	Only scratches are visible	No pits. Sample seemed to have etched along the grains.	No pits. Sample seemed to have etched along the grains.

Ingot 11	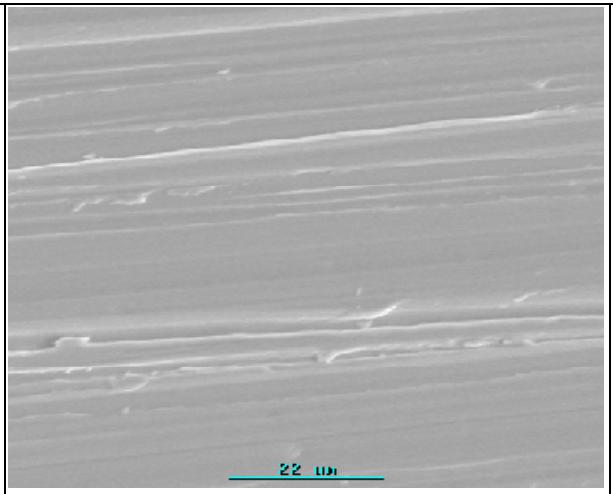	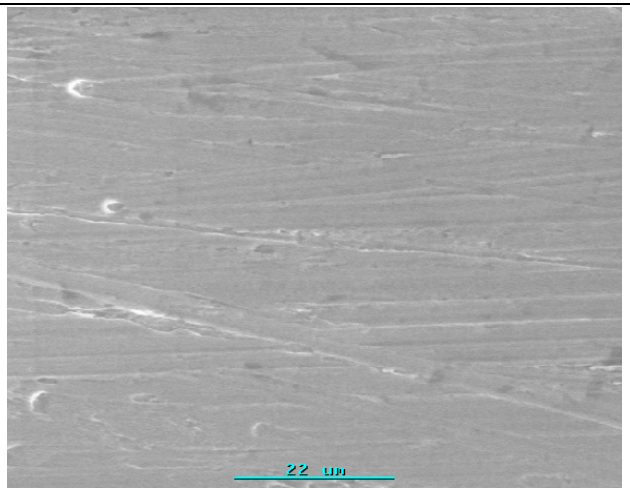	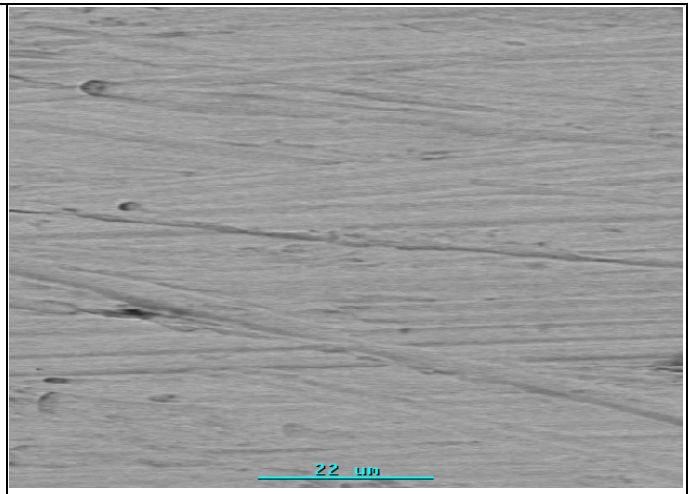
	Only scratches are visible	No evidence of corrosion	No evidence of corrosion

ngot 12	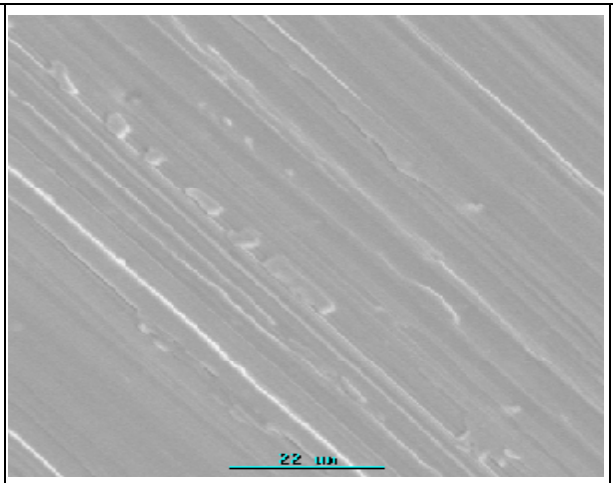	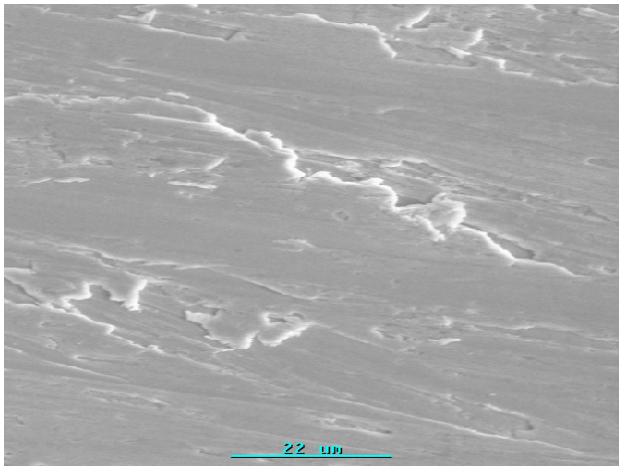	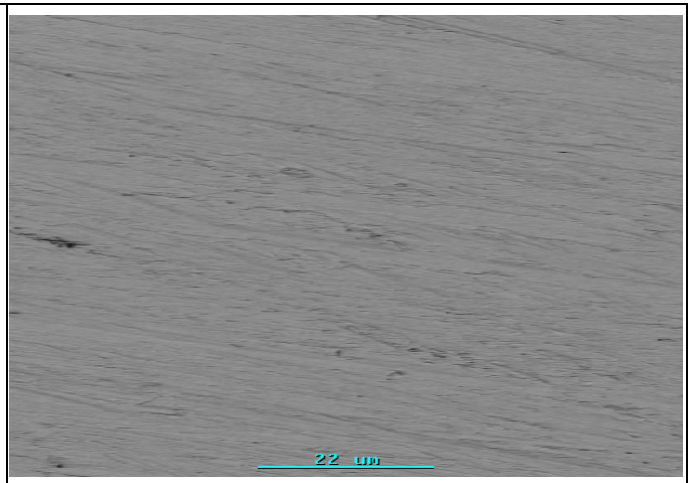
	Only scratches are visible	No evidence of corrosion	No evidence of corrosion

AISI 304	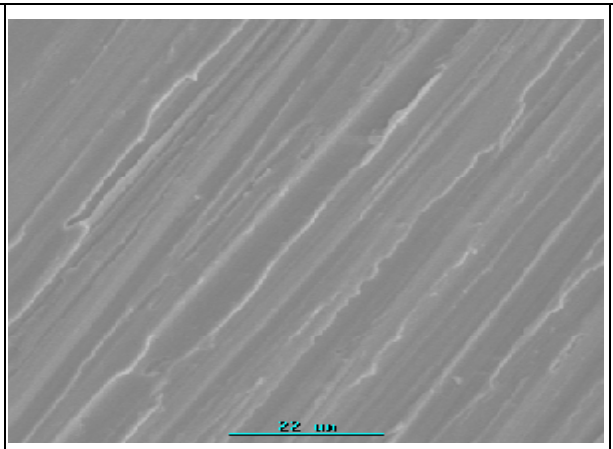	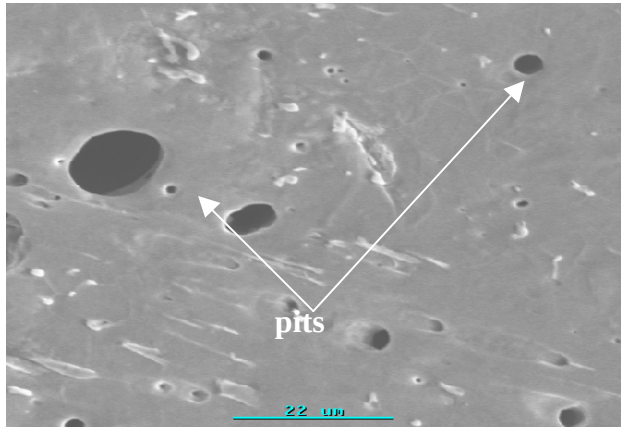	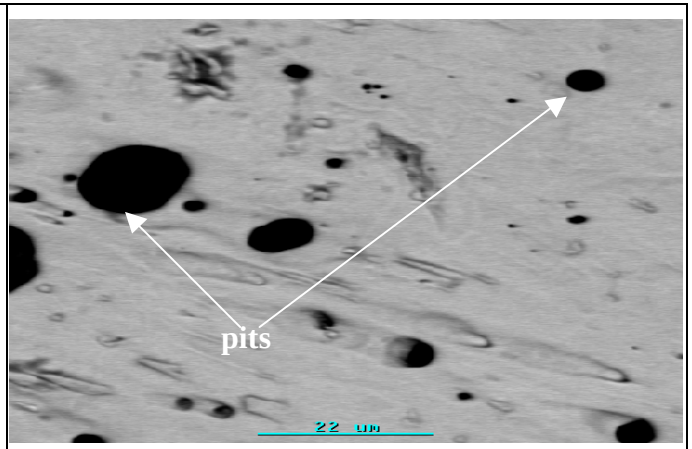
	Only scratches are visible	**Pits had formed in the alloy**	**Pits had formed in the alloy**

Appendix I: Current molybdenum and nickel prices

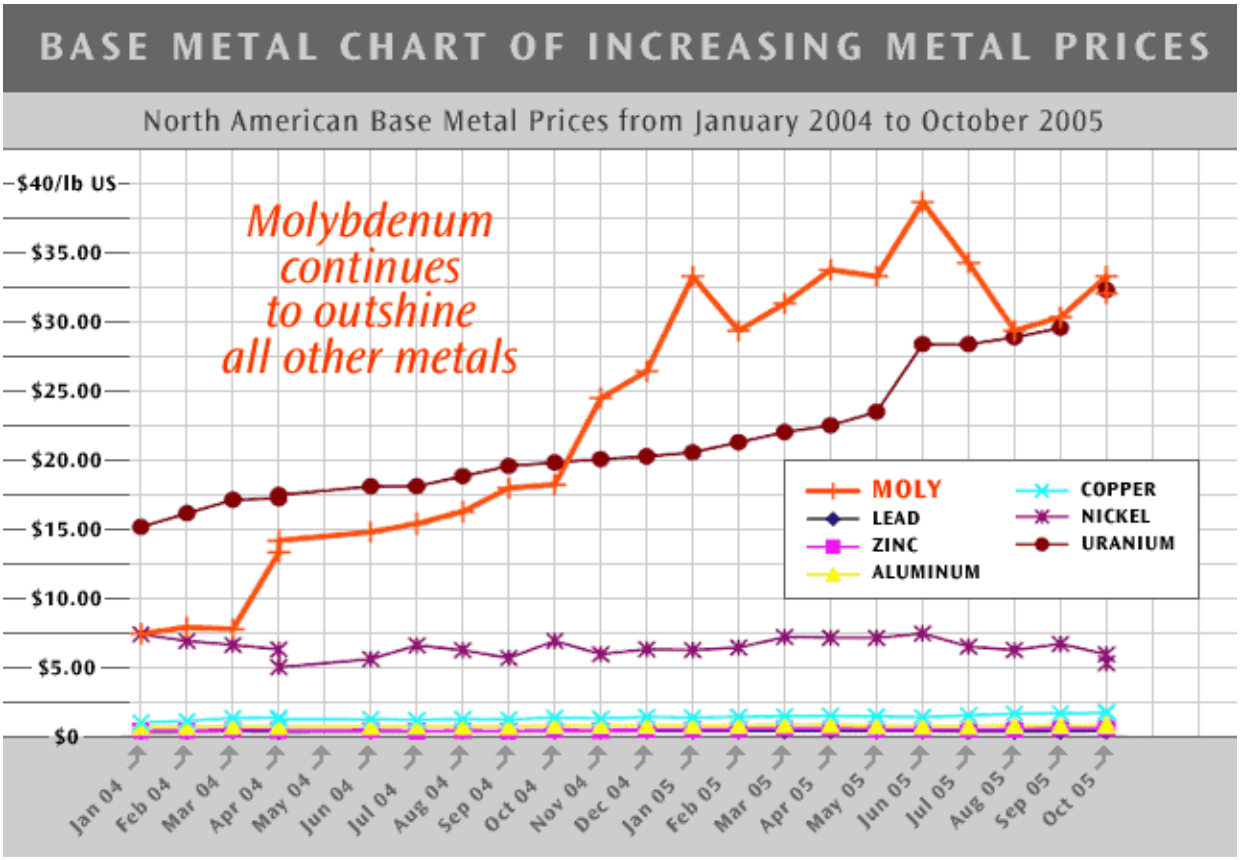

Figure I. 1: Molybdenum and Nickel prices [Adanac, 2005]

According to Adanac-Moly-Corp, a North American molybdenum producing company, molybdenum currently costs $34/lb, which is higher than the current $5/lb nickel price.